

---

# **Bacterial Inactivation using Radial Mode Ultrasonic Devices**

---

By

Graham Hunter MEng AIMEchE

A doctoral thesis submitted in fulfilment of the requirements for the award of Doctor of Philosophy (PhD) of the University of Glasgow



University of Glasgow | Department of Mechanical Engineering

© Graham Hunter 2008

---

## Acknowledgements

---

I would like to take this opportunity to thank those without whom this PhD would have been impossible.

Prof. Margaret Lucas – Margaret has been my principal supervisor for the duration of this project and her expertise and guidance throughout has been of immense value. Not only this, she was instrumental in finding the funding needed for the project to go ahead. From the first concept of combining ultrasonics with fluids to the completion of this thesis she has been both supportive and encouraging allowing me to develop the project in the direction I was interested in.

Dr. Ian Watson – Ian has been my second supervisor and his knowledge of coupling engineering with microbiology has been significant in developing the project to its fullest potential.

Dr. Roger Parton – Roger got involved in the project when we decided to look at doing the experimental side of the project and needed some expertise from the microbiology end. Having kindly allowed us to use the facilities within the Institute of Biomedical and Life Sciences (IBLS) department meant the experimental work could be done properly. Also, his knowledge and input on the project from the microbiological viewpoint has been very valuable.

Mrs. Irene Haughton – Irene is the technician that taught me the microbiological methods used in this thesis and her knowledge and help when I have been struggling in the lab was greatly appreciated.

Mechanical Engineering workshop staff – The technicians in the department have always been approachable, friendly and helpful throughout the design process of several of the parts constructed for the tests. Particularly Mr. Brian Robb who has always made sure the bits of kit were made when I needed them to the highest standards possible.

I would also like to thank Euan McCulloch (hopefully now Dr.) and Dr. Alan MacBeath for their support and banter. Particularly Euan who has had to put up with me shouting at the computer on more than one occasion. They have not just been work colleagues but friends.

Finally, I thank my family and friends for their continued support and encouragement over the last three years. This PhD has been a difficult challenge and they have always been behind me when I needed it most.

---

## **Abstract**

---

Bacterial inactivation is vitally important in many industrial processes and in particular those manufacturing products for human consumption. The consequences of poor inactivation processes can result in severe illness and death. To prevent this, several techniques have been developed over the years to ensure products are free from harmful bacteria. In the vast majority of cases either thermal or chemical inactivation is used in liquid products. Pasteurisation and boiling have been accepted methods of rendering a product free of pathogenic bacteria for centuries, as has the addition of small amounts of chlorine to water. Unfortunately, the use of thermal and chemical methods has a detrimental effect on the nutritional value, taste and texture of the product. Also, bacteria are living organisms and as such are subject to evolution. In fact, the rate at which bacteria multiply probably makes them the fastest evolving organisms on the planet. This means that bacteria are likely to evolve resistance to inactivation methods over a period of time and new methods will be required to aid the inactivation of pathogens. The use of ultrasonic vibrations to cause cavitation and thus bacterial inactivation has been shown to be successful. This method causes physical inactivation of bacteria by disrupting the bacterial cell wall thus adding a new tool in the arsenal against pathogens.

This project investigated the bacterial inactivation capacity of radial and probe type ultrasonic horns. Radial horns were designed using finite element analysis and validated using experimental modal analysis. Several radial horns were investigated, tuned to the R0 and R3 modes, while probe type horns tuned to a longitudinal mode. A finite element model has been created to estimate the acoustic fields created by these devices, where water is the load medium, and therefore where zones of cavitation could be expected to occur. This finite element model is validated against photographic and chemiluminescent visualisation studies of the cavitation field. A microbiological study was carried out to



determine the bacterial efficiency of these devices in a static (non-flow) system. This study used the organisms *Escherichia coli* and *Staphylococcus aureus* as the test organisms as they are non-pathogenic, well understood, easy to handle, and are useful indicators of bacterial inactivation performance that have been extensively studied. Further to the positive results from these tests, a continuous flow radial horn system was designed and constructed. This was used to test the bacterial efficiency of the radial horn device in a continuous flow situation. Results on the effect of flow rate and ultrasonic amplitude on the bactericidal effect on the two bacterial organisms used are presented.

---

# Contents

---

Acknowledgements	i
Abstract	iii
Contents	v
Table of Figures	viii
<b>Chapter 1 – Introduction</b>	<b>1</b>
1.1 History of bacterial inactivation	1
1.1.1 Pasteurisation	1
1.1.2 Chlorination	2
1.1.3 Ultraviolet light	3
1.1.4 Ozone	4
1.1.5 Ultrasonic vibration	5
1.2 Aims and Objectives	13
<b>Chapter 2 – Literature Review</b>	<b>16</b>
2.1 Introduction	16
2.2 Ultrasonic devices	17
2.3 Cavitation	19
2.3.1 Historical overview	20
2.3.2 Stable cavitation	22
2.3.3 Transient cavitation	24
2.3.4 Applications of cavitation	24
2.3.4.1 Ultrasonic cleaning	25
2.3.4.2 Ultrasonic homogenisation and emulsification	25
2.3.4.3 Sonochemistry	26
2.3.4.4 Bubble fusion	28
2.3.4.5 Medical	28
2.3.4.6 Microbiological applications	29
2.4 Introduction to bacteria	30
2.5 Microbiological studies	34
2.6 Continuous flow studies	36
2.7 Conclusions	39

---

<b>Chapter 3 – Horn Design</b>	<b>40</b>
3.1 Introduction	40
3.2 Finite element method	40
3.3 Experimental modal analysis	41
3.3.1 Excitation devices	43
3.3.1.1 Ultrasonic Piezoelectric Transducers	43
3.3.2 Excitation signal	43
3.3.3 Response measurement devices	44
3.3.3.1 Laser Doppler vibrometer	44
3.3.4 Signal processing	47
3.3.5 Frequency Response Function (FRF)	49
3.3.6 EMA curve fitting methods	52
3.3.7 Post processing and visualisation	53
3.4 Horn designs	54
3.4.1 Nomenclature	54
3.4.2 Radial horns	55
3.4.3 Probe horn	76
3.4.4 Booster horn	78
3.5 Ultrasonic Amplitudes	84
3.6 Discussion and Conclusion	85
 <b>Chapter 4 – Cavitation and Visualisation</b>	 <b>87</b>
4.1 Introduction	87
4.2 Finite element models	87
4.2.1 Probe model	88
4.2.2 Radial horn models	92
4.3 Visualisation	94
4.3.1 Introduction	94
4.3.2 Methods	95
4.3.3 Results	96
4.3.4 Discussion	107
4.4 Model verification	109
4.5 Conclusions	111
 <b>Chapter 5 – Bacterial Inactivation under no flow conditions</b>	 <b>114</b>
5.1 Introduction	113
5.2 Microbiological methods	113
5.3 Results	117
5.4 Discussion	126
5.5 Conclusions	131

---

<b>Chapter 6 – Preliminary study of bacterial inactivation under flow conditions</b>	<b>133</b>
6.1 Introduction	133
6.2 Adaptation of horn design	133
6.3 Method and materials	135
6.4 Results	136
6.5 Discussion	137
6.6 Conclusions	138
<b>Chapter 7 – Conclusions</b>	<b>139</b>
<b>Chapter 8 – Future work</b>	<b>145</b>
References	147
Bibliography	160
List of Publications	161

---

## Table of Figures

---

Figure 1-1	Ultrasonic probe horn	7
Figure 1-2	Radial horn with attached ultrasonic transducer	8
Figure 1-3	Sonic or ultrasonic processing apparatus	8
Figure 1-4	Heat Systems Inc. patented system	9
Figure 1-5	Radially vibrating annular horn	10
Figure 1-6	Vessel shaped/dimensioned to concentrate ultrasound vibrations in the centre of well	11
Figure 1-7	Flow through device for the ultrasonic destruction of micro organisms in fluids	11
Figure 1-8	Cylindrical transducer for the purpose of causing bacterial inactivation	12
Figure 1-9	Continuous flow method of inactivating bacteria using MHz ultrasound	13
Figure 2-1	Piezoelectric Transducer	18
Figure 2-2	Aspherical collapse of a cavitation bubble close to a rigid surface	25
Figure 2-3	Cell structures (a) Prokaryote cell and (b) Eukaryote cell	31
Figure 2-4	Bacterial cell shapes. (a) Eschericia Cole (rod), (b) Staphylococcus aureus (sphere) and (c) Borrelia burgdorferi (spiral)	32
Figure 2-5	Bacteria Cell wall structure. Gram negative (left) and Gram Positive (right)	33
Figure 3-1	Finite elements (a) 8 node linear brick element and (b) 20 node quadratic brick element	41
Figure 3-2	Experimental modal analysis set-up	42
Figure 3-3	Piezoelectric Transducer	43
Figure 3-4	Schematic of a laser Doppler vibrometer	44
Figure 3-5	Polytec 3D LDV	47
Figure 3-6	Effect of non-periodic measurements on FRF's (leakage)	48
Figure 3-7	Effect of windows on leakage (a) Gauss window, (b) Hanning window and (c) Hamming window	49
Figure 3-8	Single degree of freedom system with mass $m$ , stiffness $k$ and damping $c$	50
Figure 3-9	Block diagram of an FRF	51
Figure 3-10	Cross section view of the parts in a radial horn	54
Figure 3-11	Radial horn with attached transducer elevation picture	55
Figure 3-12	Radial modes of vibration (a) R0, (b) R1, (c) R3	56
Figure 3-13	Design process for the design of radial ultrasonic horns	57

Figure 3-14	Simple radial horn (left), dimensions used (right)	58
Figure 3-15	R0 <sub>ID30</sub> radial horn modes from 10-30 kHz. Solid black line indicates undeformed shape.	60
Figure 3-16	Radial horn design	64
Figure 3-17	R0 <sub>ID30</sub> Radial horn design including tuned connecting cylinder and flange mode shape at 20 kHz. Deformed shape shown in green and undeformed shape shown in transparent grey. (a) Elevation, (b) End Elevation, (c) Isometric.	65
Figure 3-18	(a) R0 <sub>ID30</sub> mode radial horn displacement contours for a 10µm input displacement, large displacements shown in red with small displacements are blue. (b) R0 <sub>ID30</sub> radial mode horn stress contours for a 10 µm input displacement. Displacements are shown in metres with stresses in N/m <sup>2</sup> .	66
Figure 3-19	EMA measurement points for R0 <sub>ID30</sub> horn	67
Figure 3-20	EMA captured data (black) and curve fit (red) for point 1 in the X direction	68
Figure 3-21	EMA captured data (black) and curve fit (red) for point 1 in the Y direction	68
Figure 3-22	EMA captured data (black) and curve fit (red) for point 1 in the Z direction	69
Figure 3-23	Comparison of the FE predictions (left) and the experimental modal test (right) for the R0 <sub>ID30</sub> mode radial horn	71
Figure 3-24	Comparison of the FE predictions (left) and the experimental modal test (right) for the R3 <sub>ID50</sub> mode radial horn	72
Figure 3-25	EMA captured data (black) and curve fit (red) for point 1 in the X direction	72
Figure 3-26	EMA captured data (black) and curve fit (red) for point 1 in the Y direction	73
Figure 3-27	EMA captured data (black) and curve fit (red) for point 1 in the Z direction	75
Figure 3-28	(a) R3 <sub>ID50</sub> mode radial horn displacement contours for a 10µm input displacement, large displacements shown in red with small displacements are blue. (b) R3 <sub>ID50</sub> radial mode horn stress contours for a 10 µm input displacement. High stresses are shown in red while low stresses are blue.	76
Figure 3-29	Comparison of R3 <sub>ID50</sub> mode radial horn using FEA ((a), (c), (e)) and EMA ((b), (d), (e)) for the R1 mode ((a), (b)), R0 mode ((c), (d)) and R3 mode ((e), (f))	77
Figure 3-30	20 kHz ultrasonic probe horn	78
Figure 3-31	Comparison of the FE predicted mode shapes and natural frequencies (left) with those found using EMA (right), blue lines denote the undeformed condition while red denotes the deformed shape	79
Figure 3-32	Analysis of the displacements and stresses in the probe horn	81
Figure 3-33	Elevation view of the 5 section design. Each section shown in a different colour	82
Figure 3-34	Analysis of the displacements and stresses in the initial booster horn design	83
Figure 3-35	Analysis of the displacements and stresses in the modified booster horn design	84

Figure 3-36	Analysis of the displacements and stresses in the final booster horn design	84
Figure 3-37	Comparison of the FE predicted mode shapes and natural frequencies (left) with those found by EMA (right)	85
Figure 4-1	Contour plots of the pressure generated by a 20 kHz ultrasonic probe in cavities of depth (a) $0.25 \lambda$ (b) $0.5 \lambda$ (c) $0.75 \lambda$ (d) $1.0 \lambda$ . Pressure magnitude is shown in $\text{N/m}^2$	89
Figure 4-2	Pressure variation through fluid cavity depth using 20 kHz probe horn for various fluid depths $0.25 \lambda$ (green), $0.5 \lambda$ (black), $0.75 \lambda$ (blue) and $1.0 \lambda$ (red)	90
Figure 4-3	Pressure distribution through fluid cavity for depths of (a) $0.75 \lambda$ and (b) $1.0 \lambda$	91
Figure 4-4	Contour plot of the pressure field generated by the three radial modes of vibration R0 (top), R1 (middle) and R3 (bottom) alongside graphs showing the pressure distribution through the cavity	93
Figure 4-5	Pressure through the fluid generated by R0 mode radial horns with varying inner diameters	94
Figure 4-6	Photographs of the cavitation field generated by the R0 <sub>ID30</sub> radial mode horn (a), the R3 <sub>ID50</sub> mode radial horn (b), the R0 <sub>ID50</sub> horn (c) and the probe horn (d)	97
Figure 4-7	Aluminium foil specimens subjected to cavitation by R0 <sub>ID30</sub> mode radial horn with 0.5 gain booster attached for 2 s (top row), 4 s (2 <sup>nd</sup> row) 6 s (3 <sup>rd</sup> row), 8 s (4 <sup>th</sup> row) and 10 s (bottom row) at 1.5, 2.3, 3.8 and 7.3 $\mu\text{m}$ ultrasonic amplitudes	99
Figure 4-8	Aluminium foil specimens subjected to cavitation by R0 <sub>ID50</sub> mode radial horn for 2 s (top row), 4 s (2 <sup>nd</sup> row) 6 s (3 <sup>rd</sup> row), 8 s (4 <sup>th</sup> row) and 10 s (bottom row) at 1.8, 2.5, 3.7 and 4.8 $\mu\text{m}$ ultrasonic amplitudes	101
Figure 4-9	Aluminium foil specimens subjected to cavitation by R0 <sub>ID30</sub> mode radial horn with 2.0 gain booster attached for 2 s (top row), 4 s (2 <sup>nd</sup> row) 6 s (3 <sup>rd</sup> row), 8 s (4 <sup>th</sup> row) and 10 s (bottom row) at 1.3, 1.7, 2.9 and 5.7 $\mu\text{m}$ ultrasonic amplitude	103
Figure 4-10	Photographs of chemiluminescence of luminol solution for pH12 [(a), (c), (e), (g)] and pH9.5 [(b), (d), (e), (h)] for the R0 <sub>ID30</sub> mode radial horn [(a), (b)], the R3 <sub>ID50</sub> mode radial horn [(c), (d)], the R0 <sub>ID50</sub> mode radial horn [(e), (f)] and the probe horn [(g), (h)]	106
Figure 4-11	Chemiluminescence of the probe horn at pH12 with adjusted brightness	107
Figure 4-12	Comparison of aluminium foil tests using the R0 <sub>ID30</sub> horn at 1.5, 2.3, 3.8 and 7.3 $\mu\text{m}$ after 10s sonication	109
Figure 4-13	Comparison of photographs, chemiluminescence and FEA predictions for the R0 <sub>ID30</sub> mode radial horn, the R3 <sub>ID50</sub> mode radial horn and the probe horn	110
Figure 5-1	Sketch of experimental set-up. (1) 20 kHz Ultrasonic Transducer, (2) Radial Horn, (3) Radial horn cavity (volume of fluid containing bacteria), (4) Ice packing, (5) Plastic insert, (6) Rubber gasket, (7) Aluminium mounting flange, (8) Tuned mounting	114

---

	cylinder	
Figure 5-2	Temperature increase of R0 <sub>ID30</sub> mode radial horn and liquid at different input vibration amplitude	118
Figure 5-3	Temperature increase of R3 <sub>ID50</sub> mode radial horn and liquid at different temperatures and power levels, with and without the booster horn	118
Figure 5-4	Temperature increase of R0 <sub>ID50</sub> mode radial horn and liquid at different input vibration amplitude	119
Figure 5-5	Bacterial inactivation using the R3 <sub>ID50</sub> radial horn at vibration input amplitudes of 1.3, 1.7, 2.5, 3.0 and 5.7 $\mu\text{m}$ using <i>E. coli</i> K12	121
Figure 5-6	Bacterial inactivation using the R0 <sub>ID30</sub> radial horn at vibration input amplitudes of 1.5, 2.3, 3.8 and 7.3 $\mu\text{m}$ using <i>E. coli</i> K12	122
Figure 5-7	Bacterial inactivation using the R0 <sub>ID50</sub> radial horn at vibration input amplitudes of 1.8, 3.7 and 4.8 $\mu\text{m}$ using <i>E. coli</i> K12	123
Figure 5-8	Bacterial efficacy of the R0 <sub>ID30</sub> , R3 <sub>ID50</sub> , R0 <sub>ID50</sub> and probe horns at an intensity level of 14.8, 3.2, 2.6 and 12.6 $\text{W}/\text{cm}^3$ respectively using <i>E. coli</i> K12	124
Figure 5-9	Effect of initial concentration on bacterial efficacy of the R0 <sub>ID30</sub> , R3 <sub>ID50</sub> and probe horn on <i>E. coli</i> K12	125
Figure 5-10	Bacterial efficacy of the R3 <sub>ID50</sub> mode radial horn on <i>S. aureus</i> 24 for exposure times up to 5 min, samples taken at 30 s intervals	126
Figure 5-11	Bacterial efficacy of the R3 <sub>ID50</sub> mode radial horn on <i>S. aureus</i> 24 for exposure times up to 30 min, samples taken at 5 min intervals	126
Figure 5-12	Relationship between the D-value and power input	128
Figure 6-1	Flow through design for the radial horn	134
Figure 6-2	Deformed mode shapes for the radial horn flow through device (a) R0, (b) R1, and (c) R3 modes	135
Figure 6-3	Continuous flow experimental arrangement	136
Figure 6-4	Bacterial inactivation of <i>E. coli</i> K12 using the continuous flow set up for vibration input amplitudes of 2.3 and 7.6 $\mu\text{m}$	137
Figure 6-5	Bacterial inactivation of <i>S. aureus</i> 24 using the continuous flow set up	137



---

## Chapter 1 – Introduction

---

### ***1.1 History of bacterial inactivation***

In the Middle Ages, illness and disease were rife. Many millions died from what are now preventable or curable illnesses. During the second cholera outbreak of 1829-1851, it was often safer to drink ale than water. It was only in 1849 when John Snow went against the widely accepted miasma theory of disease, and hypothesised that the mechanism for the spread of disease was contaminated water, that germ theory began to gain acceptance [1]. Several years later Robert Koch and Louis Pasteur separately confirmed germ theory [2]. At around the same time, mechanisms were being developed to make food and drink products microbiologically safe for human consumption. This work was instigated by Pasteur who developed the pasteurisation method for milk and wine in 1862 [3]. The widening acceptance of germ theory was the beginning of the fields of microbiology and epidemiology and since then there has been investigations into other mechanisms that can be used to make a product microbiologically safe including heat, chemicals (particularly chlorine), radiation (particularly UV) and ultrasound.

#### **1.1.1 Pasteurisation**

Pasteurisation is a method of heat treatment for liquid food products. The nutritional value of these food products deteriorates significantly with exposure to high temperatures and so the use of boiling is inappropriate. There are currently two available standards for the pasteurisation of food products for human consumption, the high temperature short time (HTST) and ultra high temperature (UHT) methods. The aim of pasteurisation is not to sterilise the product but to reduce the number of

pathogenic and spoilage bacteria significantly, typically a 5 log reduction in bacterial numbers is required. The HTST method requires that the fluid be heated to 63 °C and held there for at least 30 minutes before being rapidly cooled to around 4 °C. The UHT method requires the fluid to be heated to 138 °C for at least 2 seconds before being cooled. The pasteurisation method is normally used for the treatment of dairy products such as milk, cream, and cheese but can also be used for the treatment of fruit juices. Pasteurisation of dairy products is important to ensure they are fit for human consumption and can prevent tuberculosis, diphtheria, polio, salmonellosis, strep throat, scarlet fever and typhoid fever. However, the temperatures used during the process causes some protein denaturation to occur which lowers the quality of the product [4]. There are also potential health benefits that are removed with the pasteurisation process due to the destruction of particular enzymes, 'friendly' bacteria, and immunoglobulins which aid the immune system [4]. Also, there is some concern that there are pathogenic bacteria that are resistant to the pasteurisation process and can find their way into the human food chain. The recent discovery of *Mycobacterium avium paratuberculosis* (MAP) in pasteurised milk samples which is suspected of causing Crohn's disease has caused concern amongst health officials who are now re-evaluating the pasteurisation process [5, 6]. It is therefore necessary to strike a balance between the necessity for a product to be microbiologically safe whilst maximising the nutritional value of the product. Treatment of water to standards suitable for human consumption has more available options than that of liquid food products described above. Boiling of water is probably the most simple of these and has been used to disinfect water for many centuries. Chlorination, Ozone and UV radiation are other popular and well established mechanisms for bacterial inactivation.

### **1.1.2 Chlorination**

Chlorine was first discovered in 1774 by a Swedish pharmacist by the name of Carl Wilhem Scheele but its germicidal properties were not discovered until 1846 when Ignaz Semmelweis, head of Vienna General Hospital's First Obstetrical Clinic, introduced hand washing with chlorinated lime solutions to combat the rampant mortality of child bed fever [7]. His measures brought the mortality rate from 10-35 % to below 1 %. Since then the use of chlorine as a germicide has spread worldwide and is currently a cheap and effective method for ensuring water is microbiologically safe. It

has also been reported as “probably the most significant public health advance of the millennium” by Life magazine [8]. The bactericidal mechanism of chlorine is caused by the chemical reaction that takes place when it is combined with water. This reaction causes hypochlorous acid and hypochlorite ions to be created. The hypochlorous acid causes the vast majority of the bactericidal effect with the hypochlorite ions causing less than 1 % of the kill [9]. The chlorine molecule easily enters micro-organisms through their cell walls and kills the organisms by destroying several of the vital components required for the organism to survive. This is an extremely quick process and *Escherichia coli* cells have been shown to become inactivated within 100 ms of exposure to hypochlorous acid [9]. The major advantages in using chlorine to achieve a microbiologically safe product are that it is quick to act, cheap and efficient at destroying most pathogens present. Also, since low chlorine doses are not harmful to humans, leaving some residual chlorine in the finished product will mean infection after treatment can be significantly reduced. Disinfection by chlorination can, in certain circumstances, cause some problems. Chlorine can react with organic products in the water to produce compounds that are potentially carcinogenic [10]. It has also been shown that fresh water bacterial strains are becoming more resistant to the chlorination process [11], indicating that in future it will be less effective if the bacteria can evolve a resistance to the treatment. Furthermore, chlorine has little or no effect on the viability of cryptosporidium cysts [12], a pathogenic organism found in water courses such as rivers and streams. These organisms currently require to be filtered out using slow sand filtration or inactivated using ozone or ultraviolet light.

### **1.1.3 Ultraviolet Light**

Ultraviolet light occurs at wavelengths between 4 nm and 400 nm, below visible light in the electromagnetic spectrum. The most lethal wavelengths to organisms are the UV-C spectrum between 200-280 nm with a peak germicidal efficiency occurring at 264 nm [13, 14]. Ultraviolet light in the UV-C spectrum is not encountered naturally on Earth due to the atmosphere absorbing this spectrum of light before reaching the surface and can only be created using specially designed lamps. The germicidal effect of ultraviolet light was first discovered by chance in 1877 by Downes and Blount [15] who observed bacterial growth in a bottle held in the shade but not in the sunlight and correctly concluded that an aspect of the sunlight caused an inhibition to bacterial growth.

Research over the next 30 years concluded it was the ultraviolet spectrum of sunlight that caused a germicidal effect. In 1903 Neils Finsen was awarded a Nobel Prize for his work in treating tuberculosis of the skin with ultraviolet light [16]. Ultraviolet light disrupts the DNA of microbial organisms thus causing their death or removing their ability to replicate. UV-C is an extremely efficient method of reducing the bacterial load of a product and an organism needs only to be exposed to the light for a few seconds before it is rendered inactive. Advantages of this system include its effectiveness in permeable fluids, its relatively low cost, and ease of installation and maintenance. It is also effective in the inactivation of cryptosporidium due to the UV light targeting the DNA and does not require the organism to absorb a molecule like chlorine. There are several drawbacks in using ultraviolet radiation. Firstly, the fluid in which the device is operating must be permeable to UV light, otherwise the penetration of the UV light will be minimal and low bacterial numbers will be inactivated. Secondly, if the product is not homogeneous and contains significant numbers of suspended solids (say, orange juice with pulp) then this will severely inhibit the use of ultraviolet light to make the product microbiologically safe. Finally, the product has no residual inactivation capacity, unlike chlorination, thus the product must be transported aseptically to prevent the risk of infection after treatment.

#### **1.1.4 Ozone**

Ozone ( $O_3$ ) was discovered initially by the Dutch chemist Van Marum who noticed a characteristic smell around his electrifier but did not pursue it further [17]. Later, Christian Schönbein further investigated Van Marum's observations and in 1839 declared this was caused by a distinct chemical substance he called ozone [18]. Further tests to elucidate the nature of this chemical substance were carried out by several researchers and in 1845, de la Rive discovered ozone could be produced by arcing pure dry oxygen coming to the conclusion that it was a form of allotropic oxygen [18]. This was then confirmed by several other researchers [18]. It was not until 1865 that the molecular form of ozone was unravelled by Soret whose experiments concluded that ozone consisted of three bonded oxygen molecules ( $O_3$ ) [18]. Ozone is formed naturally in the Earth's atmosphere through a reaction between  $O_2$  and ultraviolet radiation and protects its inhabitants from harmful ultraviolet radiation from the sun by effectively converting the ultraviolet radiation into heat energy.



It had also been discovered through the various research studies into ozone that it is a very reactive substance which has caused some complications for experimental work. Ozone is an extremely powerful oxidising agent, only surpassed by fluorine [19], and will aim to lose a single oxygen atom such that it may reach its more stable state of diatomic oxygen,  $\text{O}_2$ . Early experiments on the use of ozone as a germicide were carried out in France by de Meritens in 1886 [20]. Since then ozone has been found to be effective against bacteria, viruses, fungi, and moulds [21]. Reports on the use of ozone to treat wounds have been cited since World War I. Water treatment plants utilizing ozone to inactivate bacteria and viruses have been widely developed in Europe and Asia (less so in America) with the first ozone water treatment plants constructed in Germany (Paderborn and Weisbaden in 1902 and 1903). The mechanism of disinfection by ozone is cell lysis. Unlike chlorine which must be taken up by the organism through diffusion, ozone causes the disruption of the cell wall through lipid peroxidation (i.e. free radicals ‘steal’ electrons from the cell membrane causing damage to the cell). Once inside the cell the ozone proceeds to oxidise, and hence destroy, DNA, RNA, enzymes and proteins essential to cell survival [22]. Using ozone to achieve a microbially safe product has advantages in that it leaves no residual smell or taste, unlike chlorination, and it is an extremely effective germicide; much lower doses are required for ozone treatment compared to chlorine and organisms such as cryptosporidium are much more susceptible to ozone than chlorine. Unlike chlorination, ozone will not leave a residual disinfectant and so the treated water must be transported aseptically to the end user for consumption. Unfortunately, ozone has also been shown to produce small amounts of the suspected carcinogen Bromate [19]. Ozone is well established in the microbiological treatment of water, however there seems to be little research or application of this technology to liquid food products such as milk and fruit juices.

### **1.1.5 Ultrasonic Vibration**

Ultrasonic vibrations are generally defined as mechanical vibrations having a frequency greater than the upper limit of the human hearing range, about 20 kHz. Ultrasound has

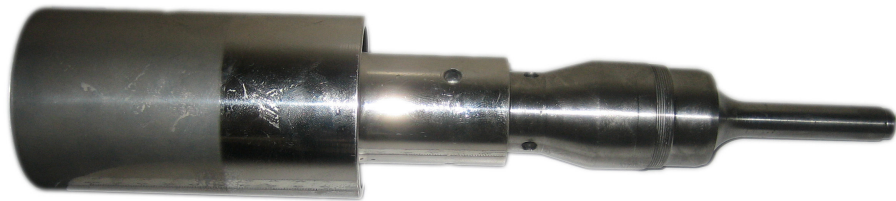
been utilised in nature by animals such as bats and dolphins that use it as their primary sensory function to visualise their environment and locate prey, this is known as echolocation. The ability to create mechanical ultrasonic vibrations came with the discovery of the piezoelectric effect by Pierre and Jacques Curie in 1881 [23] and the first practical application came during World War I with the development of sonar for the detection of submarines. Since then its use as an imaging tool has been extended to medical diagnostics as well as to non-destructive testing of materials and structures. Biologically, ultrasound is safe in low power applications, however as the power is increased some interesting effects begin to take place. At high power, ultrasonic vibrations can cause cavitation, a process whereby bubbles in the fluid are formed and subsequently collapse violently. The destructive power of ultrasound was first observed by Langevin who observed the killing of fish subjected to a beam of ultrasound [24]. Professor R. W. Wood who worked alongside Langevin described his work with high power generators thus;

*“At the arsenal at Toulon I witnessed many of the experiments with the high power generators. One was mounted in a large wooden tank filled with sea water, and when the Poulsen arc was started and the frequency adjusted for resonance the narrow beam of supersonic waves shot across the tank causing the formation of millions of minute air bubbles and killing small fish which occasionally swam into the beam. If the hand was held in the water near the plate an almost insupportable pain was felt, which gave one the impression that the bones were being heated.”*

This was to be the start of the field of high power ultrasonics. In 1926, Alfred Loomis and Prof. Wood expanded upon Langevin’s work to elucidate the chemical and biological effects of high power ultrasound and were the first researchers to create an ultrasonic horn by drawing a glass tube to a tapered point to concentrate the ultrasonic energy [24]. The use of cavitation in nature to stun or kill prey has recently been demonstrated in the closure of shrimp claws [25]. It has also been suggested that dolphins can focus their ultrasound to stun or kill their prey [26]. Also, the US military has recently been reprimanded for the use of very high power sonar which was

responsible for the deaths of several whales in the area where it was deployed [27]. In this case the deaths were due to gas embolisms in the animal's ear however it is likely this was caused by a decompression sickness like syndrome rather than pure cavitation. In the case of micro-organisms, the mechanism of cell death is through the exposure to high pressure shock waves developed upon the collapse of a cavitation bubble.

Since Langevin's initial studies, there have been some attempts to scale up and commercialise systems using ultrasound for the bacterial inactivation of waste water, dairy products and fruit juices. The majority of the systems currently used at the laboratory scale are based on a longitudinally vibrating probe device such as the one shown in Figure 1-1.



**Figure 1-1 Ultrasonic probe horn**

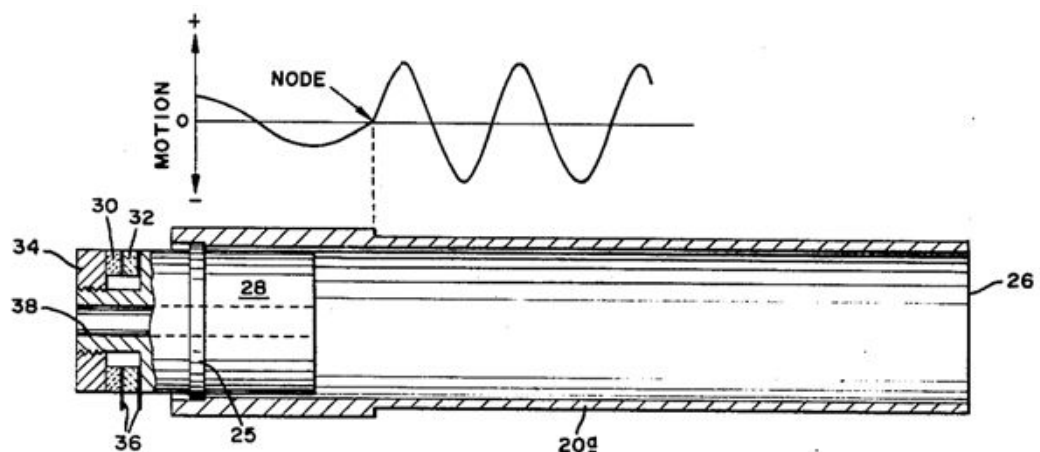
This type of system is ideal for treating small volumes of fluid in a batch process and has been used for many years. In the processing of liquids under no flow conditions using ultrasound there has been very little innovation from the probe system. This is probably due to the efficiency of the system at the laboratory scale. However, due to the nature of the cavitation field generated by these devices they are not particularly suitable when there is a continuous flow of fluid to be treated. Treatment of flowing fluids is the application area where most innovations have come from and there are several patents outlining ideas to solve the problem of continuous flow processing with ultrasound. A selection of these patents and commercial systems are examined to give an overview of what is available and the ideas which have so far been presented.

The majority of the work presented in this thesis focuses on the use of ultrasonic horns vibrating in a radial mode similar to that shown in Figure1-2.



**Figure1-2 – Radial horn with attached ultrasonic transducer**

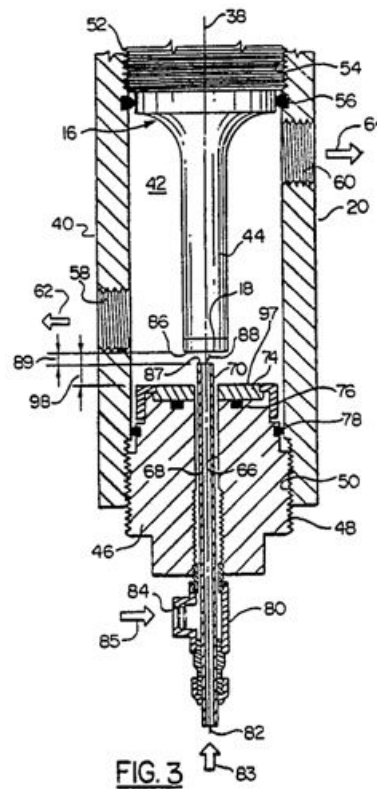
These modes involve the structure having a number of nodes around the circumference of the structure which define the mode shape. For example, the fundamental mode, R0, vibrates in a form whereby the diameter gets uniformly smaller and larger throughout the cycle. The third radial mode, R3, on the other hand has six nodes equally spaced around the circumference. These modes are discussed in more detail in Chapter 3, section 3.4.1. One of the earliest patents for using radial mode ultrasonic vibrations for continuous processing was obtained in 1977 by Branson Ultrasonics Corporation for “sonic or ultrasonic processing apparatus” (Figure 1-3). The device consisted of a tubular resonator connected at the node point of a transducer vibrating axially. At the node point of the axial transducer the majority of the motion is in the radial direction which allows excitation of the tubular section. The tubular section is designed to resonate radially at the frequency of the axial transducer.



**Figure 1-3 - Sonic or ultrasonic processing apparatus**



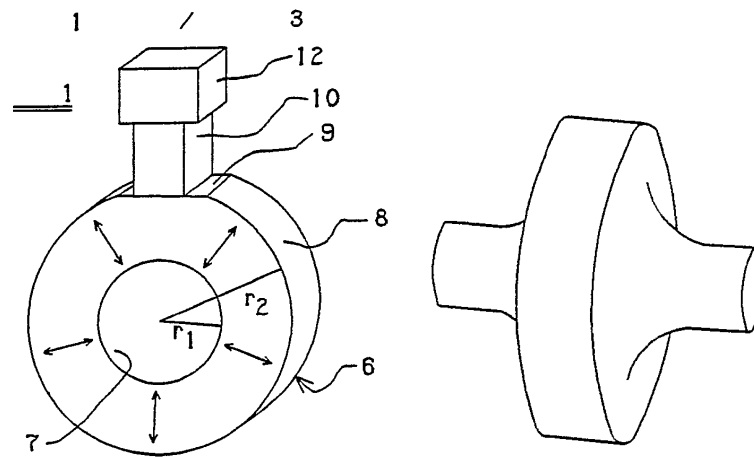
In 1990, Heat Systems Inc. obtained a patent (UK patent GB 2,236,959 A) for a system of treating a fluid with ultrasound in a flow through process. This system, shown in Figure 1-4, was an adaptation of the popular probe device used in batch operations. It involved enclosing the probe within a cell and injecting the fluid through a tube into the centre of the cavitation zone with the tip of the probe placed only millimetres from the exit of the tube. The processed fluid would exit the cell from an outlet tube.



**Figure 1-4 –Heat Systems Inc. patented system**

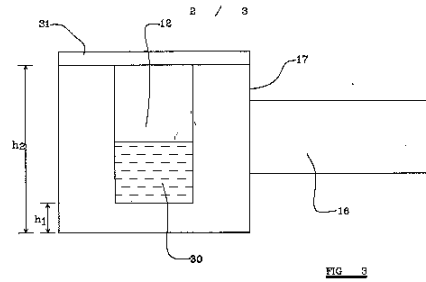
Three years later FFR Ultrasonics filed a patent (UK patent GB 2,285,142 A) for a device which most similarly resembles the radial ultrasonic device used in these studies. The device, shown in Figure 1-5, is a radially vibrating annular horn used for the purpose of fluid processing. In the patent application FFR claim that this type of device has advantages over the traditional probe system. They cite that the probe systems have a practical upper limit on the energy that can be transferred to the fluid (30-50 Watts per litre). Above this level decoupling and the generation of vapour at the probe/ fluid interface can occur preventing further increases in power from being transferred to the fluid. It is claimed that such a device as described in the patent can overcome these

issues. The patent also describes methods for using the device in a continuous flow operation. In 2004, an independent inventor (Piers Benedict Clark) filed a patent in the US (US 2004015499A1) for an ultrasonic treatment device similar to that of FFR Ultrasonics. The patent cites issues with material in the sewage causing blockages in the system and proposes an improvement by using a funnel to direct the flow through the centre of the cavity, thus allowing the vast majority of the fluid to be treated by the high intensity cavitation field generated in the centre of the ultrasonic devices.



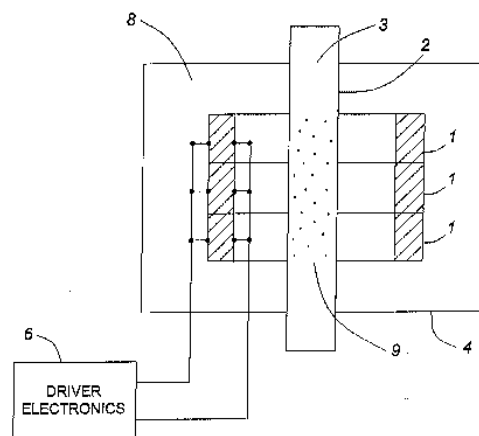
**Figure 1-5 - Radially vibrating annular horn**

In 2001, FFR Ultrasonics filed another patent for a “Vessel shaped/dimensioned to concentrate ultrasound vibrations in the centre of well” (UK patent 2,374,560 A). The device described is similar to that described in their 1990 patent above. The major difference between the two is that the device described in this patent has a solid base and the fluid is contained in the centre of the device (Figure 1-6). This patent cites the concentration effect of radially vibrating horns as the primary advantage in delivering higher energy intensities than is available with the probe device or ultrasonic cleaning baths. Though this device does not allow for continuous flow, it is similar to the device used in this study and is cited here for completeness.



**Figure 1-6 - Vessel shaped/dimensioned to concentrate ultrasound vibrations in the centre of well**

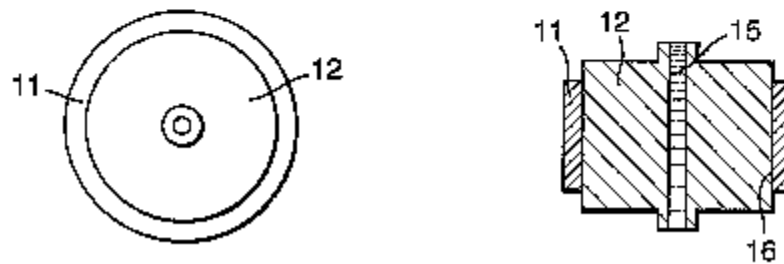
In 1991, the Canadian Government applied for a patent for a “flow through device for the ultrasonic destruction of micro organisms in fluids” (European patent EP 1,254,669 A1). The patent describes a device to treat contaminated fuel onboard a ship, though it could be applied to any fluid containing undesirable microbes. This device (Figure 1-7) incorporates a pipe through which the contaminated fluid is fed, ceramic transducers through which the vibrations are applied, and a transmission fluid. The inventors had discovered that applying the transducers directly to the pipe caused serious erosion problems and to overcome this, the ultrasonic vibrations were applied to a transmission fluid under enough pressure to suppress cavitation. The vibrations were then transmitted through the fluid into the pipe containing the fluid to be processed. Since the fluid to be processed is not under significant pressure, cavitation occurs due to the vibrations and the microbial contaminants are inactivated.



**Figure 1-7 - flow through device for the ultrasonic destruction of micro organisms in fluids**

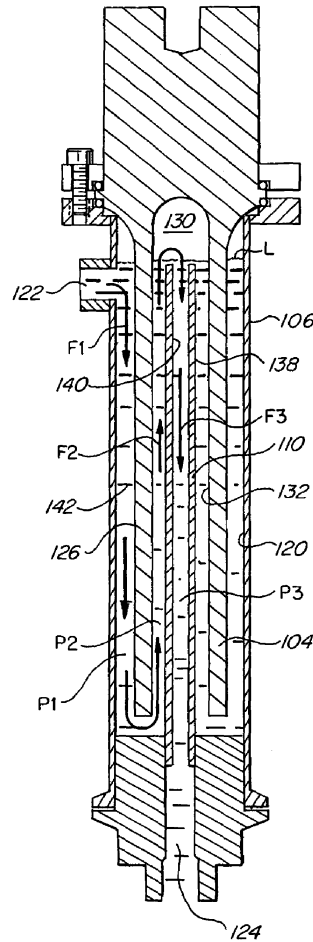
In 2004, the UK government submitted a Canadian patent (CA 2538028 A1) for a cylindrical transducer for the purpose of causing bacterial inactivation. This patent

(Figure 1-8) describes a device aimed at inactivating small volumes of bacteria at much higher frequencies (298 kHz) than used in this study (20 kHz). The patent cites the shortcomings of current devices in their bulkiness and heat generation which is not ideal for some forms of microbial analysis. The device consists of a steel cylinder through which the fluid to be treated is passed. Attached to the steel cylinder is a piezoceramic transducer operating at the desired frequency in a radial mode of vibration. The steel cylinder allows significant heat dissipation, thus allowing for cavitation to take place in the fluid without the fluid heating significantly during processing.



**Figure 1-8 - Cylindrical transducer for the purpose of causing bacterial inactivation**

In 2006, the Battelle Memorial Institute obtained a patent (US 7,022,505 B2) for a continuous flow method of inactivating bacteria using MHz ultrasound. Interestingly, this patent cites the inactivation of bacteria without the process of cavitation taking place and thus gains an advantage of extended product life, due to the lack of erosion normally associated with processes using cavitation. An embodiment of the invention is shown in Figure 1-9.



**Figure 1-9 - continuous flow method of inactivating bacteria using MHz ultrasound**

Despite all the patents and commercial systems available there is relatively little published work verifying the claims made in the patents which may explain why there is a slow take up of this technology by industries that could use it to their benefit.

## **1.2 Aims and objectives**

The work reported in this thesis investigates the use of high power ultrasonic devices for the bacterial inactivation of suspensions. The research focuses on the use of radially vibrating devices operating at 20 kHz and also uses a traditional probe type device for comparison. The hypothesis of the research is that an ultrasonic device used for the purpose of bacterial inactivation of fluid mediums will be more effective using an ultrasonic device vibrating radially compared to traditional longitudinally vibrating probe devices. The tuned radial mode is the R0 mode shape. This mode is characterised by a vibration response where the diameter of the radial horn expands and contracts

uniformly. It is hypothesised that the ultrasonic energy imparted to the fluid using the radial horn will be concentrated in the centre of the fluid cavity and cavitation will take place causing significant bacterial inactivation. The benefits of using such a system would include the significant reduction in wear from the device and ability to easily incorporate it into conventional continuous flow processes. Currently the use of probe devices for bacterial inactivation causes cavitation to occur at the probe tip where the vibration amplitudes are the greatest. This causes significant erosion of the horn tip which is usually made of titanium to give a better working life, and these tips must be replaced on a regular basis. It is hypothesised that since the radial horn concentrates the energy in the centre of the fluid cavity away from the vibrating face that the issue of wear caused by cavitation will be significantly reduced. In order to investigate these hypotheses, radial horns were designed using finite element analysis and were then manufactured. Experimental modal analysis was then carried out on the horns to confirm their modal characteristics. Due to the design of the radial horns, the fundamental (R0), first (R1) and third (R3) radial modes occur within a small frequency band. This makes it beneficial to investigate the influence of mode shape on the bactericidal effect of radial horns, thus radial horns vibrating in R0 and R3 modes have been investigated for their bactericidal efficacy of *Escherichia coli* K12 and *Staphylococcus aureus* strain 24. The use of a commercial probe device (Jencons VCX 400 with standard 13mm titanium tip) for bacterial inactivation has also been investigated such that comparisons between the two systems may be made. Furthermore, the fundamental aim of the research is to incorporate these devices in continuous flow operations to inactivate bacteria without the need for separate pre and post processing stages. The radial horn vibrating in the R0 mode was redesigned to allow for a continuous flow operation and parameters such as flow rate, vibration input and bacterial species have been investigated.

This research has made several contributions to the body of knowledge in the field. Firstly, the pressure fields generated by radial mode ultrasonic devices vibrating in different modes have been determined using FEA with investigations into the effect of geometry and amplitude. Verification of these models in the form of visualisation studies adds to the body of research currently available. Further, this research has shown

that radially vibrating ultrasonic devices can be more effective in enacting bacterial inactivation in fluid media than a traditional probe device. A preliminary study on the use of these devices in continuous flow environments paves the way for further detailed analysis to improve this system.

---

## Chapter 2 - Literature Review

---

### **2.1 Introduction**

It has been known for a long time that sound waves have the ability to kill living organisms; this was demonstrated in World War II where it was observed that SONAR systems were killing fish [28]. Research was carried out to determine the cause of these deaths and a phenomenon known as cavitation was identified.

The use of ultrasound to inactivate bacterial cells has been of interest for many years. Initial research indicated that it was not a cost effective method of inactivating cells [29], however, with the recent development of more efficient transducers, interest in this area has gathered momentum. Alternative methods for reducing the bacterial load of liquid food products as well as waste water treatment are being sought to improve the quality of the end product. Inactivation methods in the food processing industry rely heavily on heat inactivation through processes such as pasteurisation, while the water industries rely on the introduction of chemicals to inactivate cells. These methods are satisfactory, however, they do reduce the quality of the end product. Exposure to high temperatures and chemicals (particularly chlorine) causes detrimental effects to the taste of the end product. The use of chemicals is also highly regulated, with legislation on their use becoming tighter. It has also been shown that bacterial cells are becoming more resistant to these treatments [30] or that these treatments may not be as effective under certain conditions. For example, Grant and Klijn [31, 32] have found that *Mycobacterium avium paratuberculosis*, found in cows milk, can be resistant to pasteurisation processes if found in large concentrations. Thus, there is a need for the development of new technologies which do not rely on these inactivation mechanisms. Maintaining a high quality product that is microbiologically safe requires that the minimum amount of heat and chemical processing is introduced, while at



the same time ensuring bacterial numbers are kept within acceptable limits. Ultrasonic processing is one way to achieve this outcome through non-thermal inactivation.

## **2.2 Ultrasonic Devices**

High frequency mechanical vibrations can be created most efficiently using two types of transducer: the magnetostrictive transducer and the piezoelectric transducer, each having their own advantages and drawbacks.

In the early applications of ultrasound in industry, magnetostrictive transducers were more popular for the generation of high power ultrasonic vibrations. Magnetostriction is a property found in materials, such as cobalt, iron, nickel and ferrite, which causes them to physically contract in the presence of a strong magnetic field. When the magnetic field is switched off the material returns to its original shape. Thus, by alternating the electromagnetic field at the desired frequency these materials vibrate at that frequency. Magnetostrictive transducers have several advantages; they are robust and durable and can provide large driving forces, ideal for industrial applications. However, there is an upper frequency limit for these transducers of about 100 kHz, since the contracting material cannot respond fast enough to the magnetostrictive effect. Also, these devices generate considerable heat and thus require to be cooled considerably if in operation for a considerable length of time.

The piezoelectric effect, discovered by the Curie brothers, led to the development of ultrasonic transducers based on this effect. They discovered that materials such as quartz and topaz expand or contract when subjected to an applied voltage, returning to their original state when the voltage is removed. Thus, by applying an alternating voltage at the desired frequency, these materials vibrate at that frequency. Early transducers were based on quartz, but quickly moved to ceramics containing

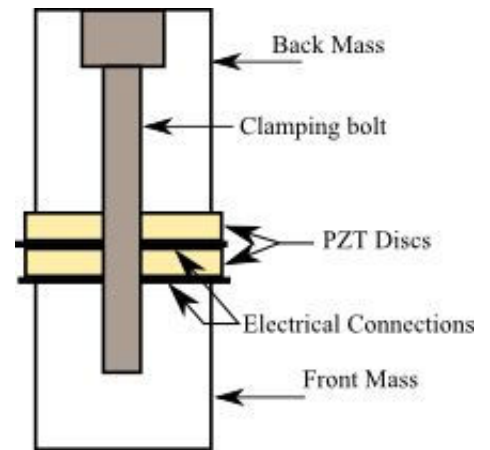


Figure 2-1 - Piezoelectric Transducer

piezoelectric materials due to the fragility and poor machinability of quartz. Transducers today are commonly made from lead (plumbum) zirconate titanate (PZT) due to the greater piezoelectric coefficients and electromechanical coupling compared to quartz. These transducers normally consist of several PZT annular discs clamped between two metal blocks (Figure 2-1). This configuration protects the PZT discs and the metal blocks also act as a heat sink to prevent overheating, though during extended operation even these transducers will require a more effective cooling mechanism. Piezoelectric transducers can produce amplitudes in the order of 10-20 microns and can, depending on their dimensions and construction, work at much higher frequencies than magnetostrictive transducers. In fact, the upper limit of frequency is currently not limited by the transducer but by the ability to generate electrical signals of higher frequencies.

The practical use of ultrasonic vibrations can be split into two distinct areas: diagnostic ultrasound and power ultrasound.

Diagnostic ultrasound normally uses the higher ultrasonic frequencies in the MHz range at significantly lower amplitudes. This has been successfully used in the medical industry to monitor the development of a foetus within the womb [33]. In the construction industry it has been widely used to detect flaws and cracks hidden within structures using non-destructive testing (NDT) [34].

Power ultrasound uses the lower ultrasonic frequencies usually between 20-100 kHz, at high amplitudes to cause different phenomena depending on the application. Power

ultrasound has been used successfully for many industrial applications such as machining [35], cutting [36], cleaning [37], casting [38], extruding [39], and welding [40], where benefits in improved performance, lower energy usage or faster processing times have been achieved.

### **2.3 Cavitation**

When ultrasonic vibrations of high amplitude are passed through a liquid, then a phenomenon known as cavitation can occur. Cavitation is defined as the formation and subsequent life of bubbles in a liquid. These bubbles are formed and grow when the liquid is put in a significant state of tension. Liquids, though unable to support shear stresses, can support compressive stresses and for short periods, tensile stresses. When a pressure wave is applied to a liquid it undergoes a compression and rarefaction cycle, and during the rarefaction half-cycle the pressure in the liquid becomes negative. If the magnitude of this pressure is high enough, the liquid can effectively be ripped apart causing voids or bubbles to be created [41]. Frenkel [42] carried out a theoretical analysis of the pressure required to overcome the attractive molecular forces and found that liquids should be able to support tensile stresses in the order of  $3 \times 10^9$  -  $3 \times 10^{10}$  Pa. A separate analysis by Mason [43], using an idea based on equilibrium, finds a pressure of approximately  $1.5 \times 10^8$  Pa is needed to make a void greater than van der Waals' distance in ultrapure water. In practice, however, the maximum tension that has been achieved has been in the order of tens of MPa [44] using ultrafiltration and purification techniques. Normal household tap water has a threshold closer to 0.1-0.2 MPa [45]. The huge discrepancy between the theoretical and experimental results can be explained by using the example of solids. In a solid medium the theoretical stress required to rupture a material is very much greater than that found experimentally due to flaws within the material such as micro cracks, grain structure, or contaminants within the material. These flaws cause local stresses in parts of the material to be greater than the theoretical limit whilst globally the stress is far below this limit thus the material starts to fail at these points of high stress and hence this is the reason materials fail at much lower stresses than anticipated by molecular theory. The same analogy can be applied to fluids. Microscopic particles and bubbles dissolved in the fluid or microscopic particles, such as minerals, acting as nucleation sites [46], reduce the tensile strength significantly. Abramov [45], however, claims that there is no sound theoretical basis for the presence of microscopic bubbles dissolved in fluid, as large bubbles will rise to the surface through buoyancy and be dispelled whilst the surface tension of small bubbles will

not be able to withstand the fluid pressure and hence be crushed. Thus, there is still some debate on this issue.

There are many factors that affect cavitation, its development and subsequent life. Most of these factors are either associated with the applied sound field or the properties of the liquid being used.

As the frequency of the applied sound field increases, the production of cavitation bubbles becomes more difficult to achieve due to the reduced time available in the rarefaction cycle of the acoustic wave. For example, at 20 kHz the rarefaction cycle lasts 25  $\mu\text{s}$  whilst at 20 MHz the rarefaction cycle only lasts 0.025  $\mu\text{s}$ . Thus the intensity of the sound field will need to be greater at higher frequencies to ensure the liquid cohesive forces are overcome in the shorter time period [47].

The most significant fluid properties that influence the production of bubbles are ambient pressure, temperature and viscosity. If the pressure of the fluid is raised then it will require a greater amplitude of vibration in order to create a negative pressure within the fluid. If, however, the temperature of the fluid is raised, then the threshold for the onset of cavitation has been found to decrease [47]. This may be due to the lowered surface tension and viscosity in the fluid at higher temperatures or it may be due to an increase in the liquid vapour pressure. Since it is necessary for the negative pressure to overcome the liquid cohesive forces, an increase in these forces will increase the threshold of cavitation [47]. Thus an increase in viscosity will cause an increase in the cavitation threshold. Mason and Lorimer [48] studied the effect of viscosity on the cavitation threshold and found that although there was a significant effect, it was not as dramatic as expected. They found a ten-fold increase in viscosity increased the cavitation threshold by only 30%.

### **2.3.1 Historical Overview**

The cavitation phenomenon was first investigated by Rayleigh in 1917 when ship propellers were under-performing [49]. His initial investigations yielded formulae that are still useful today which describe the time for a bubble to collapse and the pressure generated upon collapse. Plesset [50] later developed Rayleigh's initial work to derive an equation for the general motion of a spherical bubble in a liquid under external pressure.

Further work was then carried out by Noltingk [51], Neppiras [52], and Poritsky [53] to derive an equation that describes accurately the behaviour of a bubble for all types of stable cavitation, and also for transient cavitation bubbles where the speed of bubble collapse does not exceed 1/5 of the speed of sound of the fluid [54]. The difference between stable and transient cavitation is defined by the number of cycles the bubble undergoes in the sound field. Transient cavitation bubbles last only a few acoustic cycles before collapsing violently, while stable cavitation bubbles may be present in the sound field for several hundred cycles or more. During a transient collapse, however, the fluid cannot be considered as incompressible and research by several authors has yielded equations to solve this problem and a comprehensive review of their approaches has been carried out by Neppiras [54].

Transient cavitation is a threshold phenomenon and a number of researchers have carried out work in an attempt to define this threshold including Apfel [55], Flynn [56, 57] and Blake [58]. There is both a lower threshold and an upper threshold beyond which transient cavitation will not occur.

Blake [58] carried out an analysis in order to determine the lower threshold limit due to the surface tension forces within the bubble. This analysis only accounted for surface tension effects and did not take into account inertial and viscous effects. He found that the minimum pressure required to obtain explosive growth from a bubble of initial radius  $R_0$  under an ambient pressure  $p_0$  can be calculated as:

$$P_B = p_0 + 0.77 \frac{\sigma_l}{R_0} \quad (2-1)$$

where  $P_B$  is known as the Blake threshold pressure and  $\sigma_l$  is the surface tension of the fluid. The Blake threshold is generally accepted as the lower limit to transient cavitation.

Research by Flynn [56, 57] aimed to define the upper limit of bubble radius that could exhibit transient cavitation behaviour. This research found that the ratio of maximum bubble radius to initial radius ( $R_{max}/R_0$ ) must be at least 2 in order for the bubble to collapse violently. Apfel [55] argued that  $R_{max}$  could be estimated to be:

$$R_{max} = \frac{4}{3\omega} (P_A - p_0) \sqrt{\frac{2}{\rho P_A}} \left( 1 + \frac{2}{3 p_0} (P_A - p_0) \right)^{\frac{1}{3}} \quad (2-2)$$

Where  $P_A$  is the magnitude of the applied pressure field and all other symbols are as previously defined. This estimate predicts  $R_{max}$  is independent of  $R_0$  during transient cavitation. If the frequency of insonation, fluid properties, ambient pressure and applied pressure are known, as they normally are, then an estimate of the upper bound bubble radius that will undergo transient cavitation,  $R_{max}$ , may be found.

Initial work by Apfel [55] in the early 1980's combined the work of several researchers to create acoustic cavitation prediction diagrams based on theoretical thresholds for the growth of bubbles by different mechanisms. These charts are useful in indicating what type of cavitation can be expected from experiments. Later work by Holland and Apfel [59] extended this work to fully include the effects of surface tension. Apfel and Holland [60] related the transient cavitation threshold, frequency and initial bubble radius to achieve results which show, for any given frequency of insonation and applied pressure, the range of bubble sizes that will undergo transient collapse. It clearly showed that there is a minimum pressure below which no transient cavitation will occur and that this threshold increases with frequency. It also showed that the greater the applied pressure is above this threshold then bubbles of a greater size distribution will undergo transient cavitation. This research proved that transient cavitation could occur within the frequencies and pressures used in medical diagnostic equipment. It also implied that there is no upper limit to the frequencies that can cause cavitation provided the amplitudes are significantly high. This contradicts earlier research by Alliger [61] who stated that cavitation could not occur above 2.5 MHz though he did not elaborate as to why this was the case.

In the literature, cavitation has been separated into two types; stable (non-inertial) or transient (inertial). When bubbles oscillate under the action of an alternating pressure field for many thousands of cycles they are termed as stable cavitation bubbles [56, 57]. If however, the bubbles grow at an explosive rate and collapse suddenly (within a few cycles) then these bubbles are known as transient cavitation bubbles [56, 57].

### **2.3.2 Stable Cavitation**

The term stable (or non-inertial) cavitation is given to bubbles that oscillate for many hundreds of cycles under the action of a time varying pressure field. If the bubbles are

present in the fluid for a considerable amount of time under the action of a time varying pressure wave, then they may grow through mass diffusion from the liquid into the bubble, a process known as rectified diffusion. During stable cavitation it is usually assumed that since evaporation and condensation take place much more rapidly than the bubble dynamics, the vapour pressure within the bubble remains constant at the equilibrium value.

However, this is not the case for the gas content of the bubble, a gas that will also be dissolved in the liquid. Harvey [62] suggested a mechanism by which bubbles experiencing stable cavitation in a sound field may undergo a steady increase in radius. This rectified diffusion is caused by the pumping of gas, initially dissolved in the liquid, into the bubble using the energy of the sound field. The growth of these bubbles can be explained through the ‘area effect’. During the compression phase of the applied acoustic wave the bubble is forced to contract thus reducing the bubble volume and increasing the gas pressure inside the bubble, this will cause the gas to diffuse from the bubble into the liquid. In the rarefaction cycle of the acoustic wave, the bubble will grow in size greater than the equilibrium radius due to the tensile forces. This will cause gas to diffuse from the liquid into the bubble. However, since the diffusion of gas from or to the liquid is proportional to the surface area of the bubble, the gas flow is not symmetric and hence there is a net gas inflow to the bubble causing it to grow with each cycle.

Stable cavitation can cause an effect known as microstreaming. Microstreaming occurs when oscillating bubbles in a sound field produce a vigorous circulatory motion. These oscillating bubbles can be pushed by an acoustic force produced from the travelling wave and a non-circulatory shearing flow in the surrounding fluid may result. The fluid velocity is greatest near the bubble surface and decreases with increasing distance from the bubble. Because of this velocity change with respect to distance from the bubble surface, a gradient exists in the region of fluid around the bubble [63]. Other small bubbles are attracted into the sound field and these can create microcurrents around themselves that spread into the liquid [64].

Due to the complex motion of oscillating bubbles within a fluid under a time varying pressure field, some bubbles that were initially stable in nature may grow through rectified diffusion to become large enough to undergo transient cavitation.

### 2.3.3 Transient Cavitation

Transient cavitation is the term given to the explosive growth of a cavity within a fluid and its subsequent violent collapse. These bubbles will last for, at most, a few cycles before expanding to at least twice their initial radius during the rarefaction cycle of the applied pressure wave before collapsing violently in the compression phase of the wave, causing large pressures and temperatures to be created at the site of collapse. Theoretical studies by Noltingk [51], Flynn [56] and Neppiras [52] allow an estimate of the temperature and pressure at the point of collapse through the following equations:

$$T_{\max} = T_0 \left( \frac{P_m(\gamma - 1)}{P} \right) \quad (2-3)$$

$$P_{\max} = P \left( \frac{P_m(\gamma - 1)}{P} \right)^{\frac{\gamma}{\gamma-1}} \quad (2-4)$$

Where  $T_0$  is the ambient temperature,  $\gamma$  is the polytropic index of the gas (or gas-vapour),  $P$  is the pressure in the bubble at its maximum size (usually assumed to be equal to the vapour pressure of the liquid) and  $P_m$  is the pressure in the liquid at the moment of collapse (usually assumed to be the sum of the hydrostatic pressure and the acoustic wave pressure ( $P_h + P_a$ )). It is assumed that during the lifetime of the transient bubble there is no time for any mass flow by diffusion of gas into or out of the bubble, however evaporation and condensation of the liquid is assumed to take place freely. Taking a typical example of an air bubble in water ( $\gamma = 1.4$ ) at an ambient temperature of 293 K ( $T_0$ ) and ambient pressure of 0.1 MPa ( $P_m$ ), these equations yield values of 5000 K and 48.5 MPa for the collapse. These high pressures and temperatures can have significant physical, chemical and biological effects.

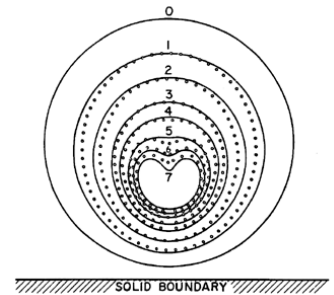
### 2.3.4 Applications of Cavitation

Cavitation has found many and varied uses in engineering, physical science (most notably in chemistry), medicine and dentistry. This section shows the extent to which cavitation has been exploited for beneficial purposes. The use of cavitation is examined for cleaning, homogenisation, sonochemistry, bubble fusion, breaking gallstones in-vivo, and cell disruption.



### 2.3.4.1 Ultrasonic Cleaning

Cleaning of surfaces and components is important in many industries for the safety or quality of products. For example, surgical instruments must be thoroughly cleaned before disinfection to ensure the highest levels of hygiene and to prevent cross-contamination and infection. Traditionally components have been cleaned by mechanical agitation either by hand or in a machine, however this is a time consuming process and the results can be highly variable in terms of the quality and consistency of the cleaned components. Also, using mechanical agitation to clean sensitive components, such as computer chips, is inappropriate as it could cause significant damage and render the component useless. It is these issues which have spurred the research into different methods of cleaning, and the use of ultrasound, to either shake contaminants off components or use controlled cavitation to assist in the cleaning process, has been researched extensively. The use of ultrasonic energy to clean surfaces has been around for several decades with one of the



**Figure 2-2 - Aspherical collapse of a cavitation bubble close to a rigid surface [158]**

first patents being obtained by Branson Ultrasonics in 1959 (US patent 2,891,176). The ultrasonic cleaning bath usually consists of a stainless steel tank with several transducers connected to the base. The tank is filled with a water/ surfactant solution into which the objects to be cleaned are placed. The surfactant reduces the surface tension in the fluid allowing more cavitation to take place. Ultrasonic cleaners normally operate between 20-50 kHz and make use of the asymmetric collapse of cavitation bubbles near boundary walls. Cavitation bubbles collapsing near boundary walls do not collapse spherically but in a manner shown in Figure 2-2. This collapse causes a high speed jet of fluid to impinge on the boundary which aids in the removal of unwanted particles adhering to the surface. Ultrasonic cleaning baths have been designed to effectively clean a variety of surfaces ranging from computer electronics to surgical instruments to archaeological artifacts and are now widely commercially available.

### 2.3.4.2 Ultrasonic Homogenisation and Emulsification

Homogenisation and emulsification are effectively the same process. The aim of these processes is to blend two immiscible liquids to create a single homogeneous liquid. Due to the immiscibility of the liquids being mixed, emulsions are unstable, do not form naturally

and require energy input to be formed. Traditionally this has involved vigorous mixing to break the dispersion liquid into smaller parts and spread it throughout the continuous liquid. Mixing, however, is not sufficient to maintain a stable emulsion as over time the emulsion tends to separate back to its constituent parts. In order to make the emulsion more stable, a chemical or surfactant is added which acts to reduce the interfacial tension between the liquids. Emulsions treated in this way can remain stable for many years after emulsification. Emulsions are used widely in industries ranging from the food industry, for products such as mayonnaise and butter, to the pharmaceutical industry, for products such as ointments. The industrial importance of this process has encouraged research into methods of improving the yield and quality of emulsions. This has led researchers to investigate the use of ultrasonic vibrations for this purpose. This area of research has been active since the early 1900's with one of the first research papers published by Wood in 1927 [65]. Since then many researchers have investigated the influences of frequency, power, exposure time, and use of emulsifiers on the quality of the emulsion obtained [66-69] and have found that the use of ultrasound in this process can bring about benefits in reduced processing time and increased quality of emulsions.

#### 2.3.4.3 Sonochemistry

The ability to use ultrasound to cause new reaction pathways, accelerate reactions and create completely different products has been of interest to chemists for many years. The field of sonochemistry started with the observations of Loomis [70] but lay dormant until about 1970, when reliable high power ultrasonic generators became commercially available. It was then that chemists started to investigate the use of ultrasound and cavitation for chemical reactions. The primary instigators in this field were Mason, an organic chemist and Lorimer, a physical chemist. Mason, having observed the intense energy used in ultrasonic cleaning baths to clean components, wondered if the energy could be used to aid his own chemical reactions and so started the field of sonochemistry. Over the last 35 years or so since its inception, this field has grown significantly and the use of ultrasound has been successfully applied to all branches of chemistry, from organic to inorganic, using either heterogeneous or homogeneous fluids.

In homogeneous fluids, cavitation can cause a series of reactions either within the bubble itself, at the bubble-liquid interface or in the liquid immediately surrounding the bubble.

Due to the large pressures and temperatures generated during bubble collapse, high energy densities can be achieved which can cause significant chemical reactions. For example, the sonication of water can produce small amounts of hydrogen peroxide as well as  $\text{OH}^\bullet$  and  $\text{H}^\bullet$  radicals [71-73]. These radicals may then travel to the bubble interface where they can react with the bulk fluid and undergo reactions with involatile species dissolved in the bulk fluid. The large shear forces generated around a collapsing bubble can also cause chemical reactions to take place. These shear forces are significant enough to break some chemical bonds [73].

Applying ultrasonic vibrations to fluids containing a large number of particles can have several effects. At low power levels the vibrations can be used to increase the homogeneity of the fluid by deaggregation and dispersion of clumps of particles. At high power levels where cavitation is present, particles have been found to fuse together. Experimental work using different particle materials found that zinc, chromium and molybdenum, with melting points of 420 °C, 1857 °C and 2617 °C respectively, showed signs of fusion whilst tungsten, with a melting point of 3410 °C, did not [77]. This gave an initial experimental insight into the temperatures created during bubble collapse.

The use of metals in chemistry as catalysts and reagents for reactions has been widely investigated and it has been shown that the generation of high speed jets owing to cavitation collapse at the surface of the metal can strip away the oxide layer present on some metals (Al, Na, Li) that prevents further reactions. The use of ultrasound in this way has shown that greater reaction rates can be achieved without the need for expensive ultra-pure chemicals [78-82].

Ultrasound has also been widely used in polymer chemistry to reduce the viscosity of solutions; this is largely due to cavitation causing degradation of the polymer chains [78-82]. Despite cavitation being identified as the cause of the effects, the precise mechanism by which the effects occur is not yet elucidated. What is certain however, is that all the factors which affect cavitation (frequency, intensity, temperature, gas content, etc.) have a considerable effect on the outcome of experimental results [78-82].

It can be seen from the above brief examples that the use of ultrasound to assist in chemical reactions has been widely investigated over the past 35 years and has been used in almost all areas of chemistry for beneficial purposes. The number of research papers and books published in the area of sonochemistry is vast considering the young age of this research area and there is no doubt that continued research in this field will yield more exciting and intriguing findings in the future.

#### 2.3.4.4 Bubble Fusion

The extreme conditions created during the collapse of a cavitation bubble have spurred some researchers into investigating the possibility of creating fusion reactions at the point of bubble collapse. The idea of bubble fusion has been around since the discovery of sonochemistry and in fact, a patent was obtained by Hugh Flynn for “A method of generating energy by acoustically induced cavitation fusion and reactor thereof” in 1982. However in the 25 years since obtaining the patent there has been much controversy in this field due to the claims made by some research groups. In 2002, Prof. Taleyarkhan and his colleagues reported the first positive results of experiments into bubble fusion which were published by the highly respected journal *Science* [83]. Since then, many research groups have tried and failed to replicate Taleyarkhan’s experiments leading to accusations of research misconduct. Investigations were carried out at Purdue University which cleared Taleyarkhan of all charges. Two years later Taleyarkhan published another paper with an improved experimental set-up to try to convince his skeptics [84] and in 2005 Xu and Butt [85] reported positive findings using a simplified experimental set up; however experts such as Prof. Suslick and Prof. Putterman remain unconvinced that all the issues with the experimental set up have been addressed properly. Until more groups can produce positive results that can be replicated independently, the idea of bubble fusion will remain just an idea.

#### 2.3.4.5 Medical

The use of ultrasound in medicine has mainly focused on the high frequency low power internal imaging techniques to examine internal injuries or assess the health of a baby in the womb. More recently however, the use of low frequency high power ultrasound has been investigated for in vivo use to destroy kidney stones, gallstones, and tumors in a variety of tissues including the liver, prostate and bladder [86-88]. This area of research is

relatively new with the earliest studies taking place in the 1930's and 1940's. Despite its young age there has been a significant effort in the medical community to apply high intensity focused ultrasound (HIFU) technology to benefit patients and thus there is a plethora of research papers and recently results of early clinical trials have been published. The main advantage of this method is that it allows the surgeon to operate on the patient without having to make any incisions, thus causing less trauma to the patient. The ultrasonic vibrations are focused accurately to a specific point in the body to treat either a tumour or hard substance. This however is no easy task due to the different acoustic properties encountered throughout the body to the target area. HIFU does, of course, have limitations in its use. Since high power ultrasonic vibrations are absorbed extremely efficiently in air, this method is not useful for use in air filled cavities such as the lungs or bowel. Also, bones can absorb or reflect ultrasonic vibrations and hence make the use of HIFU inappropriate.

#### 2.3.4.6 Microbiological Applications

It has been known for many years that high intensity ultrasonic fields can cause the disruption of cells. Initial work indicated that although ultrasound could inactivate bacterial cells, the power consumption of the devices made it unrealistic for industrial use [89]. In recent years, however, ultrasonic devices have become cheaper and more efficient and research in this area has started once again.

The main inactivation mechanism of low frequency ultrasound is widely accepted to be through cavitation [90], though different theories have arisen as to exactly how this happens. During transient cavitation the high pressure shock wave generated by the collapsing bubble is the main cause of cell inactivation [90]. Although bacteria are resistant to large static pressures it appears that they are susceptible to large pressure changes [91], [92]. It has also been shown that the high temperatures generated upon collapse are very localised and are not likely to contribute significantly to the cell inactivation mechanism [90].

During stable cavitation, cells are inactivated by the large shear stresses generated during microstreaming [93-95]. Microstreaming is an effect whereby bubbles pulsating in an ultrasonic field cause strong currents in the liquid surrounding the bubble. Other pulsating

bubbles may be attracted together and will also cause strong currents, creating a field of strong currents that may lyse cells by effectively rubbing the cell wall apart. Cavitation also has a number of non-physical inactivation mechanisms such as the release or creation of chemicals toxic to bacteria; hydrogen peroxide for example [28], or the production of free radicals, which can attack cells [82].

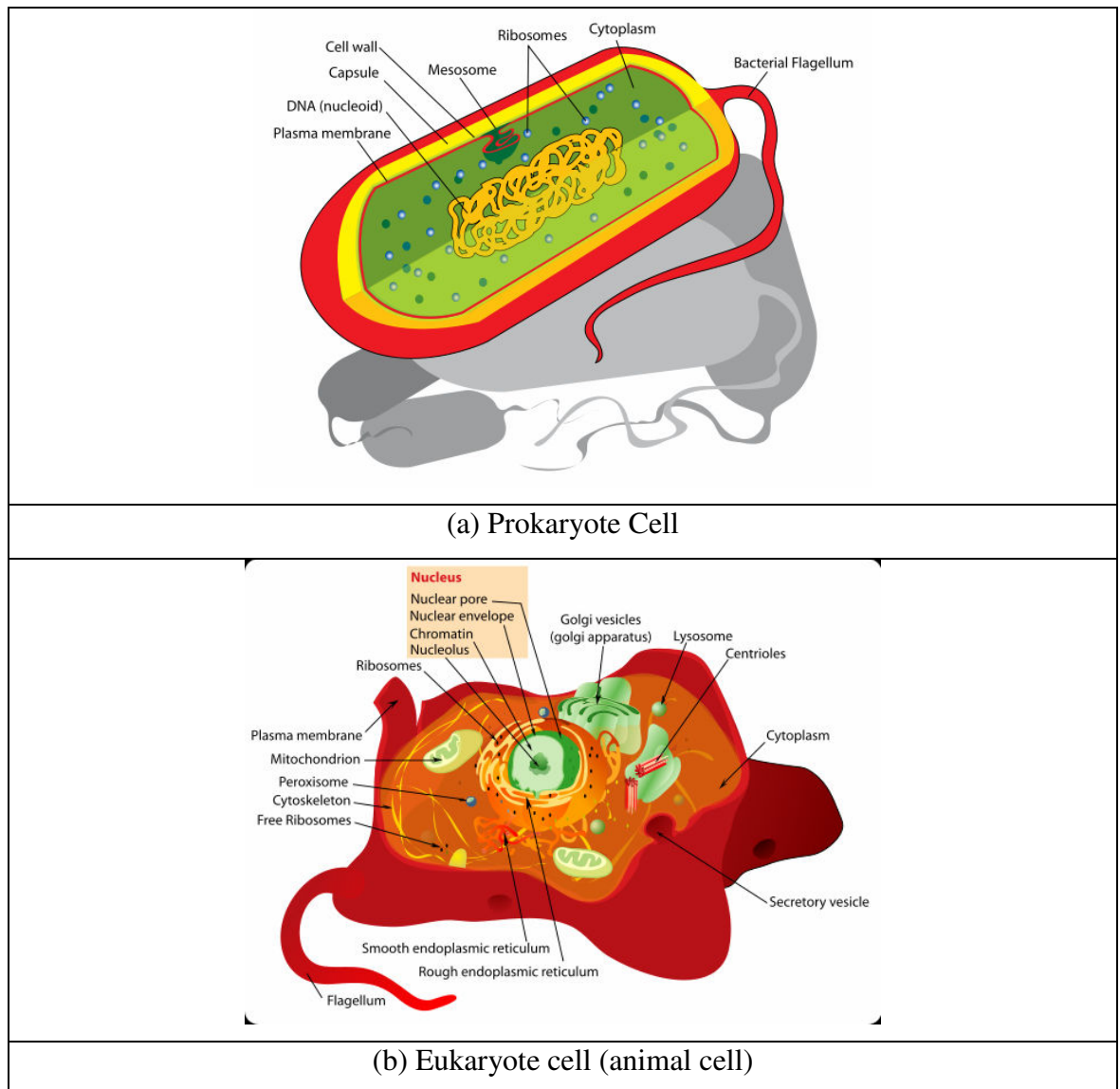
Cavitation can also be applied in a controlled manner to cells in order to insert large molecules which cannot normally enter through the cell wall. It can also be used as an alternative to using vectors such as viruses to insert DNA or RNA. This is achieved through a technique known as sonoporation. It involves applying ultrasound to create cavitation bubbles but the intensity is such that non lethal damage is caused to the cell wall. The cavitation causes the cell wall to become temporarily more permeable than normal and allows large molecules to be taken up by cells without causing cell lysis and death. This area of research is relatively new and different research groups have had differing degrees of success with some reporting high percentages of cells taking up large molecules whilst having a low number of non-viable cells and other groups have reported the complete opposite [96-102].

## **2.4 Introduction to Bacteria**

In order to fully understand the bactericidal effect of ultrasound and interpret the results of previous studies we must first understand that we are dealing with a living organism and although bacteria are single cell organisms, they are remarkably complex when examined in detail. In examining the structure of these organisms we can see where their strengths and weaknesses lie such that effective mechanisms can be used to target them efficiently.

There are three major domains that make up the living world; Bacteria, Archaea, and Eukarya. Each of these domains has evolved separately for many billions of years and each has its own unique characteristics in terms of cell structure. Humans, along with all other animals, form part of the Eukarya domain and have a much more complex cell structure than Bacteria. **Figure 2-3** shows a typical prokaryote cell and eukaryote cell. It should be noted that viruses do not feature in any of the domains. The virus is technically not a living organism and must infect a host cell in order to obtain the components required to complete one of the fundamental requirements for living organisms, reproduction.

Bacterial cells are much smaller than eukaryote cells. Animal cells vary in size from 10  $\mu\text{m}$  to 100  $\mu\text{m}$  whilst bacteria cells can vary between 1  $\mu\text{m}$  and 10  $\mu\text{m}$ . All living cells have certain components that are required for the cell to function. **Figure 2-3** shows the internal structure of (a) prokaryote and (b) eukaryote cells.

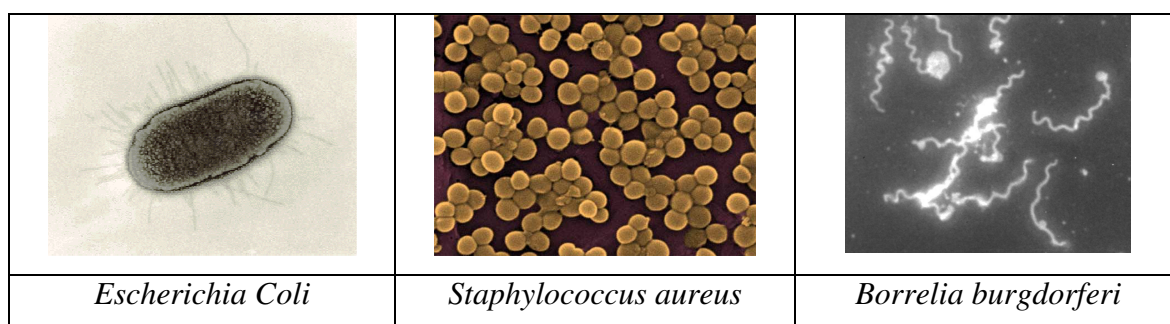


**Figure 2-3 - Cell Structures. (a) Prokaryote cell [159] and (b) Eukaryote Cell [160]**

In general, bacteria are prokaryote with plant and animal cells being eukaryote. It can be seen that both types of cell contain a cell wall, cytoplasmic membrane, ribosomes, and cytoplasm. The major difference between the cells is the prokaryotes lack of a well defined nucleus. The cell wall provides structural strength to the cell while the cytoplasmic membrane acts as a barrier between the inside and outside of the cell and allows the cell to

absorb nutrients and other substances needed by the cell. The cytoplasm of bacterial cells is where the functions for cell growth, metabolism, and replication are carried out. Ribosomes translate the genetic code from the molecular language of nucleic acid to that of amino acids - the building blocks of proteins. Proteins are the molecules that perform all the functions of cells and living organisms.

Bacteria generally have one of three shapes: rods, cocci (spherical), or spiral, these are illustrated in **Figure 2-4** by the bacteria *Escherichia Coli* (rods), *Staphylococcus aureus* (spherical) and *Borrelia burgdorferi* (spiral).

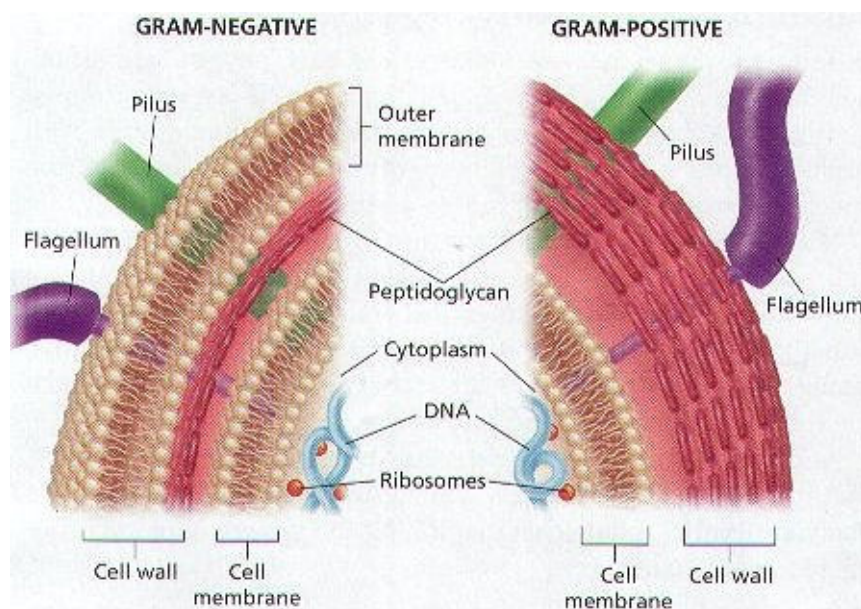


**Figure 2-4 - Bacterial cell shapes.** (a) *Escherichia Cole* (rod  $\approx 2 \mu\text{m}$  long) [161], (b) *Staphylococcus aureus* (sphere  $\approx 1 \mu\text{m}$  diameter) [162] and (c) *Borrelia burgdorferi* (spiral 20-30  $\mu\text{m}$  long) [163]

They are single cell organisms that reproduce asexually through binary fission i.e. the original cell grows then splits into two daughter cells that grow and split into another two cells, thus the bacteria grows exponentially from 1, 2, 4, 16, 256, ...etc... assuming there is sufficient nutrition available. The mechanism by which this occurs is beyond the scope of this background material though an adequate and easily digested description may be found in Brock [103]. In general, there are four phases to the growth of bacterial organisms in a growth medium; lag, exponential, stationary and death. Bacteria inoculated into a fresh growth medium will not grow immediately but will become accustomed to their surroundings before growing; this is known as the lag phase. Once the bacteria are satisfied that the conditions are suitable they will grow at an exponential rate. This continues until either there is no more nutrition available or there is a waste product build up which inhibits further growth, thus the bacterial population stays constant during the stationary phase. After some time, some bacterial cells may die and a reduction in population occurs, this is generally exponential but at a much slower rate than the exponential growth phase.



Another important feature which indicates the structure of the cell is whether the cell is gram-positive or gram-negative. Bacteria cells can be differentiated by a staining mechanism whereby gram-positive cells take up a purple staining solution and gram-negative cells do not. This is due to differences in the composition of the bacterial cell wall. **Figure 2-5** shows a diagrammatic representation of the cell walls of a gram-positive organism and a gram-negative organism.



**Figure 2-5 - Bacteria Cell wall structure. Gram negative (left) and Gram Positive (right) [164]**

It can clearly be seen that gram-negative bacteria have a more complex cell wall structure compared to the gram-positive bacteria. The bacterial cell wall is an extremely important structure to the survival of the cell, it provides the cell with strength and rigidity and without it the contents of the cell would leak to the environment and the cell would die. The cell wall is a polymer made up from sugar molecules and amino acids. In gram-positive bacteria the cell wall is much thicker than in gram-negative bacteria. Typically gram-positive bacteria cell walls are 20-80 nm thick whilst the gram-negative measure only 7-8 nm [104]. The periplasm layer in gram-negative bacteria is responsible for the transport of molecules to the cell for nutrition as well as the alteration of substances toxic to the cell. In *Escherichia coli* this layer is about 12-15 nm thick and has a gel-like consistency thus providing little structural support to the cell. The outer membrane of gram-negative bacteria provides structural support to the cell but is also frequently toxic.

Some species of bacteria have evolved to create extremely hardy structures to ensure their survival called spores. Spores are notorious for their ability to survive extreme conditions including heat treatments, harsh chemicals, physical processing and radiation and can lie dormant for possibly millions of years before becoming active again.

There are many different kinds of bacteria that interact with the world in different ways. Many are used in a positive sense to create medical drugs, clean oil spills and are partly involved in the cheese making process amongst many other uses mankind has found for these life forms. There are some, however, that are pathogenic i.e. they can cause disease. Examples of bacterial disease include Botulism, Plague, Tuberculosis, Gonorrhoea and many more. Hence it is important to kill or inactivate these pathogenic bacteria where they may come into contact with humans. Different types of bacteria have different strengths and weaknesses and thus there is no set methodology for killing or inactivating them. In general, for the bacteria found in food products (including dairy products) and those found in dirty water, there are a few well developed inactivation methods used including thermal, chemical, pressure, or a combination of these.

## **2.5 Microbiological Studies**

There are many factors that will affect the rate of bacterial inactivation using ultrasound technology. Mason [29] found that using higher frequency ultrasound (850 kHz), an increase in bacterial numbers was observed. He postulated that this was due to the bacterial cells being declumped. Interestingly, when ultrasonic treatment is used in conjunction with chlorination then the frequency of insonation and order of treatments plays a significant role in the inactivation of cells. In Mason's study substantially higher inactivation rates were observed when applying low frequency (20 kHz) ultrasonics simultaneously with chlorination or when high frequency insonation was used as a pre-treatment. In the case of the 20 kHz results this is due to the fact that at lower frequencies the bubbles have time to grow to a sufficient size in order to collapse violently [60]. There will also be a greater range of bubbles excited in the lower frequency range [60]. This shows that there are different mechanisms at different ultrasonic frequencies, the higher frequencies appear to have a separation effect whilst the lower frequencies seem to have a direct inactivation effect.

There have been many studies investigating different species of bacteria, including *Escherichia Coli* [105-109], *Staphylococcus Aureus* [110], *Bacillus Subtilis* [111-114], *Listeria Monocytogenes* [115] and *Salmonella* [116] as well as the yeast *Saccharomyces cerevisiae* [117-124]. Many authors [28, 125, 126] have reported that ultrasonic treatment is less effective on Gram-positive organisms due to their thicker cell wall, compared to Gram-negative organisms. However, Scherba [90] found no such correlation and hypothesises that the inner cytoplasmic membrane may be the target of the ultrasonic treatment. The physical shape of the bacterial cell also influences inactivation. It has been found that coccus (sphere) shaped cells are generally more resistant to ultrasonic treatment than rod shaped cells [127, 128]. This is probably due to the higher structural strength of a sphere shaped structure compared to a rod shaped structure.

Ultrasonic treatment on its own is an inefficient method of inactivating bacteria as it takes excessively long exposure times to reduce the bacterial count sufficiently [129, 130]. Hence, the use of ultrasound in combination with traditional bactericidal technologies, such as heat, chemicals and ultraviolet light, has been successfully investigated by several authors [131-136]. Initial pioneering work in this area was carried out by Garcia in 1989 [111], who showed a synergistic effect of heat and ultrasound for both a batch system and a continuous flow arrangement using *B. Subtilis* spores. More bacterial spores were inactivated by using both treatments simultaneously than either alone or in series. Garcia also found that using sub-lethal temperatures with ultrasonication did not affect the survival of the *B. Subtilis* species used. Other authors [134] have reported that sub lethal temperatures can make an impact on the survivability of certain species of bacteria. If the main inactivation mechanism is thought to be physical disruption of the cell wall, then this proves that even small changes in cell structure can have a significant impact on the effect of ultrasonic treatment and this should be considered if applying it in an industrial context where there may be more than one species of bacteria present. Lee et al. [112] have also reported that the survivability of bacterial cells changes drastically with the medium in which they are suspended. This may be due to changes in the ultrasonic energy penetration into the fluid [93].

Raso [113] developed Garcia's ideas and investigated the effect of ultrasound treatment combined with heat (thermosonication), pressure (manosonication) and both heat and pressure (manothermosonication) on *B. subtilis* spores. Raso found that increasing the

pressure had a beneficial effect on reducing spore numbers but that this benefit ceased above 500 kPa. This may be caused by the increased violence of cavitation at higher pressures, however as the pressure approaches 500 kPa, there are less and less bubbles undergoing cavitation and hence fewer bacterial spores can be inactivated. An increase in ultrasonic amplitude from 90-150  $\mu\text{m}$  was found to exponentially increase the number of bacterial spores inactivated [113]. This would be expected as the range of cavitation bubbles and cavitating volume will increase with increased amplitude of vibration. Interestingly, Raso found that using temperatures below 70 °C had no effect on spore survival but above these temperatures, spore survival dropped dramatically. Spore survival went from 20 % at 70 °C (20 kHz, 117  $\mu\text{m}$ , 300 kPa) to 0.2 % at 90 °C for 6 minutes ultrasonic exposure. Using only thermal treatment yielded survival points of 100 % and 40 % for 70 °C and 90 °C respectively, thus the use of ultrasonic treatment had a significant impact on spore survival. Further work by Pagan [115] in the same year reported decimal reduction times (D-value) for *S. Faecium*, *L. Monocytogenes*, *S. Enteritidis*, and *A. Hydrophilia* under heat treatment, manosonication, and manothermosonication conditions. The D-value is defined as the time taken to cause a single log reduction in viable cells and is widely used in the literature since bacterial inactivation generally follows first order death kinetics. This is to say that a constant proportion of viable cells are inactivated per unit time according to Eq.2-5.

$$N_t = N_0 e^{k t} \quad (2-5)$$

Where  $N_t$  is the number of viable bacteria after time,  $t$ .  $N_0$  is the initial number of bacteria and  $k$  is a death rate constant. Pagan [115] also reported an additive inactivation effect for *L. Monocytogenes*, *S. Enteritidis*, and *A. Hydrophilia* while *S. Faecium* displayed a synergistic effect. Thus the effect of ultrasonic treatment in combination with traditional methods is highly dependant on the organism being treated.

## **2.6 Continuous flow studies**

Currently the majority of devices used for the disruption of cells are probe type devices that resonate in the longitudinal mode at the desired operational frequency. These devices typically have tip vibrational amplitudes in the region of 100  $\mu\text{m}$  but this will vary considerably depending on the design of the horn and the materials used in its construction. When these devices are placed in a fluid then a cavitation cloud can be created near the tip. In fact, Campos-Pozuelo [137] has observed that a probe type device vibrating in the

ultrasonic range at intensities high enough to cause cavitation will create a cone like bubble field. As a consequence of creating the cavitation field at the horn tip, the cavitation can cause pitting and erosion damage to the device. Also, the scalability of these devices is limited to small volumes.

Previously most of the research has concentrated on static batch type systems. Exceptions have been early research by Garcia [111] and more recently work by Villiamiel [138], Mason [29] and Zenker [139]. The research by Garcia [111] and Villiamiel [138] has taken the traditional probe type device and modified the set up to allow for a flow of fluid. Mason [29] used some more novel set-ups, though few details were provided.

Of the very few studies to be done on the use of ultrasonic devices in continuous flow systems, the two of most significance are those by Villiamiel [138] and Zenker [139]. Both these authors have adapted the set up of a traditional probe device in order to obtain a flow through system and both authors attempt the same type of work; comparing conventional treatments with ultrasonically assisted ones for batch and continuous processes. These authors used devices operating at 20 kHz. The main differences between these studies are the power of the devices used, the flowrates, and the organisms used. The table below summarises these differences.

	Villiamiel [138]	Zenker [139]
Max Power	150 W	800 W
Max Flowrate	50 ml/min	1 l/min
Volume of Sonication Cell	18.76ml	117ml
Gram-positive organism	<i>Streptococcus thermophilus</i>	<i>Lactobacillus acidophilus</i>
Gram-negative organism	<i>Pseudomonas fluorescens</i>	<i>Escherichia coli K12 DH 5 <math>\alpha</math></i>

**Table 2.1 – Experiment variables used in the studies carried out by Villiamiel [138] and Zenker [139]**

Though not directly comparable, it is interesting to note that both authors came to the same conclusions. These authors found that a significant decrease could be observed in bacterial survival when ultrasound treatment was applied simultaneously with mild heat treatment. This benefit diminishes at higher temperatures with Villiamiel and Zenker finding the thresholds at 61 °C and 65-67 °C respectively. This will be due to the reduction in cavitation effects at higher temperatures combined with the increased thermal inactivation effect. In their studies, Villiamiel found that ultrasound and heat treatment had

an additive effect whilst Zenker observed a synergistic effect, thus the death kinetics of these combined processes is not yet fully understood and further research into this area is required. Both authors did, however, find that the gram-negative organism was more susceptible to treatments than the gram-positive organism and that longer treatment times resulted in increased inactivation. Zenker also observed that at flowrates greater than 28 l/h, there was little difference in inactivation between the thermal and ultrasound-assisted treatment, probably due to the short residency time of the fluid in the ultrasonic field. Zenker's research also showed that the D-value decreased exponentially from 39.4 to 19.4 s as the amplitude of vibration was raised from 50 to 160  $\mu\text{m}$  at a constant temperature of 60 °C. This will be due to an increased cavitation effect at larger amplitudes. Not only can the cavitation become more violent but the volume of the cavitation field can also increase with increased amplitudes. The unique aspect of these studies is that they are the only studies that attempt to relate the inactivation rates of different methods with the energy input requirements and in this respect both authors are in agreement. These authors find that the ultrasonic assisted treatments require a greater energy input than traditional heating methods. There are, however, other benefits of ultrasound assisted treatments that may offset the additional energy requirements; these authors cite the increased quality of the end product as an advantage. Other advantages may include the fact that the ultrasonic treatment has a physical rather than thermal inactivation effect and this is a new line of attack in the treatment of water and liquid food products. Also, by using two separate inactivation mechanisms bacteria are required to evolve to combat both at the same time. If a single mechanism is used, heat for example, then those bacteria most resistant to the treatment may survive the process and multiply. On an evolutionary scale it could be expected that this will cause bacteria to become more resistant to the treatment as it facilitates their survival, such that eventually new treatment processes will be required. This risk can be minimised by forcing the bacteria to evolve defences against multiple lines of attack simultaneously.

Research on the use of devices that do not fit the traditional probe design for cell inactivation is lacking. Papers by Mason [29] and Borthwick [139] are rare exceptions with Mason using two commercial systems and Borthwick a radial mode device operating at 267 kHz. Although the aim of Borthwick's work is for small scale cell disruption in the order of ml, Mason [29] has investigated systems that aim to treat litres of fluid.

## **2.7 Conclusions**

It has been shown that ultrasonic treatments can cause physical inactivation of bacterial cells through cavitation. Ultrasonic treatments used on their own take too long to be useful to industry. However, as has been shown by many authors, combining ultrasonic treatments with conventional heat or chemical treatment can be a very effective way of inactivating bacterial cells. Questions still remain over the energy consumption of these methods compared with traditional methods and until these are resolved then the technology will not be adopted widely in industry.

Research in this area is slow but gathering some momentum with more groups taking an interest in this area of ultrasonics. There is still much research to be done in this area in determining the interaction between bacterial cells and cavitating bubbles as well as determining how different cell structures are affected by cavitation. More research is required into devices that do not fit the standard probe design as well as developing upon the initial research into continuous flow arrangements.

---

## Chapter 3 – Horn Design

---

### ***3.1 Introduction***

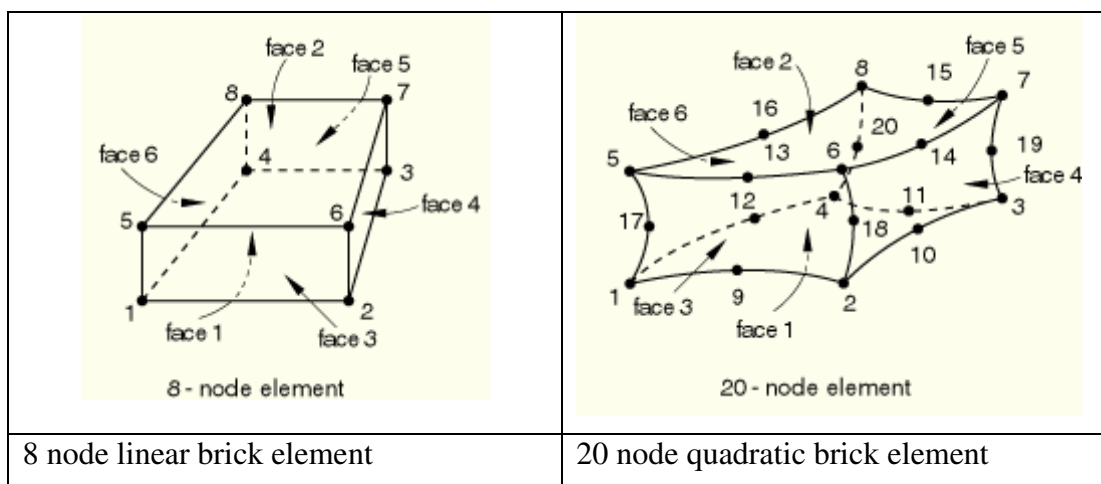
The ultrasonic horns and boosters used in this work are designed using finite element analysis with their natural frequencies and associated mode shapes confirmed using experimental modal analysis. In this chapter an overview of the finite element method to obtain natural frequencies and mode shapes as well as experimental modal analysis techniques are presented. The design and analysis of the devices used in the microbiological studies carried out in Chapters 5 and 6 are then shown.

### ***3.2 Finite Element Method***

The finite element method can be applied to structures to determine the stresses, strains and displacements generated by an applied loading condition. In dynamic problems it can also be used to determine the eigenvectors and eigenvalues of a structure and hence the mode shapes and associated frequencies at which they occur. ABAQUS 6.5 was used in these studies to determine the modal parameters of the horn designs. In order to extract the eigenvalues and eigenvectors from the model, ABAQUS has a choice of two solvers: the subspace solver and the Lanczos solver. The Lanczos solver is used in these studies as it is faster at extracting large numbers of eigenvalues compared to the subspace solver [140]. Full 3D models of the devices were created in order to capture the asymmetric modes, which would not be extracted from models utilising geometric symmetry. The 3D nature of the models also allows the capture of any modes which vary through thickness which would not be possible using a 2D approach. The models are meshed using 20 node quadratic brick elements. Quadratic elements are a necessity in this type of analysis to obtain accurate results, the use of linear elements results in a significant number of non-



existent plate type modes being generated which causes a massive increase in computation time.



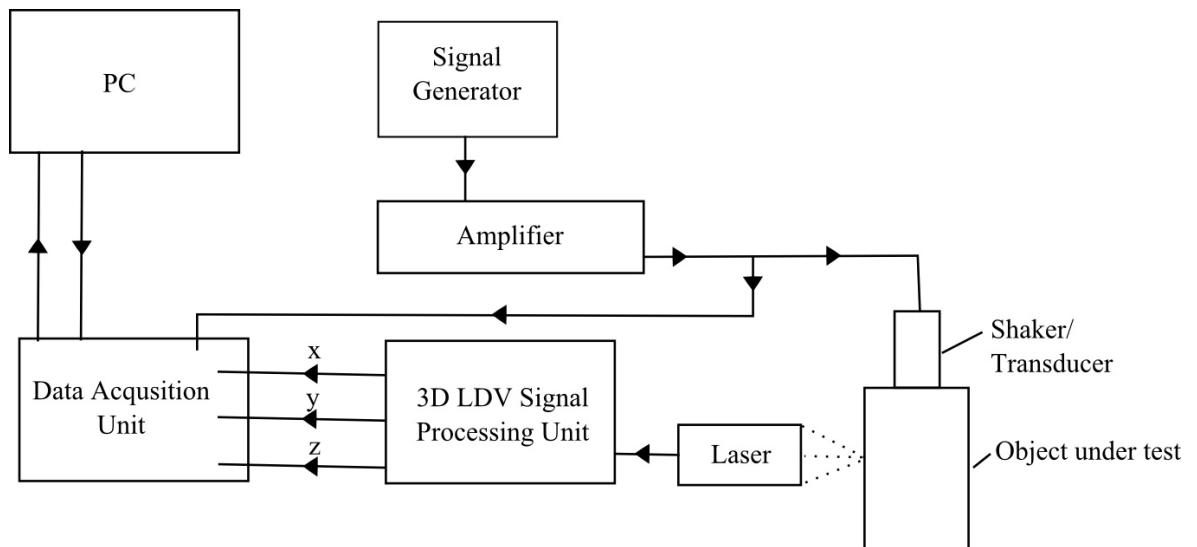
**Figure 3-1 – Finite elements (a) 8 node linear brick element and (b) 20 node quadratic brick element [165]**

Figure 3-1 shows a linear and quadratic element. The major difference is that the quadratic brick element has 20 nodes as opposed to 8 nodes for the linear brick element. The mid-side nodes of the element, away from the vertices, allow the quadratic elements to deform according to a quadratic equation ( $Ax^2 + Bx + C$ ) as opposed to the linear elements which may only deform according to the linear equation ( $Ax + B$ ). Although there are more nodes using quadratic elements, the added flexibility allows for efficient modal parameter extraction whereas the use of linear elements can result in a number of spurious modes being calculated, increasing the overall solution time drastically. Also, the choice between the use of brick elements as opposed to tetrahedral elements is deliberate. As far as is practically possible, brick elements should be used for the extraction of modal parameters since tetrahedral elements are generally considered to be stiffer and will put the mode frequencies slightly higher than they should be. Recently, 15 node quadratic tetrahedral elements have been found to give accurate results compared to brick elements but solution times are slightly longer due to the higher mesh density required for convergence [169].

### 3.3 Experimental Modal Analysis

Experimental modal analysis (EMA) is a procedure whereby the response of a structure subject to a vibrational load can be examined and the mode shapes, frequencies and damping parameters extracted. Figure 3-2 shows a schematic diagram of a typical modal

testing set-up. It can be seen that there are several parts required to carry out an experimental modal analysis.



**Figure 3-2 – Experimental modal analysis set-up**

Firstly there is a PC to control the process and handle the mathematics involved in extracting modal parameters from the test data provided by the data acquisition unit. A signal generator is used to provide the desired input waveform to the structure such that all the frequencies in the range of interest are excited. This signal may require to be made greater and an amplifier is used for this purpose. This signal is then passed to the excitation device and is also passed to the data acquisition unit to provide the input signal required to determine the frequency response functions (FRFs). The excitation device vibrates the test structure and the response of the structure is usually measured using an accelerometer or Laser Doppler Vibrometer (LDV). The response measurement is then fed into the data acquisition unit to provide the output signal required to determine the FRFs. The data acquisition unit passes the data to the PC in order for it to perform a fast Fourier transform (FFT) to change the time domain data captured by the test into more useful frequency domain data which can be interpreted in terms of modal parameters. There are several important assumptions that are made when carrying out a modal test. Firstly it is assumed that the system under test is linear such that the response of the structure will be proportional to the applied force. There are methods for dealing with non linear structures; however this is beyond the scope of this thesis. Secondly, it is assumed that the structure has reciprocity. This is to say that the response measured at a point B, due to a force applied at point A is equivalent to the response at A due to a force applied at B. Thirdly, in

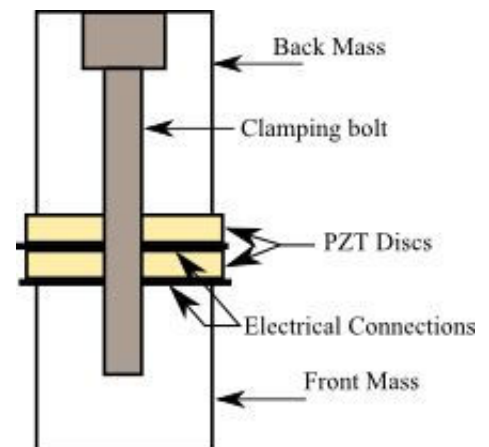
order to apply a FFT to the signals there is a requirement of signal periodicity. Failure to satisfy this criterion results in the serious problem of leakage where a single frequency wave can appear to leak into close-by frequencies. This is examined more closely in section 3.3.4.

### 3.3.1 Excitation Devices

Excitation devices are used to provide vibration input to the modal analysis. There are generally two methods of providing this input; impact hammer and electrodynamic shakers, however neither of these methods is appropriate for this work since the frequencies of interest are higher than the capabilities of these methods. It is therefore necessary to use an ultrasonic transducer.

#### 3.3.1.1 Ultrasonic Piezoelectric Transducers

Piezoelectric transducers are used to provide vibrational input to systems where the frequency range of interest is above that capable with electrodynamic shakers. These transducers are based on the piezoelectric effect where an electrical charge applied to a material causes a mechanical extension or contraction of the material and vice versa. These materials can be designed to resonate at extremely high frequencies and are limited only by the capacity of the signal generator to provide an electrical signal at the desired frequency. Figure 3-3 shows a cross section of a typical piezoelectric transducer and its components. It can be seen that the transducer has several PZT discs mounted in pairs which are constructed to resonate in the longitudinal mode at the desired frequency. To prevent damage to the PZT discs from overstress a clamping bolt is used to ensure the device remains in a compressed state during operation. Electrical connections on the PZT discs provide the means for applying the electrical charge to cause vibration.



**Figure 3-3 - Piezoelectric Transducer**

### **3.3.2 Excitation Signal**

There are many different types of excitation signal that can be used for a modal analysis. Common forms of excitation signal include random, burst random and sine chirp. Random excitation is still widely used in modal testing though it has drawbacks. Due to the non-periodic nature of a random signal and the requirements of the FFT, leakage is a major problem though it can be reduced through the use of windows to force the random signal to become more periodic (more on windows in section 3.3.4). However, this signal type has the advantage that the random nature of the signal ensures that no two input signals are ever the same, thus when the measured signals are averaged any slight non-linearities in the system tend to be averaged out. Burst random signals apply a random signal for a set period before switching off. The capture period of this signal is such that it is periodic and thus satisfies the requirements for the FFT without the need for windows to be applied. A sine chirp signal is a quick sine sweep from a low to high frequency. Again, because the signal is periodic, no leakage occurs and there is no need to apply a window. The EMA reported in this chapter used a swept sine input signal as this was found to provide FRF's with the least noise compared to the considerably quicker random excitation signal.

### **3.3.3 Response Measurement Devices**

The response of the structure to the applied excitation must be measured in order to determine the FRFs of the system. The most common ways to achieve this is through the use of accelerometers or though non-contact methods such as laser Doppler vibrometry.

#### **3.3.3.1 Laser Doppler Vibrometer**

A laser doppler vibrometer (LDV) is the principal device used in the experimental modal analysis for the acquisition of vibration data. Figure 3-4 shows a schematic diagram of the components of a LDV.

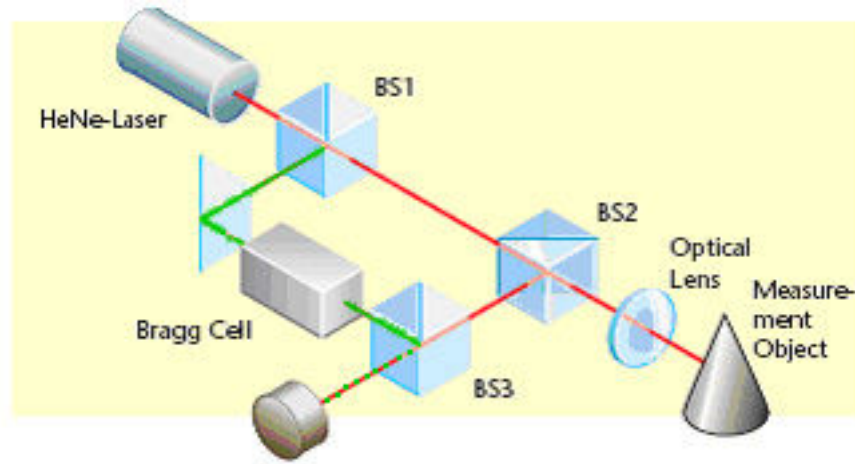


Figure 3-4 - Schematic of a laser Doppler vibrometer

A LDV works upon two principles, the Doppler shift and optical interferometry. The Doppler shift describes how the frequency of a wave will change if the source of the wave is moving relative to an observer. Since light can be treated as a wave, this principal can be applied to laser light. Thus the wavelength of reflected light is slightly different to the wavelength of the incident beam for moving objects. If the object were stationary the reflected beam would be of exactly the same frequency and wavelength. However if the object is moving toward the incident beam then the reflected beam has a shorter distance to travel and since the speed of light remains constant, the wavelength of the reflected beam must decrease. The opposite holds true if the object is moving away from the source, the wavelength will increase. The difference between the wavelength of the source beam and reflected beam can be used to determine the velocity of the object. Unfortunately, due to the high frequency of the laser beam ( $4.74 \times 10^{14}$  Hz) and the small changes in frequency it is not possible to directly demodulate the light. Thus it is necessary to use optical interferometry and the speckle effect.

Optical interferometry involves superimposing two waves to detect differences between them, this technique is extremely sensitive and is able to detect changes as small as a half wavelength of the light used. For example, a Helium-neon laser has a wavelength of 632.8 nm [141] thus using optical interferometry could detect changes as small as 316.4 nm. The intensity of two overlapping laser beams is not simply the summation of individual intensities but is given by Equation 3-1 below

$$I = I_1 + I_2 + 2 \sqrt{I_1 I_2} \cos \left[ 2 \pi \frac{(r_1 - r_2)}{\lambda} \right] \quad (3-1)$$

where  $I$  denotes intensity,  $r$  denotes the path length of the laser and the subscripts 1 and 2 denote the incident and reflected laser beams. Thus it can be seen that when the path length  $(r_1 - r_2)$  is an integer multiple of wavelengths then constructive interference occurs causing the total intensity to be four times that of a single beam. Conversely, if the path length is an integer plus one half wavelength then destructive interference occurs causing the intensity of the beam to be zero.

Figure 3-4 shows how a typical vibrometer is constructed. It can be seen that the laser beam is split into two components, a reference beam (shown in green on Figure 3-4) and a measurement beam (shown in red on Figure 3-4). This is achieved through a beam splitter (BS1). The measurement beam is then passed through a second beam splitter (BS2) before being optically focussed on the test object. The reflected beam is then passed to a third beam splitter (BS3) where it is combined with the reference beam and directed to the detector. Since the path length of the reference beam is constant then movement of the test object will produce dark and light interference fringes. A complete dark-bright cycle corresponds to one half wavelength of movement from the test object which in the case of a helium-neon laser is 316.4 nm. Unfortunately this set-up cannot distinguish the direction of movement and a Bragg cell is used for this purpose. The Bragg cell modulates the reference beam by 40 MHz thus generating a modulated fringe pattern when the object is at rest. If the object moves toward the laser this modulated frequency will decrease and conversely increase for objects moving away from the laser. Thus the system is now capable of detecting not only movement but also the direction in which it occurs.

The 3D LDV used in these studies is a Polytec CLV-3D as shown in Figure 3-5 and uses the same principal but has three laser beams 120° apart inclined at a 12° angle such that all three beams cross at a single point. This allows the velocity in all three axes to be measured accurately over a wide frequency range, up to 250 kHz in this case. This system has the advantage of being a non-contact method thus there is no effect from the added mass of an accelerometer; which is significant for lightweight test structures or those of small size. Also, since it can measure three directions simultaneously, it greatly reduces the time required to obtain measurements and reduces the complexities of using tri-axial accelerometers. Unfortunately, the 3D laser vibrometer has its limitations. It is only able to

measure velocities up to 1.5 m/s, this means that at a frequency of 20 kHz a maximum displacement of 12  $\mu\text{m}$  can be accurately measured and this displacement obviously gets smaller as the frequency increases. Due to the small amplitudes required to obtain good modal data this limitation is no great issue however, at the operating levels of power ultrasonic devices the amplitudes may be significantly large to prevent the laser vibrometer from obtaining accurate results.



Figure 3-5 – Polytec 3D LDV [166]

### 3.3.4 Signal Processing

Once the measurement signals have been collected they require to be processed to be in a useful form for the extraction of modal data. Acquiring accurate data with minimal noise is by far the most important aspect of modal testing. In order to transform data from the time domain to the frequency domain, a Fast Fourier Transform (FFT) is applied. Thus the data must satisfy the needs of this process. The major requirement of this process is that all the signals must be periodic in nature. Some forms of input signal, such as random excitation, are not periodic. Also, the response of a lightly damped structure may take an extremely long time to reduce to zero and so the response is not periodic. Periodicity is fundamental to the application of a FFT, if the data does not satisfy this need then a phenomena known as leakage occurs. This is a serious problem for the extraction of modal data as it causes a distortion in the data in the frequency domain as the signal ‘leaks’ into nearby frequencies. Figure 3-6 illustrates this problem succinctly. This figure shows the frequency spectrum of a sine wave of frequency,  $f$ , when the sampled data period is timed to be exactly a set number of wavelengths thus being periodic and when the sampled data period is slightly longer.

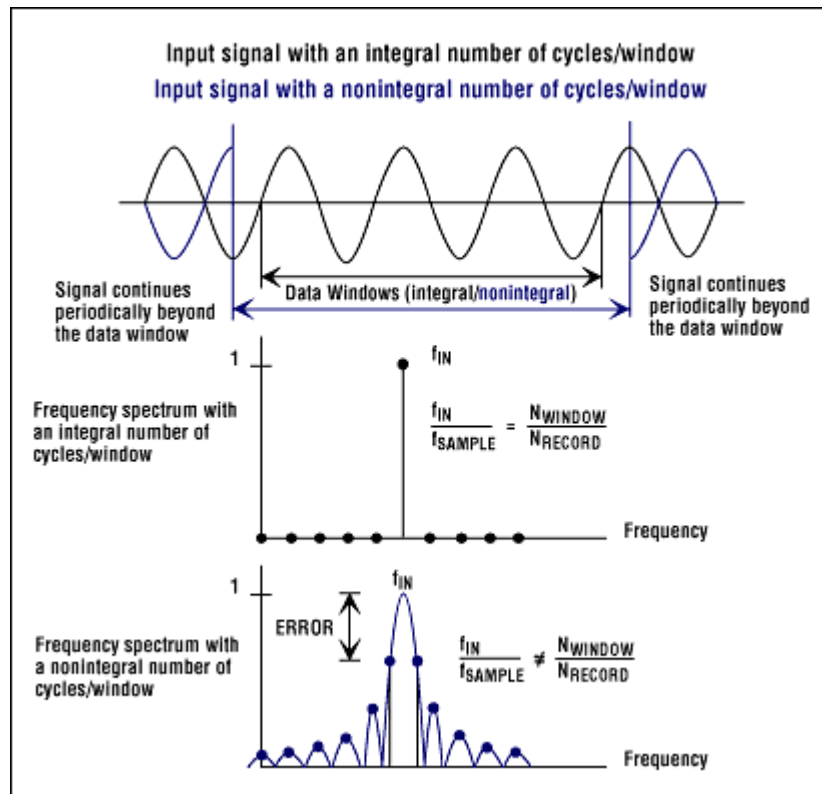
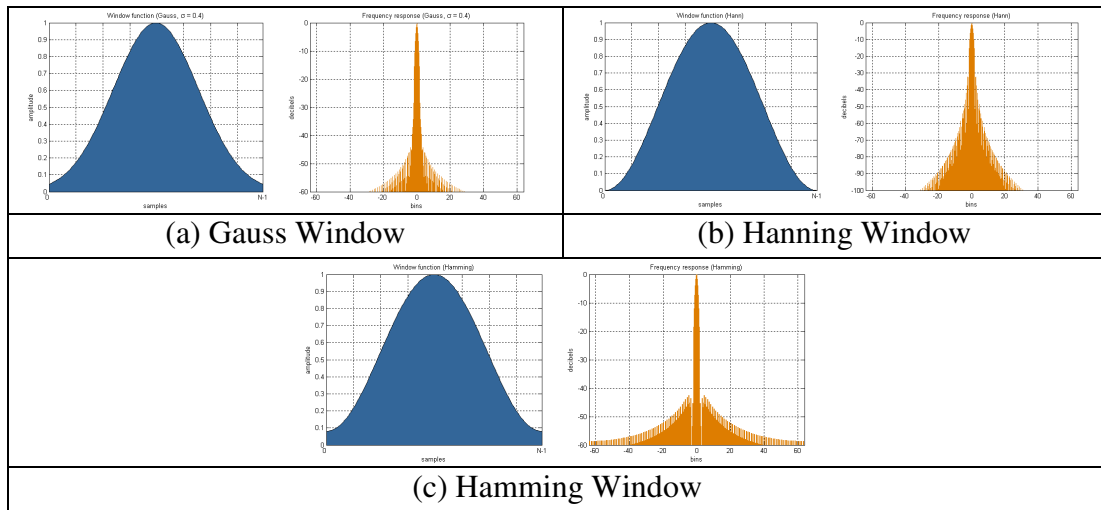


Figure 3-6 – Effect of non-periodic measurements on FRFs (leakage) [168]

In order to combat this, a window is applied to the data. This forces the data to zero at the beginning and end of the window thus satisfying the periodicity requirement for the FFT. There are many types of window available with the most popular being Gauss, Hanning, Hamming, which are used for transient signals (such as random, burst random, sine chirp) and Exponential windows which are popular with impact hammer testing. Figure 3-7 shows the effects (a) Gauss, (b) Hanning and (c) Hamming windows have on the leakage of non-periodic data.





**Figure 3-7 – Effect of windows on leakage (a) Gauss window, (b) Hanning window and (c) Hamming window**

It can be seen that compared to Figure 3-6 the application of these windows has significantly reduced the problem of leakage though it has to be noted that the only way to eliminate the problem is to capture entirely periodic data. Once the requirements of the FFT have been satisfied through the use of an appropriate signal or through windowing it is prudent to ensure that the signal quality is satisfactory. This is normally achieved by analysing the coherence of the FRF. The coherence measures how the output signal is related to the input signal. Ideally the coherence should be a value of unity throughout the frequency range of interest, although spikes will tend to occur at the points of anti-resonance. Large variations in the coherence indicate a poor measurement or problems with the experimental configuration which should be addressed before proceeding.

### 3.3.5 Frequency Response Function (FRF)

Frequency response functions are used to describe the force-response characteristics of any system. They are vital for the determination of the modal parameters; natural frequencies, damping and mode shapes. To obtain a FRF it is necessary to measure both the input force and output response of the structure under examination. Taking a single degree of freedom system as shown in Figure 3-8 with mass  $m$ , stiffness  $k$  and damping  $c$  it is possible to determine the response of the system,  $y(t)$  to a forcing input,  $f(t)$ .

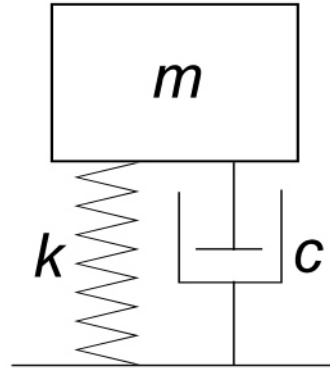


Figure 3-8 - Single degree of freedom system with mass  $m$ , stiffness  $k$  and damping  $c$

Given a forcing function of the form,

$$f(t) = f e^{i\omega t} \quad (3-2)$$

The response is assumed to be of the form

$$y(t) = y e^{i\omega t} \quad (3-3)$$

Thus the equation of motion becomes

$$f e^{i\omega t} = m \frac{d^2}{dt^2} y(t) + k y(t) + c \frac{d}{dt} y(t) \quad (3-4)$$

$$f e^{i\omega t} = (m \omega^2 + i \omega c + k) y e^{i\omega t} \quad (3-5)$$

The response can be measured as displacement, velocity or acceleration, depending on the measurement transducer used. For the LDV measurement, the velocity response is measured. The mobility FRF is defined as the ratio between the harmonic velocity response and the harmonic force, thus

$$H(\omega) = \frac{\frac{d}{dt} y(t)}{f e^{i\omega t}} \quad (3-6)$$

This gives the FRF for a single degree of freedom as

$$H(\omega) = \frac{i \omega y}{f} \quad (3-7)$$

It can be seen that the FRF is a complex function containing both real and imaginary parts thus requires to be viewed in three dimensions of phase, magnitude and frequency to be fully appreciated. However, plotting three dimensions is not practical and the FRF is normally represented as a combination of plots including magnitude v frequency and magnitude v phase. The combination of these two plots is commonly known as a bode plot.

Figure 3-9 shows the relationship between the input excitation and structure response in the time and frequency domains.

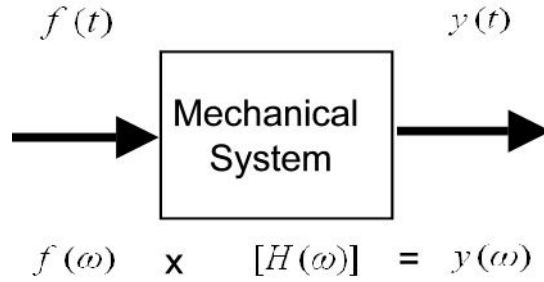


Figure 3-9 - Block diagram of a FRF

Directly measuring the input force and output velocity it is possible to obtain an FRF for each selected degree of freedom for any point in the system. However, these measurements tend to be taken in the time domain and a fast Fourier transform (FFT) is used to transform the measurements from the time domain into the frequency domain. It is likely that the signals acquired from an EMA have noise present and it is useful to know the quality of the FRF obtained at any measurement point. The quality of the FRF is defined by the ordinary coherence. This measures the degree of causality in a FRF function and varies from zero, where no proportion of the input signal is responsible for the output, to one, where all the output is caused by the input. Considering the case of a single force and single response it can be shown that the force-response equation is

$$(F_q - v_q) H_{pq} = X_p - n_p \quad (3-8)$$

where  $v$  and  $n$  are the errors associated with the input and output signals respectively. To minimise the errors associated with the input and output signals, several measurements are taken and averaged. Taking the number of measurements as  $N$ , the cross-power spectra and auto-power spectra are defined as

$$G_{XF_{pq}} = \sum_1^N X_p F_q^* \quad (3-9)$$

$$G_{FX_{qp}} = \sum_1^N F_q X_p^* \quad (3-10)$$

$$G_{FF_{qq}} = \sum_1^N F_q F_q^* \quad (3-11)$$

$$G_{XX_{pp}} = \sum_1^N X_p X_p^* \quad (3-12)$$

Where  $X_p^*$  and  $F_q^*$  are the complex conjugate of  $X(\omega)$  and  $F(\omega)$  respectively.

These spectra are the result of the application of the FFT algorithm to statistical cross-correlation and auto-correlation functions. These algorithms cannot be applied on the directly measured excitation and response signals when using random excitations as they are not periodic.

The frequency response function can be calculated using either the  $H_1$  or  $H_2$  method. The  $H_1$  method minimises noise on the output signal while  $H_2$  minimises noise on the input signal.

$$H_1 = \frac{G_{XF_{pq}}}{G_{FF_{qq}}} \quad (3-13)$$

$$H_2 = \frac{G_{XX_{pp}}}{G_{FX_{qp}}} \quad (3-14)$$

The ordinary coherence is defined as

$$COH_{pq} = \frac{G_{XF_{pq}} G_{FX_{qp}}}{G_{FF_{qq}} G_{XX_{pp}}} \quad (3-15)$$

It can be seen that the coherence function is frequency dependant and will vary between zero and one. Ideally the coherence should be unity across the frequency spectrum with spikes being observed at the anti-resonances of the system due to the very low vibrational response at these points.

### 3.3.6 EMA curve fitting methods

Once measurement data has been obtained it is necessary to fit this data to an analytical function for the modal parameters to be estimated. There are several curve fitting algorithms available and can be categorised as either local single degree of freedom (SDOF) or local multiple degree of freedom (MDOF).

Local SDOF procedures estimate modal parameters one mode at a time and are very accurate for structures with a low modal density. This method uses three procedures to determine the modal parameters of frequency, modal damping and mode shape. Firstly, the frequency of a resonant peak is taken as the modal frequency. The frequency of a resonant

peak will be visible in every FRF with the exception of those measurements taken at node points. The accuracy of this method is dependant on the frequency resolution of the measured data but can, in general, be considered a good approximation. The modal damping is estimated by measuring the width of a resonant peak at the half power points. This width corresponds to twice the modal damping in Hz. Finally, the mode shapes can be determined by taking the peak values from both the imaginary and real parts of the FRF. In this way all the modal parameters of a system can be estimated.

Local MDOF methods also work on one FRF at a time but have the capability to determine several modes simultaneously. These algorithms are useful for the determination of modal parameters for systems with high modal density or heavy damping. The complex exponential and rational fraction polynomial are the most common methods employed. The complex exponential method is used to fit experimental impulse-response data to an analytical expression of the form shown in Eq.3-16.

$$\left[ H(t) \right] = \sum_{k=1}^m e^{\frac{-\lambda_k t}{m \omega}} \sin(\omega t) \quad (3-16)$$

This method calculates the system poles in the time domain and therefore requires an inverse FFT to be applied to the data. Unfortunately, this process causes a degree of leakage distorting the data. However, this method has the advantages of being computationally efficient and numerically stable and is widely used for these reasons.

The rational fraction polynomial (RFP) method applies Eq.3-17 to the measured data where  $a$  and  $b$  are polynomial coefficients. The degrees of the polynomials need to be specified, however the degree of the polynomial on the denominator is always twice the number of modes. This method can be applied over any frequency range, meaning the accuracy at resonant frequencies can be increased by increasing the number of polynomial terms in the numerator of Eq.3-17.

$$H(\omega) = \frac{\sum_{k=0}^N a(j\omega)^k}{\sum_{k=0}^{2m} b(j\omega)^k} \quad (3-17)$$

The mode shapes can be visualised by animating the deformations at the natural frequencies of interest. This information can then be used to validate the FEA design or adjust the FEA model such that it more closely matches the experimental observations.

### 3.4 Horn Designs

#### 3.4.1 Nomenclature

Throughout this thesis, reference is made to several terms regarding the different parts associated with the radial horn design. Figure 3-10 figuratively shows the general design of a radial horn used in these studies and the parts which will be referred to.

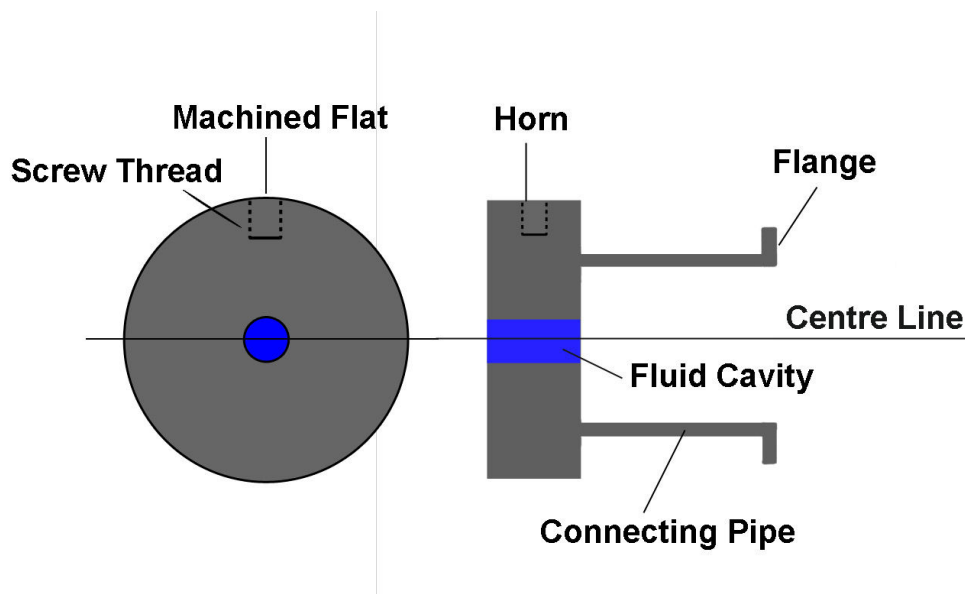


Figure 3-10 –Cross section view of the parts in a radial horn

The thick cylindrical mass is termed the ‘horn’ and this part is tuned to the desired radial mode at the operating frequency. The horn has a machined flat surface with a screw thread for the attachment of a transducer. The inner volume of the horn has been termed the ‘fluid cavity’ as this is the volume in which the bacteria laden fluid will be held for treatment. The horn is attached to a cylindrical connecting pipe which in turn is connected to a mounting flange. This cylindrical connecting pipe is tuned to ensure that its presence does not affect the vibratory motion of the horn. This allows the device to be mounted onto a surface for testing. Figure 3-11 shows an elevation view of a radial horn tuned to the R0 mode with attached transducer.



Figure 3-11 – Radial horn with attached transducer elevation picture

### 3.4.2 Radial Horns

This research is concerned with the use of ultrasonic horns operating in a radial mode to effect bacterial inactivation. These horns have been designed using the finite element package ABAQUS 6.6-4 and experimental modal analysis has been carried out using a 3D Laser Doppler Vibrometer (Polytec CLV-3D) with the ME'scope modal analysis VES package to validate the designs. Ultrasonic horns vibrating in the fundamental radial mode can be designed using an approximate analytical solution which states that the fundamental radial mode of an annular disk can be found by making the mean circumference an integral number of wavelengths as shown in Equation 3-18 [142]

$$k(R_1 + R_2) = 2n \quad (3-18)$$

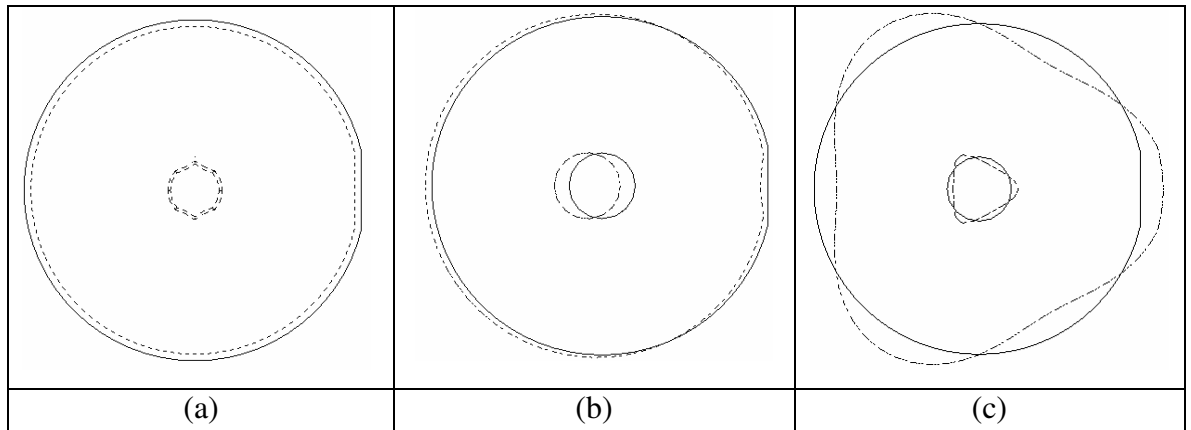
where  $R_1$  is the inner radius,  $R_2$  the outer radius and  $k$  the wave number. The wave number is defined as  $\omega/c_r$  where  $\omega$  is the angular frequency ( $\omega=2\pi f$  where  $f$  is frequency in Hz) and  $c_r$  the wave velocity which is related to the Young's Modulus ( $E$ ), density ( $\rho$ ) and Poisson's ratio ( $\nu$ ) by Equation 3-19

$$c_r = \sqrt{\frac{E}{\rho(1 - \nu)}} \quad (3-19)$$

and  $n$  is an integer which relates to the number of wavelengths of the system.

This analytical solution provides an excellent starting point from which a design process can take place, however it is not appropriate to use it as the only design tool. It has been shown that ultrasonic radial horns operating in the fundamental mode are susceptible to having several modes of vibration in a narrow frequency range [142] and particularly the R0, R1 and R3 modes are known to occur close to the fundamental mode (mode shapes shown in Figure 3-12). In order for the horn to operate as required it is imperative that these modes are separated sufficiently such that modal coupling is minimised or ideally

eliminated. Modal coupling will cause the horn to vibrate in a shape that contains portions of the pure modes and can lead to inefficiency or reduced horn life. Also, the effect of the addition of flat sections for the attachment of a transducer, and the addition of connecting pipes and flanges, cannot be incorporated into the analytical model. Thus, it is necessary to use finite element analysis in the design stage to determine the modal frequencies and shapes surrounding the fundamental mode.



**Figure 3-12 – Radial modes of vibration (a) R0, (b) R1, (c) R3**

Figure 3-13 shows the design procedure used in the development of the horns. An initial estimate of the material properties is made as the material properties are not known exactly due to small differences in the manufacture of the material. The hypothesis of this thesis is based upon the fundamental radial mode concentrating vibrations to the centre of the cavity and hence the mode to which the horn is to be designed is known to be the fundamental R0 mode. It has been shown in Chapter 2 that bacterial inactivation is due to cavitation caused by ultrasonic vibrations and that at lower ultrasonic frequencies cavitation is easier to initiate due to the longer rarefaction cycle available to create bubbles, thus it was decided to design the horn to operate at 20 kHz. Using this information and choosing a nominal internal diameter of 31 mm, Equation 3-2 was used to obtain an approximate outer diameter of the horn of 168 mm. The thickness of the horn is 45 mm which serves to place other flexural modes far higher in the frequency spectrum than the radial modes, thus during the design stage it will only be necessary to separate the radial mode frequencies and not the radial from other flexural modes.



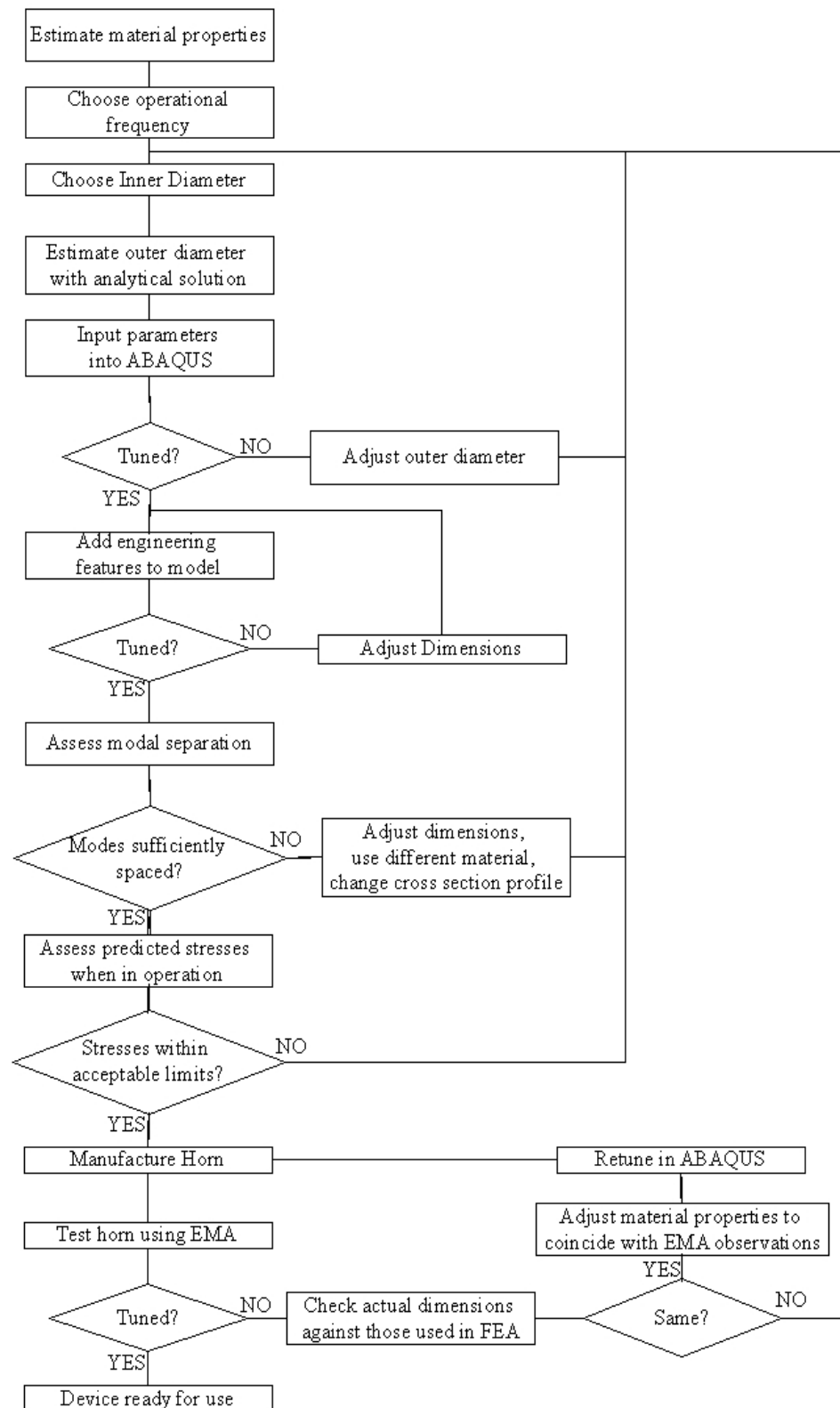
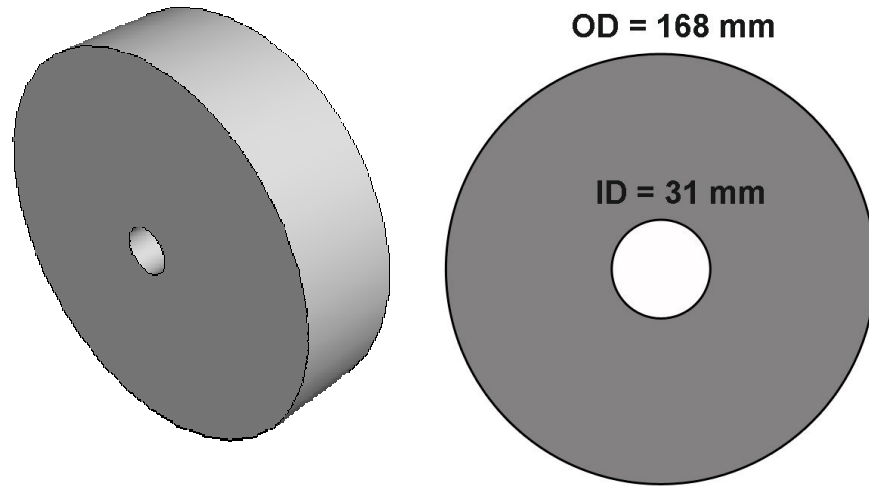


Figure 3-13 – Design process for the design of radial ultrasonic horns

ABAQUS was employed to calculate the mode shapes and associated frequencies. To this end, a mesh density study was initially carried out to ensure the results were converged (Table 3-1). The mode shapes and frequencies are extracted using the ABAQUS Lanczos solver in the frequency range of 10-30 kHz. This analysis shows that the FE model predicts there are 17 modes in this frequency range.



**Figure 3-14 – Simple radial horn (left), dimensions used (right)**

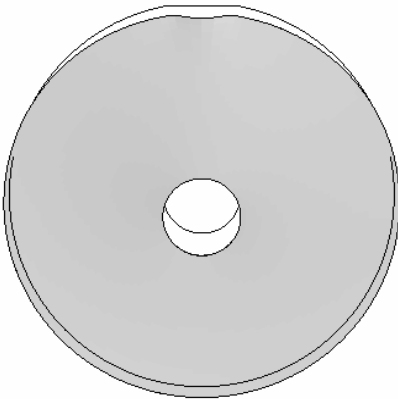
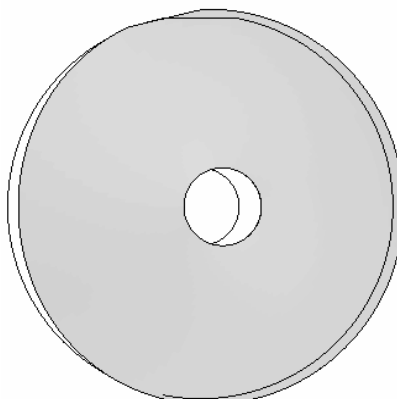
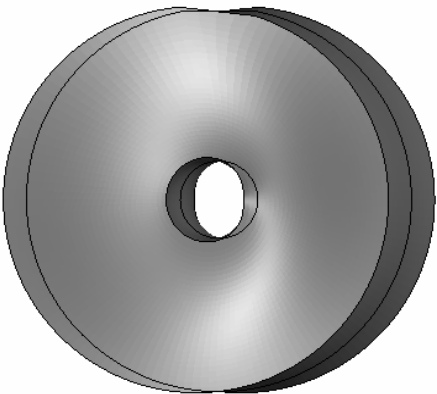

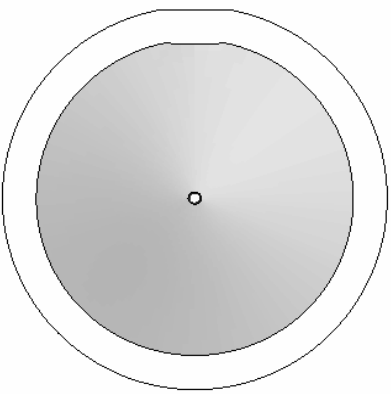
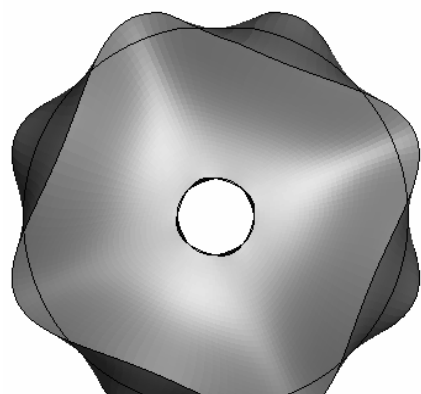
Figure 3-14 shows the radial horn referred to as  $R0_{ID30}$  while Table 3-1 shows the results from the mesh density study. It can be observed that convergence is dependent upon the mode shape and that a solution will converge with fewer elements for lower mode numbers. Table 3-1 shows that the R0 mode requires a minimum of 300 elements to reach a converged solution while the R1 and R3 modes require a minimum of 980 and 4608 elements respectively.

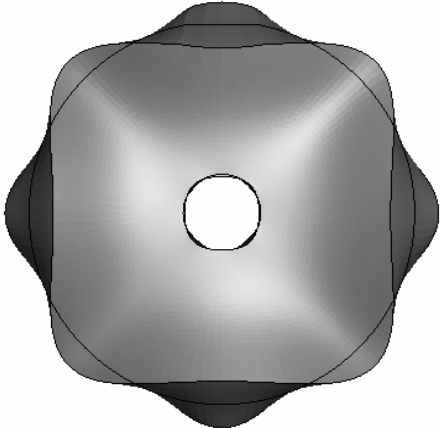
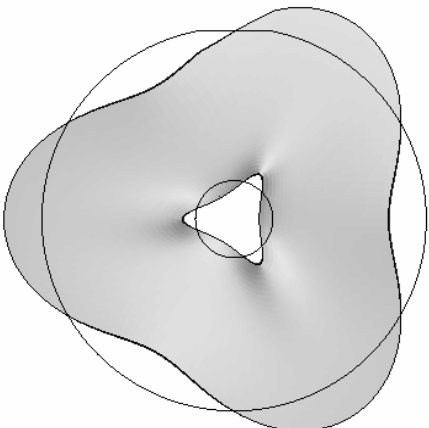
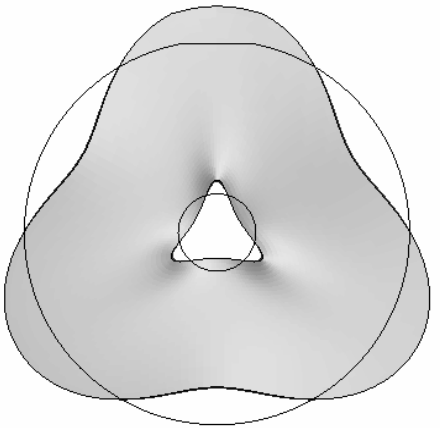
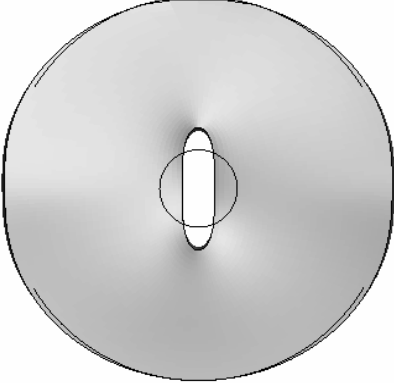
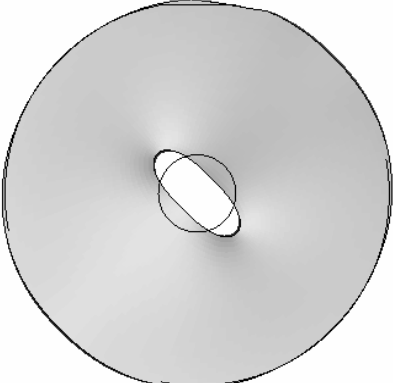
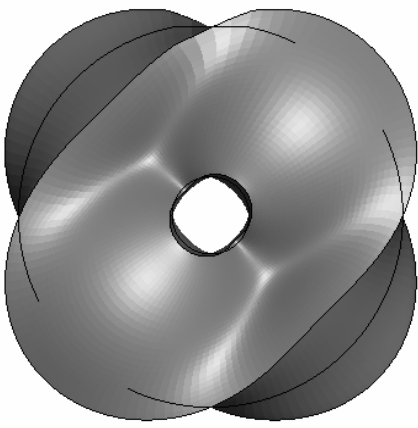
No. of Elements	R0 (Hz)	R1 (Hz)	R3 (Hz)
8	20132	17270	21679
24	20047	17011	22255
48	20043	17010	22259
72	20036	16997	22210
128	20033	16998	22158
300	20032	16985	22142
980	20032	16983	22133
1944	20032	16983	22131
4608	20032	16983	22130
5408	20032	16983	22130

**Table 3-1 – Mesh density study of the  $R0_{ID30}$  mode radial horn**

Figure 3-15 shows the predicted mode shapes and associated frequencies between 10 and 30 kHz for the R0<sub>ID30</sub> mode radial horn design. It can be seen there are 9 different modes with the analysis capturing several of the dual modes as well. Dual modes are analytical in nature due to the way eigenvectors and eigenvalues are extracted by the FE analysis. In theory they should occur at exactly the same frequency but due to small asymmetries (like the flat for the attachment of the transducer) there is often a small difference in the frequency obtained. There are 5 radial modes and 4 anti-symmetric modes in this frequency range with the R0 mode at the tuned frequency of 20032 Hz. Further, the modes above and below the tuned frequency are 1760 and 1797 Hz away from the tuned mode respectively. Previous studies suggest that a frequency separation of the tuned mode from other non-tuned modes of 1200 Hz is necessary at 20 kHz to ensure there is no significant modal coupling [167]. This figure is dependant on the specific electronics of the generator-transducer system due to the ability of modern generators to track the resonance frequency within a small frequency range. If modes are not separated sufficiently it is possible that the generator-transducer system will track to the undesired mode. It is known that the generator and transducer used in these studies can track the resonance frequency to  $\pm 1$  kHz, thus this design is sufficient to prevent modal coupling from taking place which could reduce the effectiveness of the device.

In Figure 3-15 the following nomenclature has been used for the description of mode shapes. Modes where there is no axial variation in the displacement along the horn length are defined as radial modes and are denoted by the prefix R followed by a number indicating the order of the mode. The order of the mode is defined as half the number of nodes in the mode shape. Thus a radial mode with 6 nodes would be defined as R3. Further, each mode predicted by the FEA has a dual mode which is  $\frac{1}{4}$  wavelength displaced. Anti-symmetric modes have been defined as where the mode shape is such that there is axial variation in the displacement. Again, the order of these modes is defined as half the number of nodes present in the mode shape. Further, in order to display the mode shapes sufficiently the displaced shapes have been greatly amplified.

	
(a) R1 mode, 16983 Hz	(b) R1 dual mode, 17536 Hz
	
(c) R1 anti-symmetric mode, 18244 Hz	(d) R1 anti-symmetric dual mode, 18272 Hz
	
(e) R0 radial mode, 20032 Hz	(f) R4 anti-symmetric mode, 21829 Hz

	
(g) R4 anti-symmetric dual mode, 21952 Hz	(h) R3 radial dual mode, 22100 Hz
	
(i) R3 radial mode, 22130 Hz	(j) R2 radial mode, 25952 Hz
	
(k) R2 Radial dual mode, 26112 Hz	(l) R2 anti-symmetric dual mode, 28222 Hz

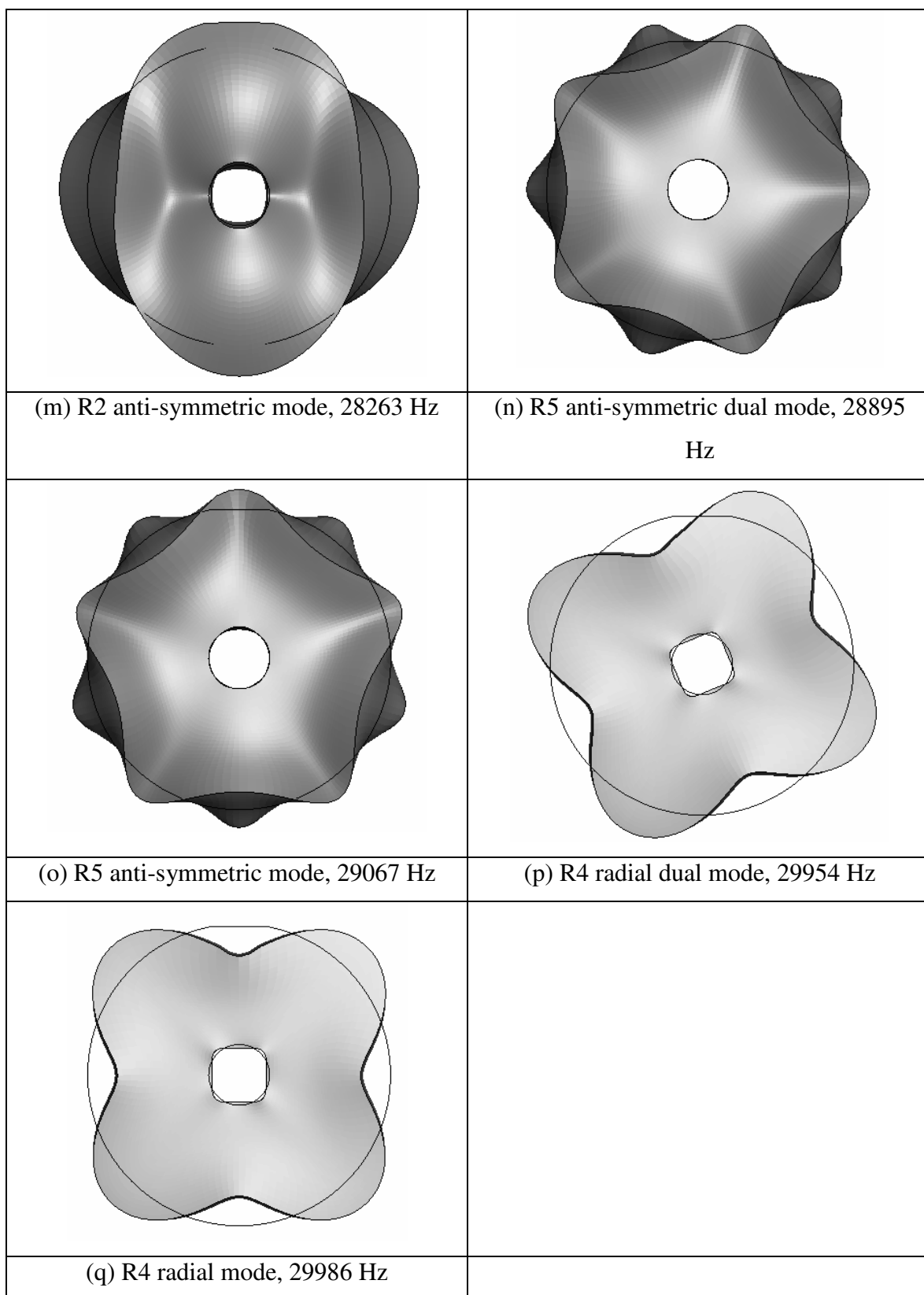


Figure 3-15 – R0<sub>ID30</sub> radial horn modes from 10-30 kHz. Solid black line indicates undeformed shape.

It can be seen that the R0 mode occurs extremely close to the desired 20 kHz operating frequency and the R1 and R3 modes are separated from the R0 mode by 3049 Hz and 2098

Hz respectively. Adjustments were then made to the horn material properties to assess the sensitivity of the design to small changes in the material, these can be seen in Table 3-2. Values were chosen to represent the typical range of stiffness and density of aluminium alloy.

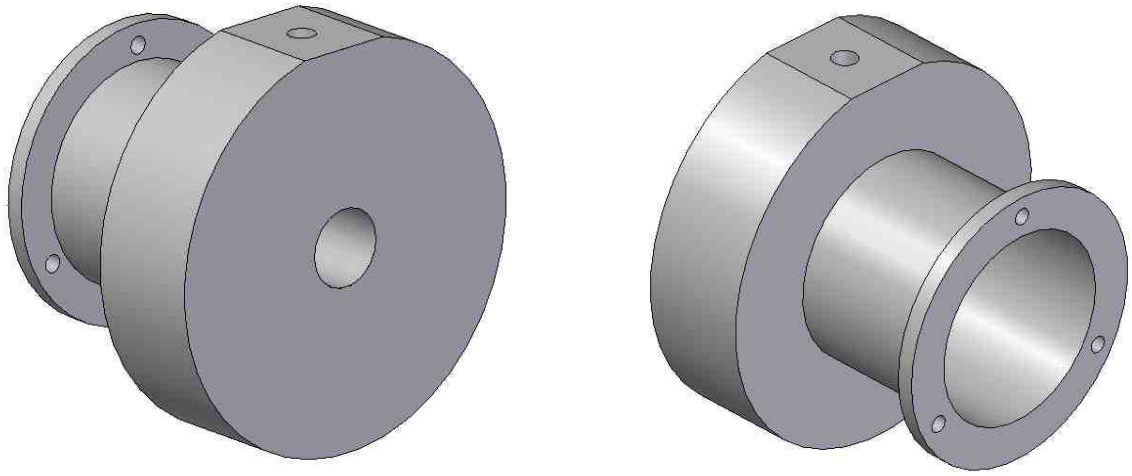
Stiffness (E) (GN/m <sup>2</sup> )	Density ( $\rho$ ) (kg/m <sup>3</sup> )	R0 (Hz)	R1 (Hz)	R3 (Hz)
69	2600	20124	17061	22232
70	2600	20269	17184	22393
71	2600	20413	17306	22552
69	2700	19748	16742	21816
70	2700	19890	16863	21974
71	2700	20032	16983	22130
69	2800	19392	16440	21423
70	2800	19532	16559	21578
71	2800	19671	16667	21732

**Table 3-2 – Effect of material parameters on FE modal analysis results**

It can be observed from these results that the horn design is not significantly sensitive to small changes in material properties as an increase in stiffness of 1 GN/m<sup>2</sup> results in the R0 mode being shifted upwards approximately 140 Hz while an increase in density of 100 kg/m<sup>3</sup> results in a downward shift of 376 Hz. Thus, the accurate determination of these properties is not required before the manufacture of the horn. Once manufactured, the horn will be tested experimentally to determine the mode shapes and frequencies with minor frequency tuning adjustments being made by skimming the outer and/or inner surfaces to achieve resonance at the desired frequency.

Since the basic design of the horn has been shown to be viable it is now necessary to consider the engineering features the horn will require to be functional. The design of the horn could be kept as it is currently, however this poses practical issues for the experimental testing stage. As the design currently stands the horn would be placed inside a pipe for testing. Due to the dimensions of the horn, the pipe would be large and it is not yet known how efficient the device will be at bacterial inactivation, thus using large volumes of fluid to be treated would be unwise. Further, it is not known how much power will be required to cause cavitation and whether the fluid loading will mean that the ultrasonic generator is unable to provide sufficient power to cause cavitation. Hence it is necessary to design the device such that a minimum fluid loading is applied while allowing experimental data on the bacterial efficacy of the device to be obtained. The horn was thus

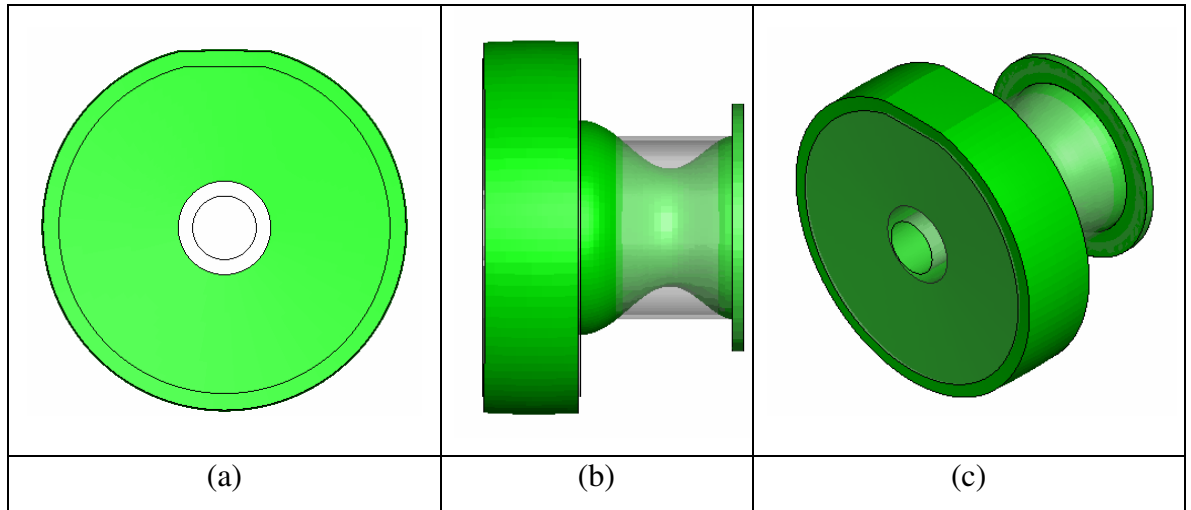
designed with a short pipe section with a connecting flange (Figure 3-16). Also, it is necessary to connect the ultrasonic transducer to the radial horn and so a small flat is incorporated on the horn.



**Figure 3-16 – Radial horn design**

This design allows for the horn to be mounted on a base and for the fluid to be treated to be placed within the cavity, keeping the treated volume and fluid loading small. In order for the maximum vibration transmission into the system it is necessary that all the parts work together dynamically, thus the pipe and flange sections should not hinder the vibration of the horn. To this end, the pipe and flange section are of length such that the end of the flange is coincident with a node point. This will mean that when connected to the base, the flange will naturally have only small vibratory motion allowing for an excellent seal at the connection to the base. The pipe diameter is such that it also vibrates in the radial mode at 20 kHz and will naturally vibrate with the horn and not oppose the motion of the horn, thus allowing the maximum energy transfer to the centre of the horn. A finite element analysis was carried out to confirm that the connecting pipe and flange operate as desired. Figure 3-17 shows the results of this analysis. It can be seen that the horn and connecting pipe both vibrate in the radial mode and thus the connecting pipe will not interfere dynamically with the vibratory motion of the horn.





**Figure 3-17 – R0<sub>ID30</sub> Radial horn design including tuned connecting cylinder and flange mode shape at 20 kHz. Deformed shape shown in green and undeformed shape shown in transparent grey. (a) Elevation, (b) End Elevation, (c) Isometric.**

A steady state finite element analysis was carried out on the horn including the pipe section and flange to determine the stresses in the horn when in operation. This type of analysis calculates the stresses and displacements of a dynamic system under constant forced vibration at a point in time when the transient effects of the force have dissipated. A typical displacement of 10  $\mu\text{m}$  was applied to the flat section of the horn and the results can be seen in Figure 3-18. The maximum stress was found to be 45.8 MPa at 10  $\mu\text{m}$  input displacement.

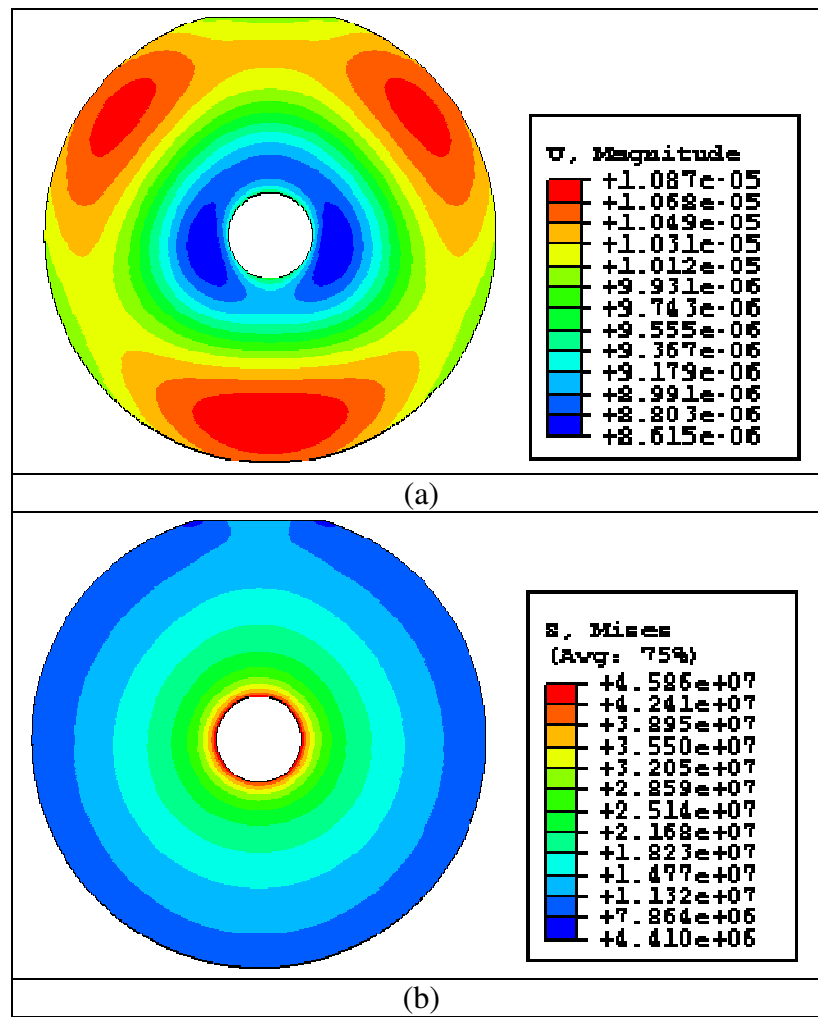
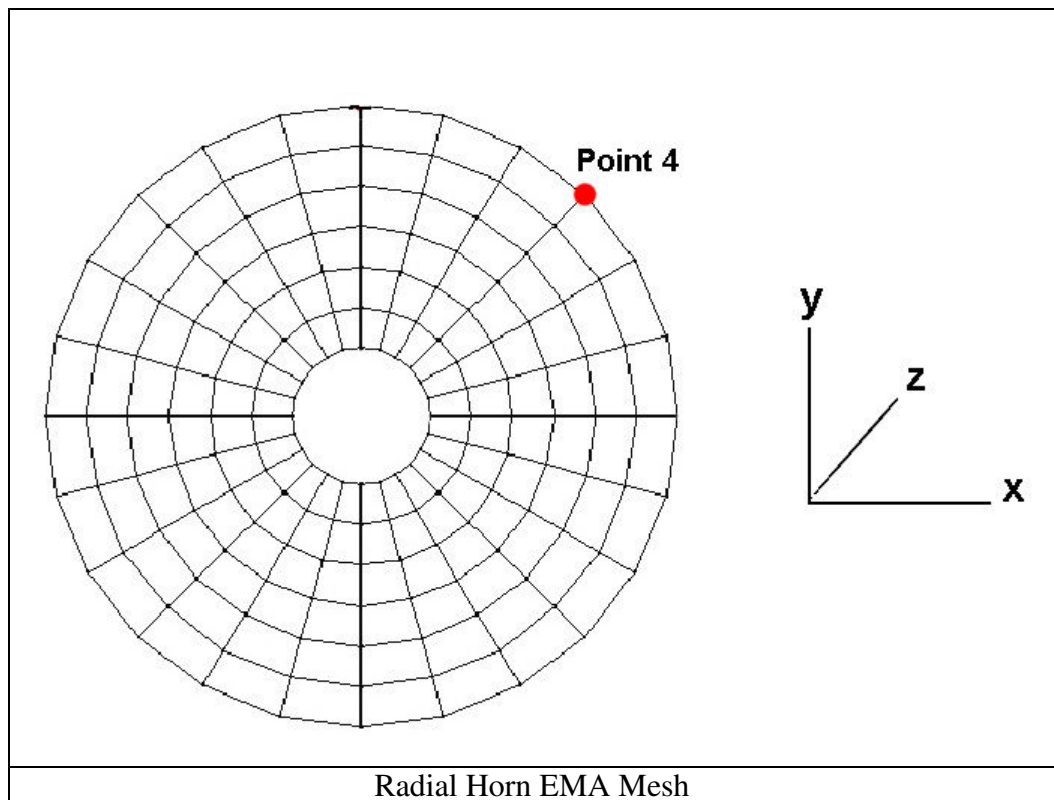


Figure 3-18 – (a)  $R0_{ID30}$  mode radial horn displacement contours for a 10 μm input displacement, large displacements shown in red with small displacements are blue. (b)  $R0_{ID30}$  radial mode horn stress contours for a 10 μm input displacement. Displacements are shown in metres with stresses in  $N/m^2$ .

From the steady state analysis it was found that for a 10 μm input displacement the inner diameter vibrated at an amplitude of 9.7 μm, giving a gain factor of 0.97. Importantly, analysing the von Mises stresses in the horn it was found that the maximum tensile stress of 45.8 MPa occurred at the inner diameter of the horn. The tensile yield stress for the horn material, aluminium 2014, is 414 MPa. Defining the safety factor as the maximum stress divided by the yield stress it can be seen that there is a safety factor of 9.04.

The analytical and numerical studies have provided a design which was manufactured by machining a solid aluminium block to the specified dimensions. In order to confirm that the horn is working in the manner to which it was designed it is necessary to carry out an experimental modal analysis. This analysis determines the actual modal parameters

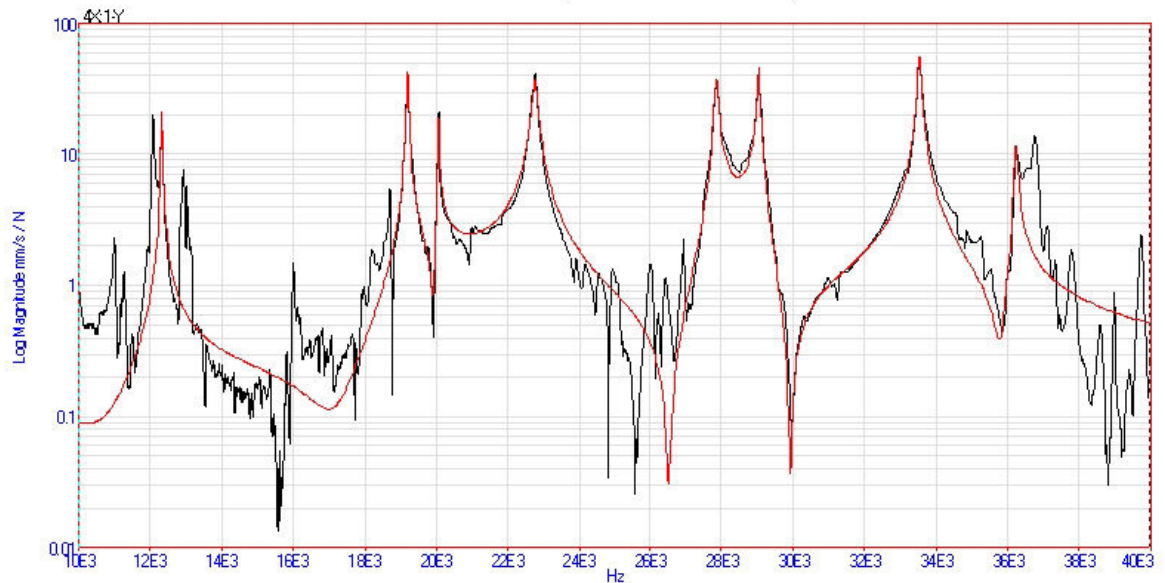
experimentally and is used to validate the finite element design. The EMA is carried out using a dataphysics SignalCalc software and data acquisition unit, amplifier, 3D LDV, 20 kHz transducer and ultrasonic horn to obtain the measurements. These measurements were then analysed using ME'Scope VES modal analysis software. In order to capture the mode shapes accurately measurements are taken from different points on the horn. Measurement points were spaced on the face of the horn such that there were 24 divisions circumferentially and 7 radially giving a total of 168 measurement points as shown in Figure 3-19. The EMA was carried out between 10-30 kHz with a frequency resolution of 12.5 Hz, the highest available. It was found that a swept sine input signal gave measurements with the least noise compared to random and burst random excitation signals, thus a swept sine input was used in the range 10-30 kHz. Measurements were obtained over four sine sweeps, i.e. measurements were obtained while the input signal swept from 10-30-10-30-10 kHz. A Hanning window was applied to ensure all captured signals obeyed the requirement for periodicity.



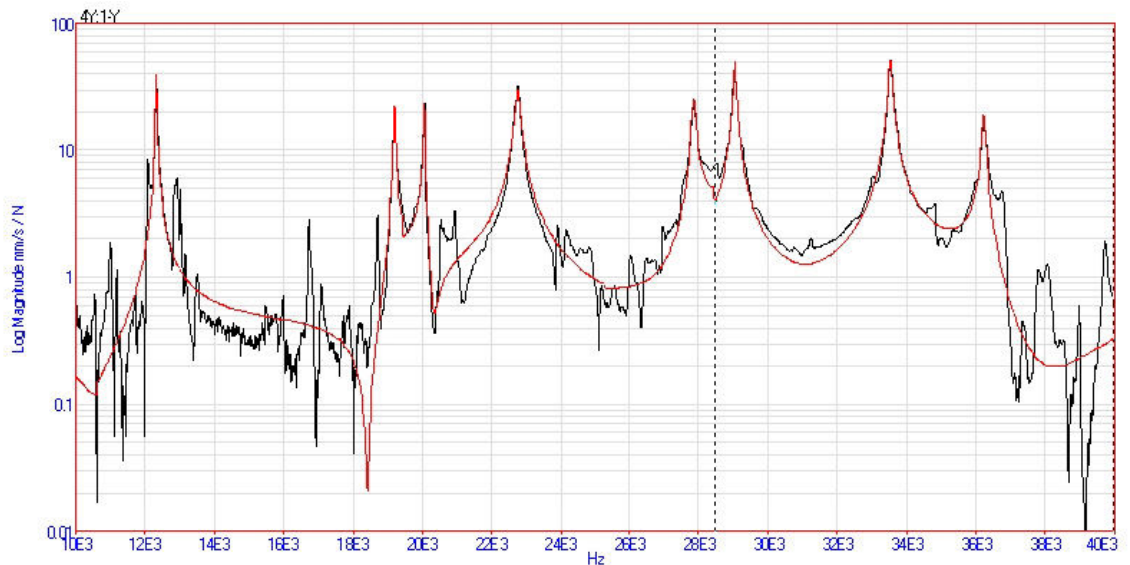
**Figure 3-19 – EMA measurement points for the radial horns**

Figure 3-20 and Figure 3-21 show the data obtained (black) and the curve fit (red) applied by the ME'Scope software for the x, y and z directions at point 4. It can be seen from these

graphs that although there are some discrepancies, overall the software has accurately identified the natural frequencies while neglecting the noise present in the measured data.

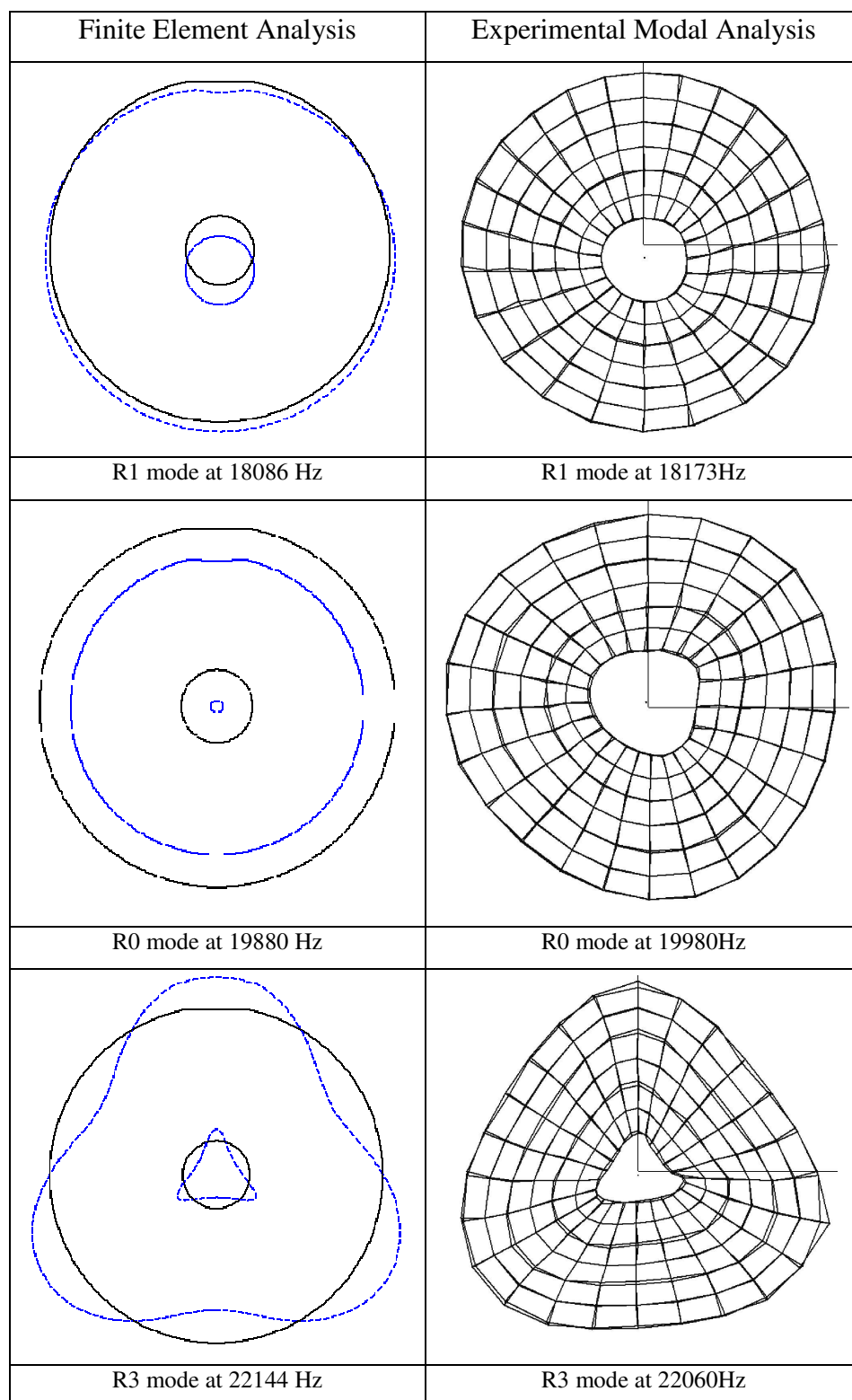


**Figure 3-20 – EMA captured data (black) and curve fit (red) for point 4 in the X direction**



**Figure 3-21 – EMA captured data (black) and curve fit (red) for point 4 in the Y direction**

Taking all the measurements and curve fit data, it is now possible to display the mode shapes at the natural frequencies. Figure 3-22 shows the mode shapes and associated frequencies of the FEA and EMA analyses. The R0, R1 and R3 modes are found to occur at 19980 Hz, 18173 Hz and 22060 Hz respectively. It can be seen that there is excellent correlation between the FEA and EMA results both in terms of mode shape and frequency, thus validating the FE design approach.



**Figure 3-22 – Comparison of the FE predictions (left) and the experimental modal test (right) for the  $R0_{ID30}$  mode radial horn**

FE and EMA analyses were carried out on a second horn to determine its modal parameters. This horn is similar in design but its inner and outer radii are 25 mm and 81.5

mm respectively. The FE model predicts that this horn vibrates in the R3 mode at 19943 Hz while the R0 and R1 modes are located lower in the frequency spectrum at 17150 Hz and 18047 Hz respectively. EMA confirms the FE results; Figure 3-23 shows the mode shapes and frequencies of both the FE and EMA analysis for this horn while Figures 3-24 and 3-25 show the EMA captured data and curve fit for the X and Y directions on point 4. Table 3-3 shows the results from the FEA mesh density analysis of this horn. Since this horn provides an opportunity to test for a different radial mode it will be used to ascertain the influence of mode shape upon the bacterial inactivation rates.

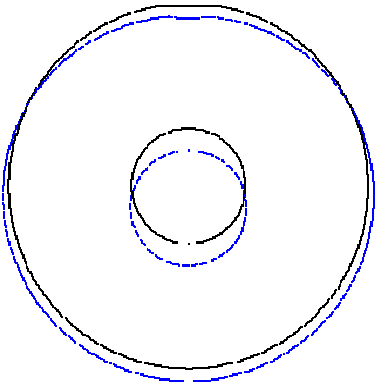
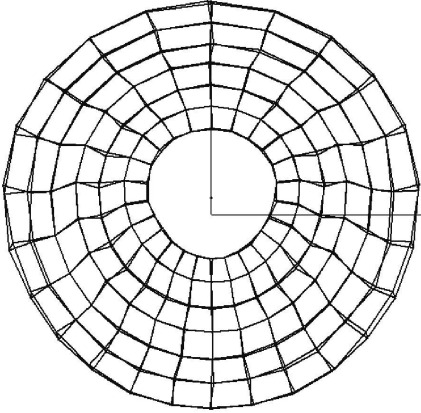
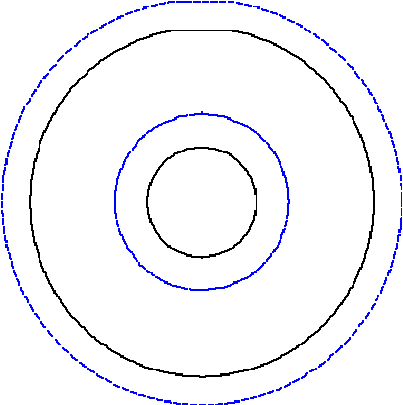
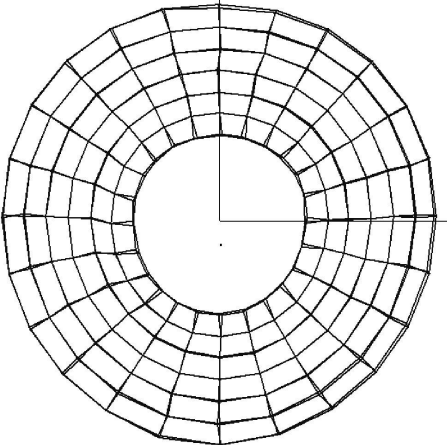
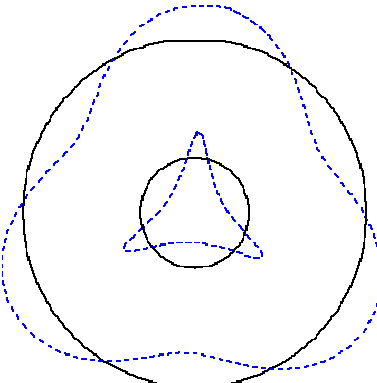
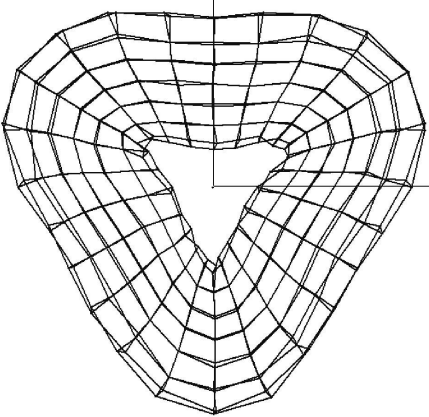
Finite Element Analysis	Experimental Modal Analysis
	
Deformed Mode Shape (R1) at 18047 Hz	R1 mode at 17800 Hz
	
Deformed Mode Shape (R0) at 17150 Hz	R0 mode at 17200 Hz
	
Deformed Mode Shape (R3) at 19943 Hz	R3 mode at 19700 Hz

Figure 3-23 – Comparison of the FE predictions (left) and the experimental modal test (right) for the R3<sub>ID50</sub> mode radial horn

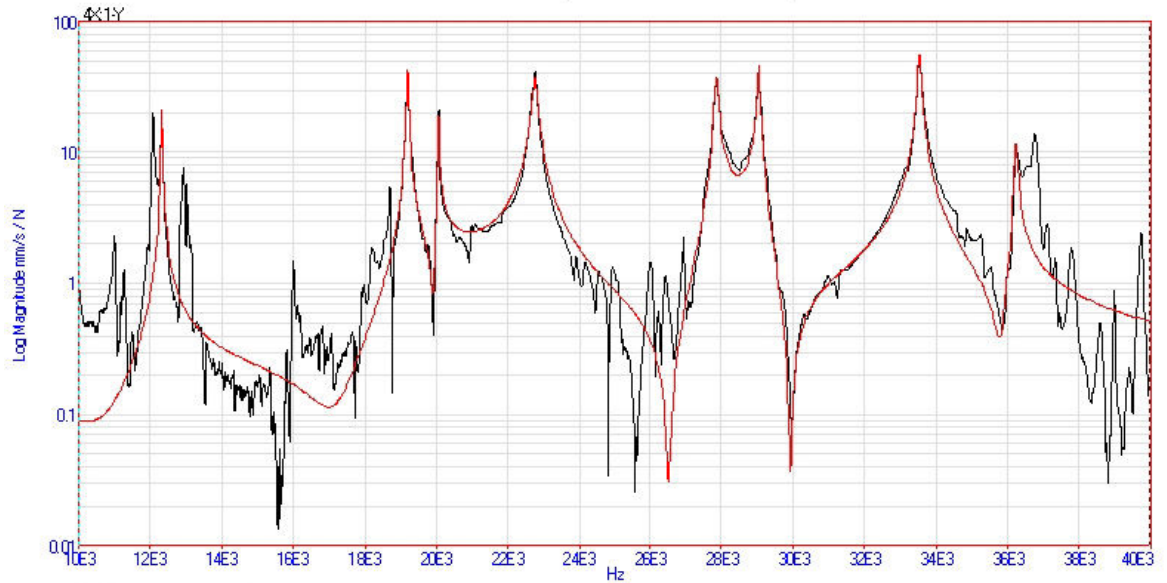


Figure 3-24 - EMA captured data (black) and curve fit (red) for point 4 in the X direction

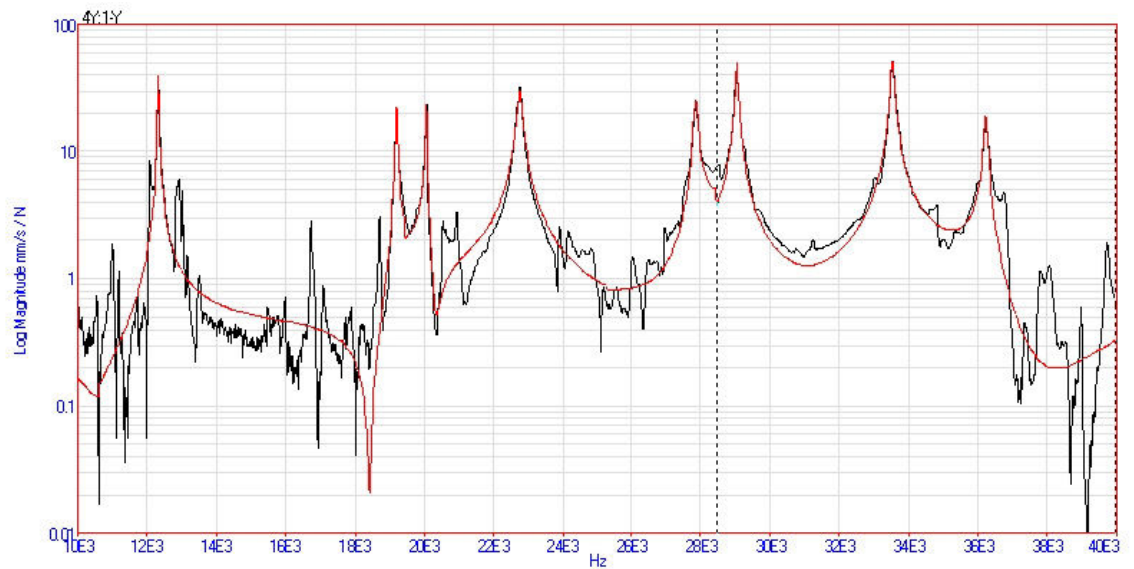


Figure 3-25 - EMA captured data (black) and curve fit (red) for point 4 in the Y direction

No. of Elements	R0 (Hz)	R1 (Hz)	R3 (Hz)
7	17207	18645	23226
11	17148	18239	20318
60	17151	18066	20094
114	17150	18051	19979
800	17150	18046	19941
1680	17149	18046	19934
3816	17149	18046	19933
6336	17149	18046	19932

Table 3-3 – Mesh density analysis of R3<sub>IDS0</sub> mode radial horn



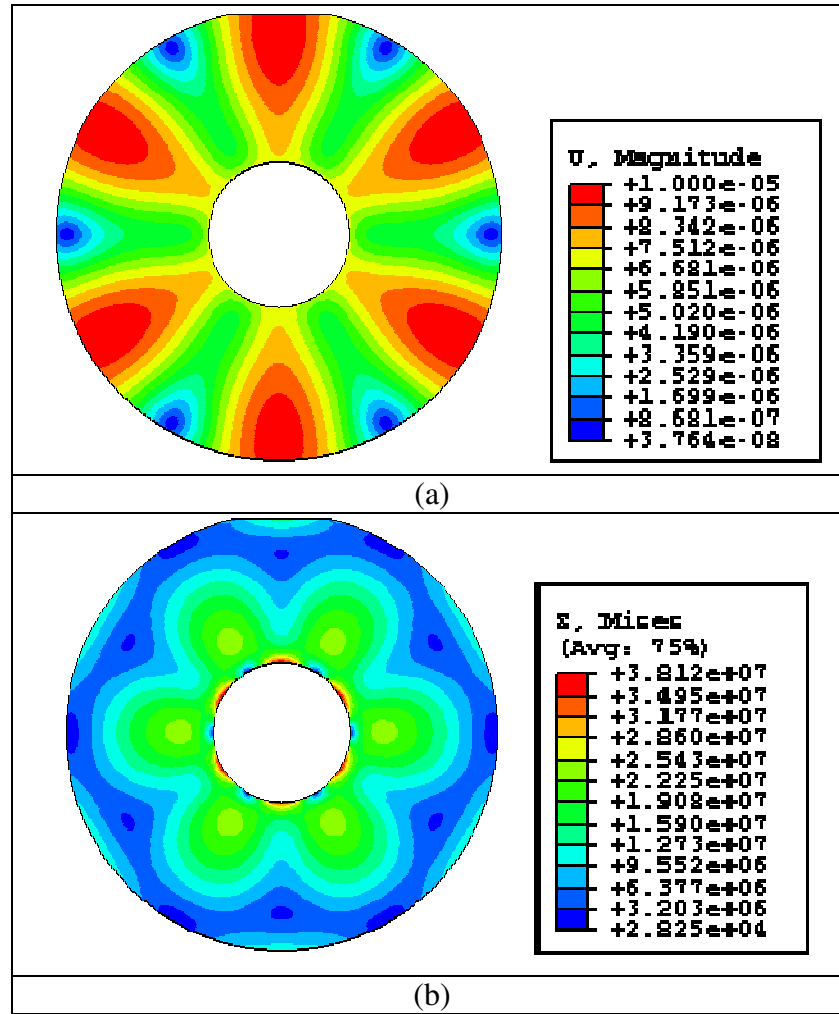
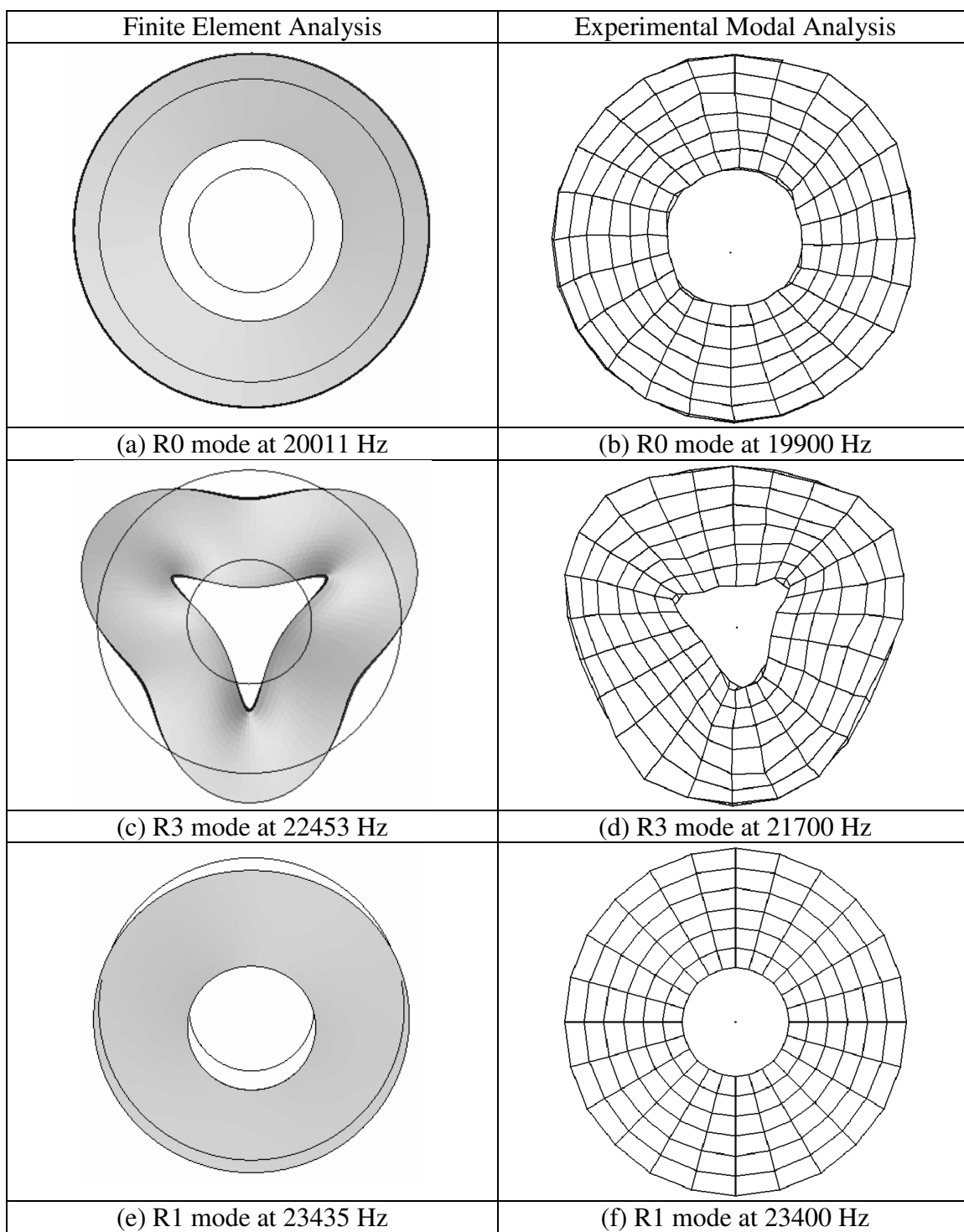


Figure 3-26 – (a)  $R3_{ID50}$  mode radial horn displacement contours for a 10  $\mu\text{m}$  input displacement, large displacements shown in red with small displacements are blue. (b)  $R3_{ID50}$  radial mode horn stress contours for a 10  $\mu\text{m}$  input displacement. High stresses are shown in red while low stresses are blue.

In order to determine the displacements and stresses in the horn a steady state dynamic analysis is required. Carrying out this analysis on the  $R3_{ID50}$  horn, it can be seen from Figure 3-26 that the maximum (red) and minimum (blue) displacements occur at the anti-node and node points of the mode respectively. The maximum displacement was found to be 10  $\mu\text{m}$ , equal to the input vibration. Furthermore, it can also be seen that the maximum stresses in the  $R3_{ID50}$  horn occur at the inner surface and are equi-spaced corresponding to the nodes and anti-nodes of the mode shape. The maximum von Mises tensile stress was found to be 38.12 MPa. This is 10.9 times lower than the tensile yield stress and can be considered safe operating conditions.

The  $R3_{ID50}$  mode radial horn was skimmed such that its inner and outer diameters were 50 and 161 mm respectively; this tuned the horn to the R0 mode (subsequently referred to as

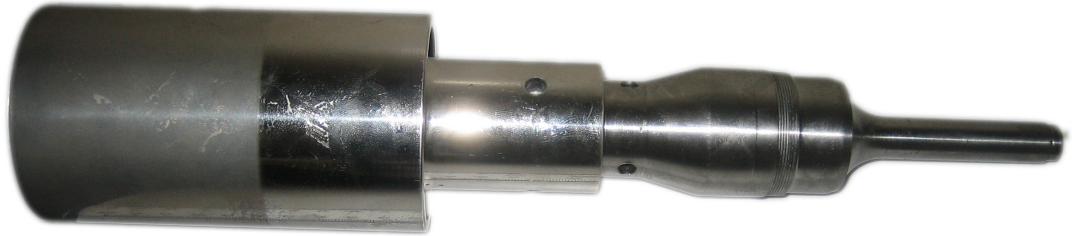
the R0<sub>ID50</sub> horn). An analysis using FEA and EMA similar to those carried out above was done in order to confirm the re-tuning. It should be noted that this re-tuning was carried out after the R3<sub>ID50</sub> horn was used for visualisation (Chapter 4) and microbiological (Chapter 5) studies and was no longer required for the project. Figure 3-27 below shows the results of the study.



**Figure 3-27 – Comparison of  $R3_{ID50}$  mode radial horn using FEA ((a), (c), (e)) and EMA ((b), (d), (e)) for the R1 mode ((a), (b)), R0 mode ((c), (d)) and R3 mode ((e), (f))**

### 3.4.3 Probe Horn

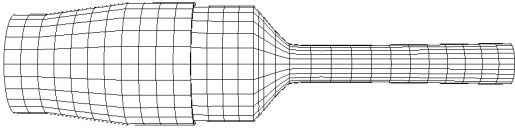
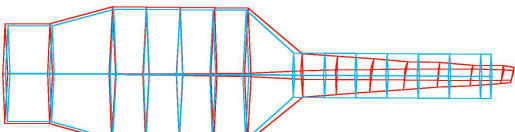
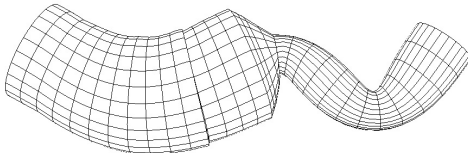
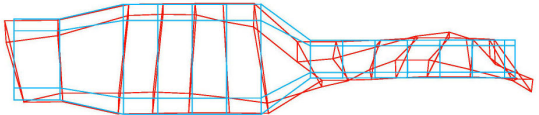
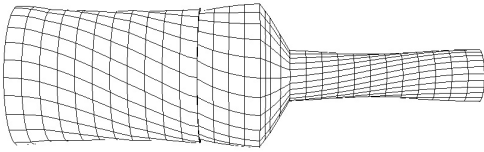
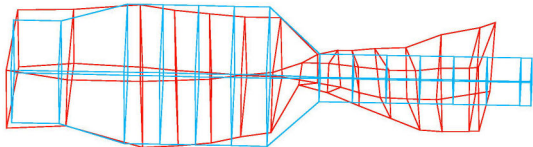
It has been shown in Chapter 2 that most studies currently rely on a probe type device (Figure 3-28) which vibrates in the longitudinal axis, causing cavitation at the tip.



**Figure 3-28 – 20 kHz ultrasonic probe horn**

These devices consist of a piezoelectric transducer attached to a horn which is shaped such that a small input amplitude is magnified to produce a large output vibration. These devices can typically produce 100  $\mu\text{m}$  output displacement for only 10  $\mu\text{m}$  input displacement. When immersed in a fluid, the large amplitude causes cavitation to occur at the tip of the device. Removable tips are used to prevent significant erosion and extend the life of the probe. These are generally made from titanium and are replaced once the pitting caused by cavitation becomes excessive. The device used in this study was a Jencons VCX 400 with a standard 13mm diameter probe and titanium tip. For completeness, the modal characteristics of this probe device were also assessed using FE and EMA methods.

The probe was assumed to be made from aluminium of similar properties to that of the radial horn and so the Young's Modulus, density and Poisson's ratio were set to 69  $\text{GN/m}^2$ , 2700  $\text{kg/m}^3$  and 0.33 respectively. The dimensions of the probe were estimated by measuring with callipers. Despite these assumptions, the FE model predicts that the longitudinal mode of the probe occurs at 20030 Hz, only 30 Hz from the operating frequency of 20 kHz. Experimental modal analysis of the horn found the probe horn to vibrate at 20026 Hz in its longitudinal mode, 4 Hz from the FEA prediction. Figure 3-29 shows a comparison of the FEA results to those obtained using EMA.

Finite Element Analysis	Experimental Modal Analysis
	
Longitudinal mode at 20030 Hz	Longitudinal mode at 20026 Hz
	
3 <sup>rd</sup> bending mode at 21442 Hz	3 <sup>rd</sup> bending mode at 21794 Hz
	
2 <sup>nd</sup> torsional mode at 23825 Hz	2 <sup>nd</sup> torsional mode at 23804 Hz

**Figure 3-29 – Comparison of the FE predicted mode shapes and natural frequencies (left) with those found using EMA (right), blue lines denote the undeformed condition while red denotes the deformed shape**

Applying a steady state analysis to the probe, the gain and stress throughout the horn can be determined. Applying an amplitude of 10  $\mu\text{m}$  to the input face of the horn, Figure 3-30 shows that an output amplitude of 76  $\mu\text{m}$  is achieved thus the horn is estimated to have a gain of 7.6. The steady state analysis also predicts that the probe horn is subjected to a maximum Mises stress of 145 MPa located at the neck. The probe is made from high strength aluminium alloy which has a yield strength in the region 414 MPa thus the stresses generated would cause no concern. It is vital that the stresses within these ultrasonic components is kept below the yield strength as localised plasticity will cause a change in the stiffness matrix resulting in the loss of the device being tuned to a specified frequency.

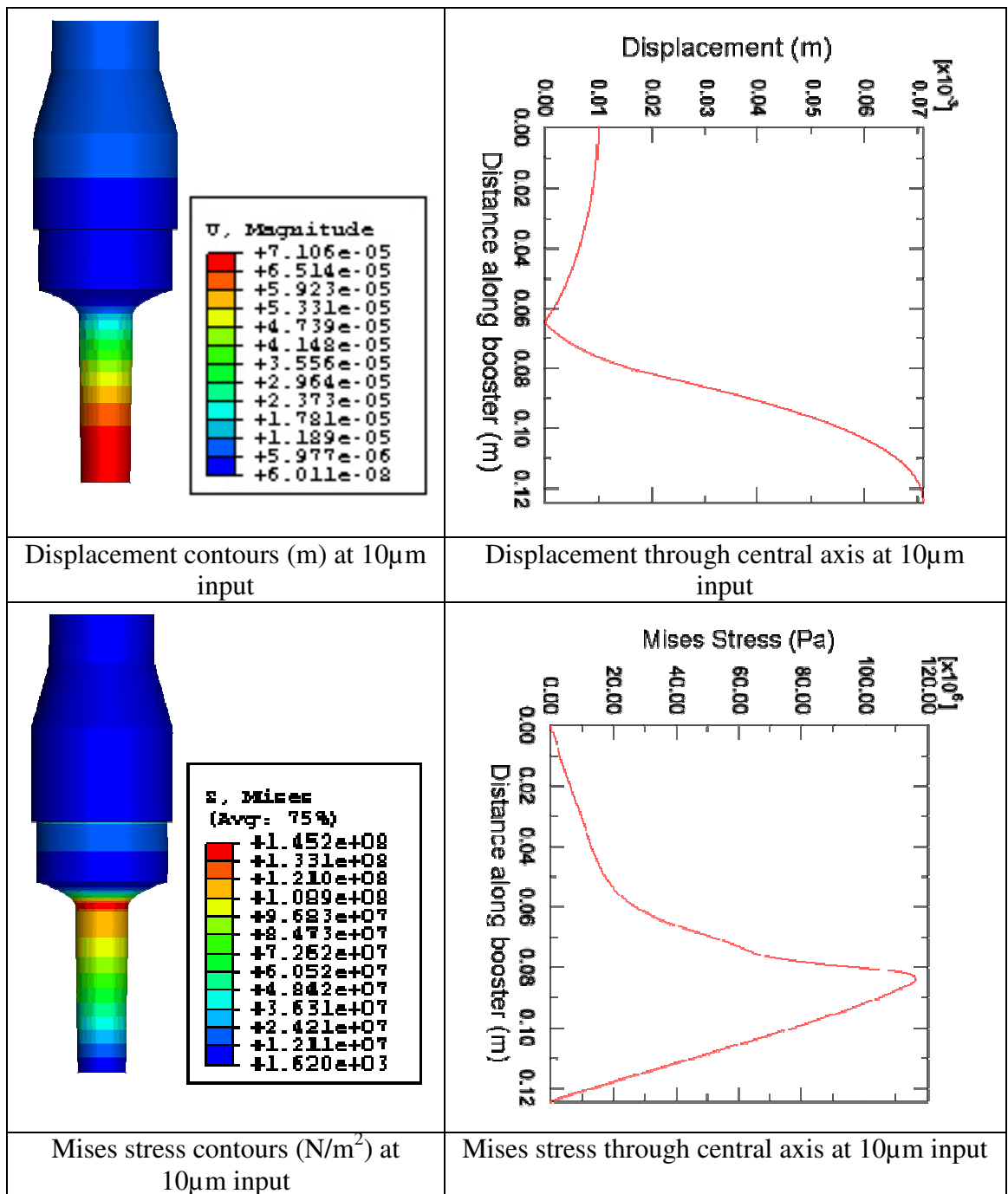


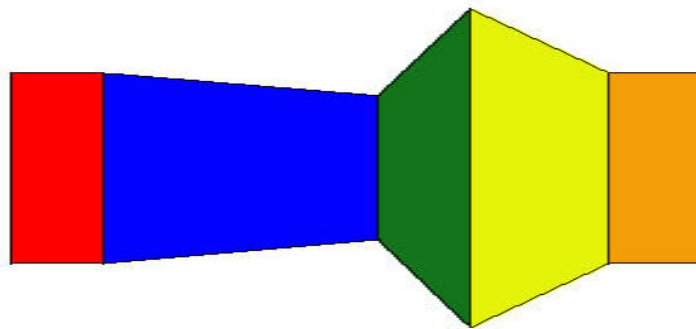
Figure 3-30 – Finite Element Analysis of the displacements and stresses in the probe horn

#### 3.4.4 Booster Horn

Since the 20 kHz transducer can provide amplitudes in the range of 4-8 µm depending on the generator setting and it is hypothesised that higher ultrasonic amplitudes will lead to a greater reduction in bacterial numbers over the same exposure time, then it is desirable to increase the range of amplitudes available. Since the ultrasonic vibrations are applied by a longitudinal transducer, it is possible to put a booster horn, tuned to the longitudinal mode

at the operating frequency, in between the transducer and the working horn. This intermediate horn can be designed to give greater or smaller amplitude at the working horn and is thus known as a booster or de-booster horn. The booster designed for use in these studies has a gain of 2, thus it may double or half the amplitude depending on the configuration used. Normally boosters are designed by reducing the cross sectional area along the length, as with the probe horn in section 3.4.3. However, it was desired that both the input and output areas of the horn be the same so that the transducer and radial horn could be attached to either end, giving a horn that could operate as a booster (gain of 2.0) or a de-booster (gain of 0.5), thus another design was sought.

Analysing the work of Peshkovsky and Peshkovsky [143] it was seen that it is possible to design a horn with gain while keeping the input and output surfaces the same cross sectional area. In general the designs conformed to the five section approach by Peshkovsky [143] (Figure 3-31) with the first and last sections requiring to be of constant cross-section. This, in addition to a couple of small location holes, will allow for the horn to be easily removed through the use of a c-spanner. Thus the number of configurations for the other three sections is reduced substantially. Finite element analysis was used to assess several possible designs (Figure 3-32 – Figure 3-34). The final design (Figure 3-34) consists of an initial circular section, a sweeping curve which reduces the cross-section before increasing it, a linear taper section and a final circular section. Using this design the gain can be adjusted by modifying the parameters of the curve section while the frequency of the longitudinal mode can be adjusted by the steepness of the linear taper section, thus allowing the design criteria to be met (gain 2,  $f = 20000$  Hz longitudinal mode, no modal coupling).



**Figure 3-31 – Elevation view of the 5 section design. Each section shown in a different colour**

The booster is made from aluminium ( $E = 69 \text{ GN/m}^2$ ,  $\rho = 2700 \text{ kg/m}^3$ ) and was modelled fully with 3D quadratic elements in ABAQUS. A frequency analysis was carried out to determine the modal characteristics and a steady-state response was carried out to determine the gain and calculate the stresses in the horn when the input amplitude is at maximum. This will ensure the booster horn does not fail prematurely.

Initial designs (Figure 3-32 and Figure 3-33) were found to be inappropriate due to the large stresses generated at corners which exceeded the yield strength of the aluminium available, thus a design which eliminated these stress concentrations was sought. The design shown in Figure 3-34 eliminated the stress concentrations and allowed the use of relatively low strength aluminium. The frequency step of the analysis shows that the longitudinal mode occurs at 20125 Hz whilst the closest modes above and below this are the 1<sup>st</sup> bending mode at 22353 Hz and the 1<sup>st</sup> torsional mode at 8706 Hz respectively as depicted in Figure 3-35. Applying unit amplitude to face A of the horn and running a steady state analysis it is found the horn has a gain of 2.01. Applying a typical input of 10  $\mu\text{m}$ , Figure 3-34 shows the stresses calculated at this frequency and amplitude. It can be observed that the maximum von Mises stress occurs at the node and is of magnitude 37.5  $\text{MN/m}^2$ , the tensile yield stress for aluminium is in the range 103  $\text{MN/m}^2$  thus the horn should be operating at 0.364 yield and thus should not fail in use.



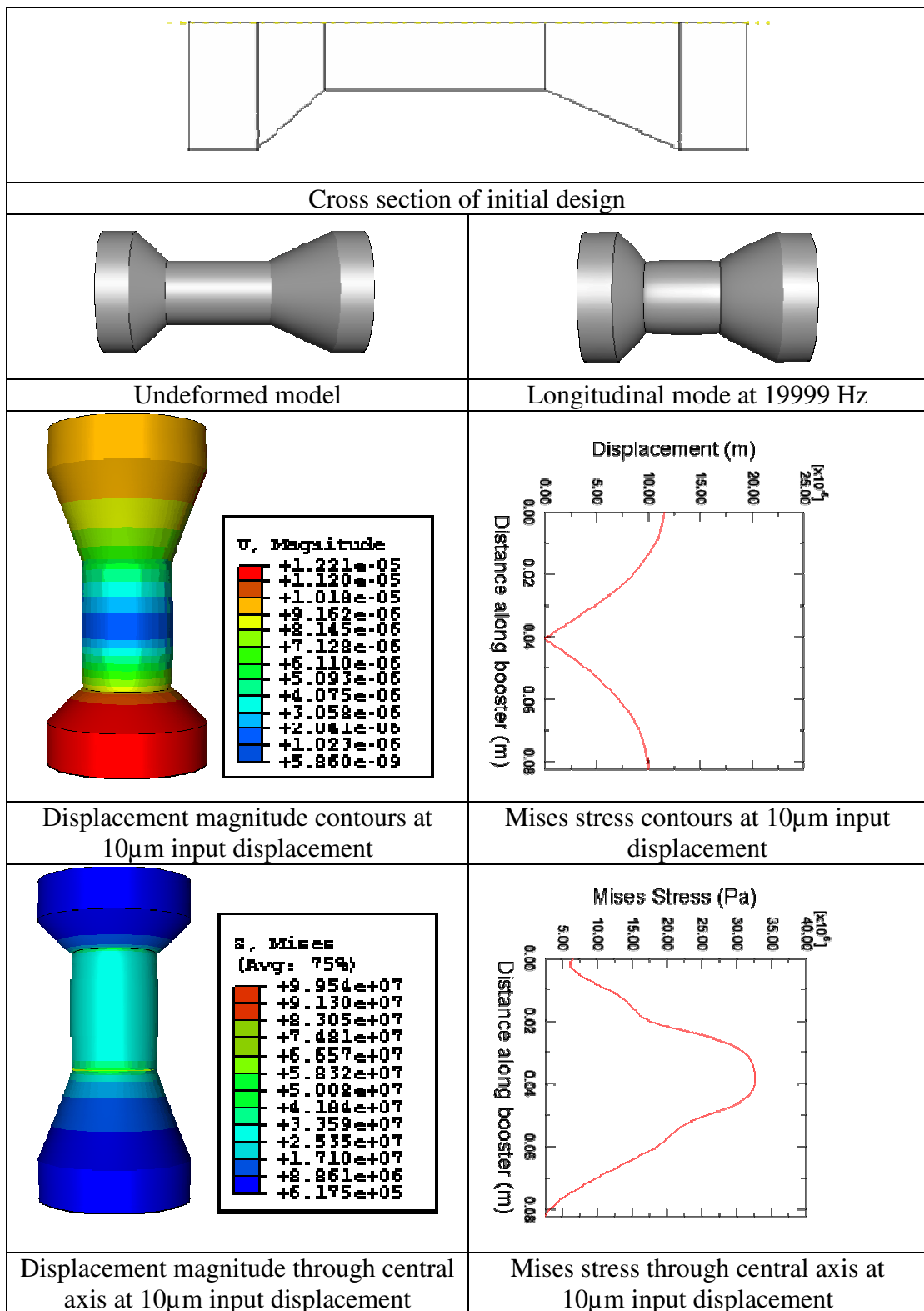


Figure 3-32 – Analysis of the displacements and stresses in the initial booster horn design

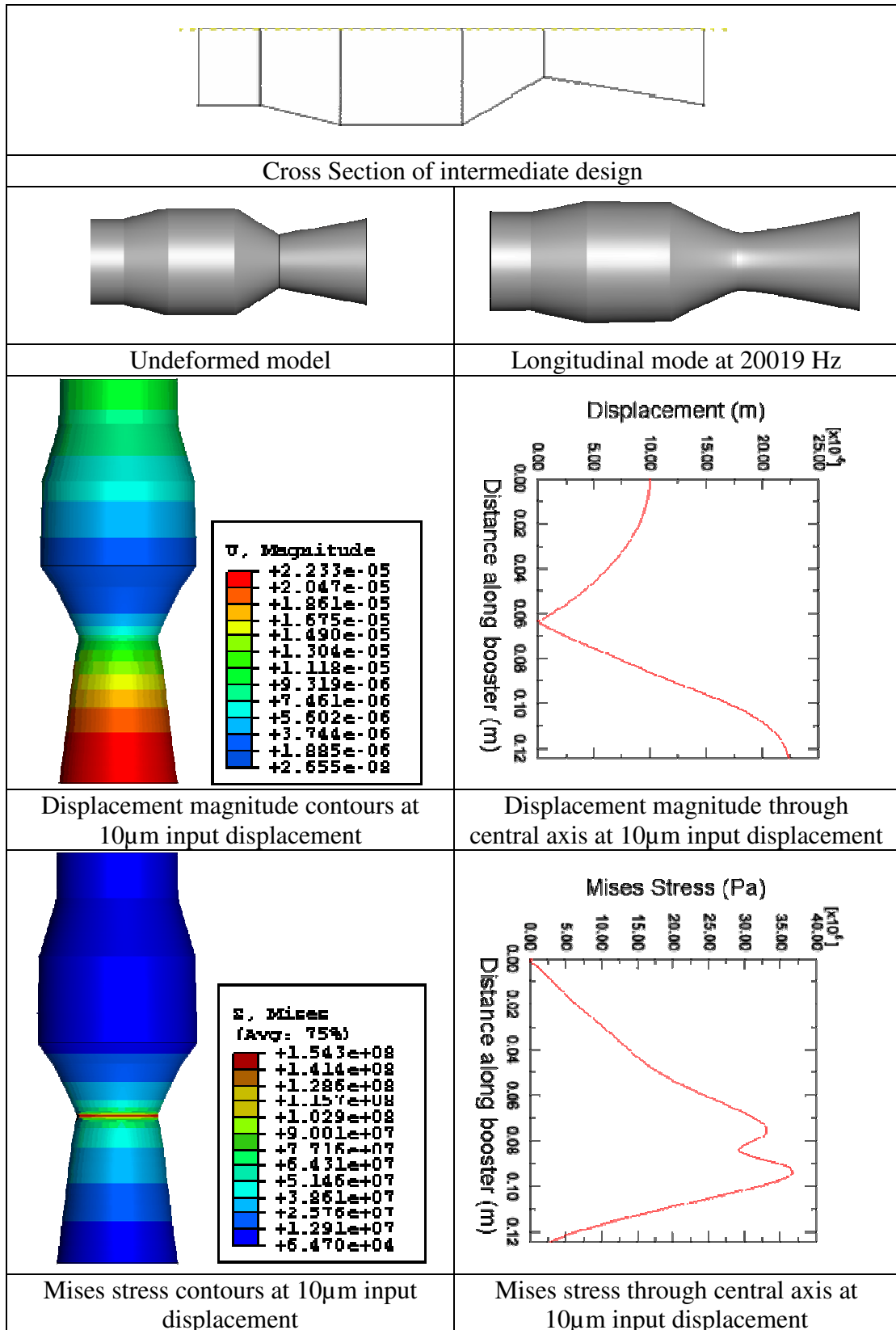


Figure 3-33 – Analysis of the displacements and stresses in the modified booster horn design

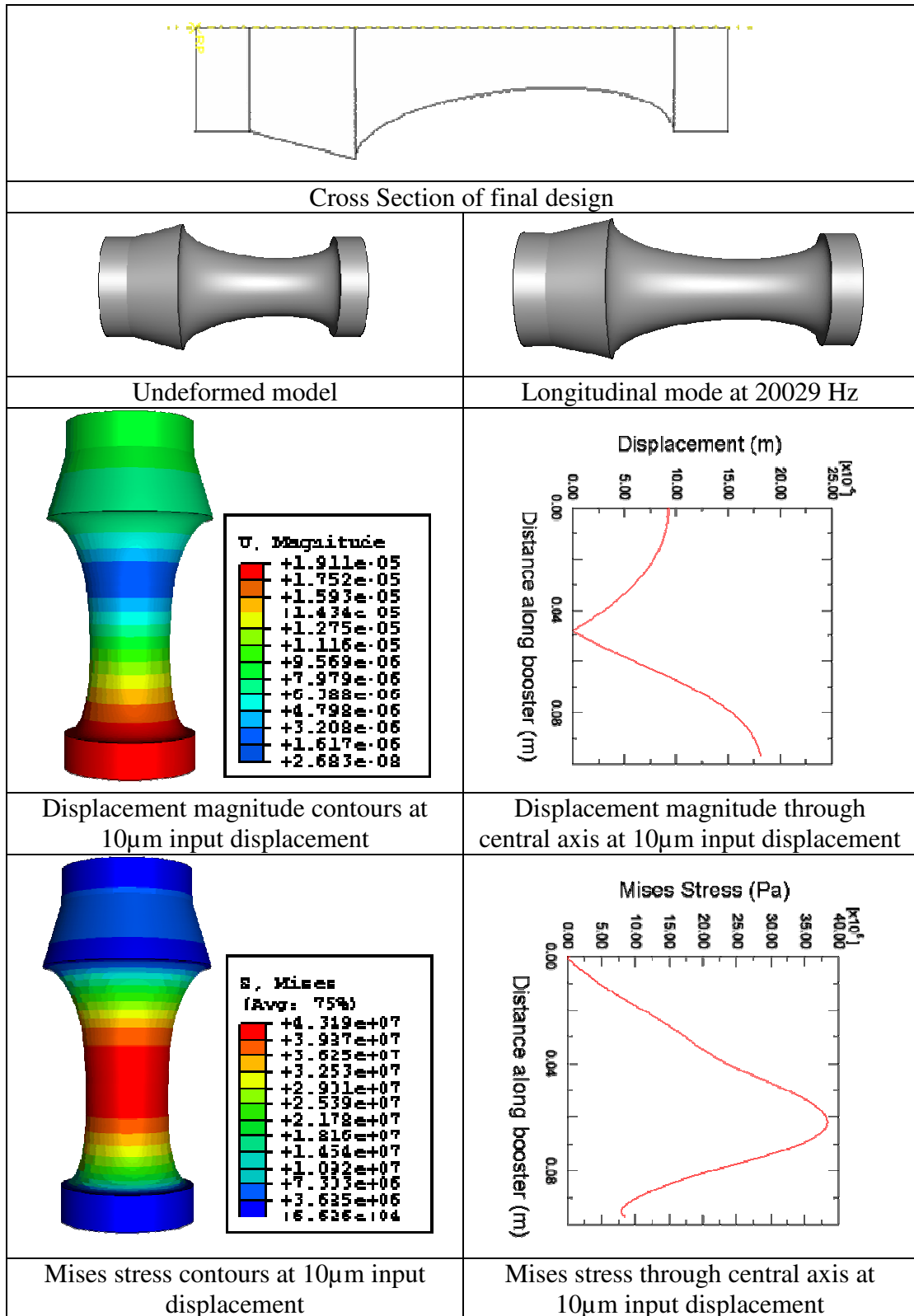


Figure 3-34 – Analysis of the displacements and stresses in the final booster horn design

Experimental modal analysis was used to confirm the FEA predictions. Figure 3-35 shows the mode shapes and associated frequencies for both FEA and EMA. It can be seen that the longitudinal mode occurs at 21000 Hz, 1 kHz above the FEA prediction. This error is likely to be due to the several factors. Engineering features such as location holes and also, the effect of the transducer have not been accounted for are not modelled in the FEA. It can be seen that the 1<sup>st</sup> torsional and 1<sup>st</sup> bending modes occur at 8470 Hz and 22300 Hz respectively. Using the data from the finite element model and correlating it with the predicted natural frequencies and observing the longitudinal mode occurs in the 20 kHz region there is a high degree of confidence that the booster horn operates as designed.

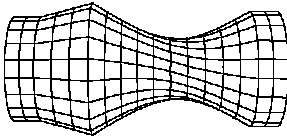

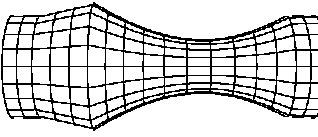
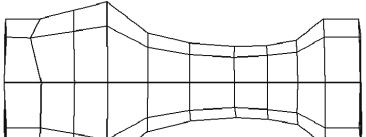
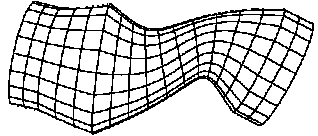
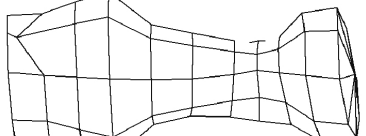
Finite Element Analysis	Experimental Modal Analysis
	
1 <sup>st</sup> Torsional mode (8706 Hz)	1 <sup>st</sup> Torsional mode (8470 Hz)
	
1 <sup>st</sup> Longitudinal mode (20125 Hz)	1 <sup>st</sup> Longitudinal mode (21000 Hz)
	
1 <sup>st</sup> Bending mode (22353 Hz)	1 <sup>st</sup> Bending mode (22300 Hz)

Figure 3-35 – Comparison of the FE predicted mode shapes and natural frequencies (left) with those found by EMA (right)

### 3.5 Ultrasonic Amplitudes

Since the primary cause of cell death through the use of ultrasonic vibration is by cavitation collapse, and cavitation intensity is governed by the amplitude of vibration, it is beneficial to measure the amplitude of vibration of the horns used in this study in all the configurations. Thus the radial horn amplitudes at the inner surface were measured using a 3D LDV while the probe horn amplitude were measured using a 1D LDV. The 1D LDV was used for the probe horn since it is vibrating in the longitudinal mode and measurement of the tip vibration is straight forward. During the tests described in the following chapters the radial horns were used in several configurations. The generator amplitude setting as a

percentage of maximum amplitude either 50 or 100 % and the booster horn either in the 0.5 or 2.0 gain configuration were used to provide a variety of amplitudes. Table 3-4 shows the measured velocities obtained from the LDV with the corresponding ultrasonic amplitude.

R0 <sub>ID30</sub>	
Velocity (mm/s)	Amplitude (μm)
292	2.3
925	7.4
190	1.5
480	3.8
R0 <sub>ID50</sub>	
Velocity (mm/s)	Amplitude (μm)
228	2.3
608	4.8
226	1.8
467	3.7
R3 <sub>ID50</sub>	
Velocity (mm/s)	Amplitude (μm)
314	2.5
716	5.7
163	1.3
214	1.7
364	2.9
Probe horn	
Velocity (mm/s)	Amplitude (μm)
4300	34.2

**Table 3-4 - Horn Amplitudes**

Amplitudes are found to range between 1.3-7.4 μm for the radial horns while the probe horn was found to vibrate at 34.2 μm. In discussing the radial horns in the proceeding chapters reference will be made to the radial horn used and amplitude of vibration.

### **3.6 Discussion and Conclusions**

This chapter has shown the process by which the radial horns were designed using analytical solutions and numerical finite element analysis and the designs verified by experimental modal analysis. Three radial horns have been assessed, two vibrate in the fundamental R0 mode having different inner and outer diameters while the other vibrates

in the third radial mode R3 at the operating frequency of 20 kHz. These horns are designed such that unwanted modes are separated from the operational mode by at least 1200 Hz, to prevent any modal coupling from occurring. The FRF's obtained from the EMA indicate no modal coupling is taking place. The horns also have a pipe and flange section to enable them to be attached to a base. This allows for a small volume of fluid to be contained in the centre cavity of the horn for treatment.

A booster horn has also been designed to increase the available range of amplitudes for testing. A booster horn with a gain of 2 was designed using finite element analysis, which had the same input and output cross sectional areas. This design allowed the booster to be used in two configurations simply by reversing it, as a gain of 2 and a gain of 0.5.

Traditionally, a probe type device has been used for bacterial inactivation and thus this type of device is used in these studies to gauge the effectiveness of the radial horn. A finite element study and an experimental modal analysis was conducted on a commercial ultrasonic probe. This has shown that the probe vibrates in the first longitudinal mode at 20 kHz with sufficient modal separation.

Ultrasonic devices designed using FEA and verified with EMA, are to be used for the bacterial inactivation of fluid suspensions. It is known that this inactivation is due to cavitation created by the vibration of the ultrasonic devices thus it is now necessary to assess these devices in terms of the cavitation fields which they generate.

---

## Chapter 4 – Cavitation Fields and Visualisation

---

### **4.1 Introduction**

This chapter reports the use of finite element (FE) analysis to predict the pressure field in the fluid cavity of a tuned radial mode ultrasonic horn. The aim is firstly to evaluate the FE models as part of the design process for radial horns such that the radial mode and fluid cavity dimensions can be optimised for bacterial inactivation. Secondly, the FE models are evaluated in terms of their ability to provide useful estimations of where in the fluid cavity bacterial inactivation is most likely to occur. Finally, the results of the radial mode horn FE models are compared with those developed for a longitudinal mode ultrasonic probe device.

The devices designed for this study are tuned to 20 kHz and are a radial mode horn operating in the fundamental radial mode, R0<sub>ID30</sub>, and one operating in the third radial harmonic, R3<sub>ID50</sub>. A third radial horn was constructed by re-tuning the R3<sub>ID50</sub> mode radial horn to the R0 mode at 20 kHz, this is referred to as the R0<sub>ID50</sub> mode radial horn. The longitudinal mode ultrasonic probe, also tuned to 20 kHz, is a Jencons VCX 400 attached to a standard 13 mm probe horn with titanium tip.

The fundamental radial mode, R0, of a cylinder produces a uniform ultrasonic vibration amplitude at the inner diameter and this horn is therefore designed to focus the ultrasonic energy at the centre of this cavity. The aim is to produce an area of low pressure where cavitation can occur in the fluid away from the vibrating face. Also, by focussing the ultrasonic energy, it is hoped to achieve a cavitation cloud at significantly lower horn ultrasonic amplitudes than is necessary with probe devices.

As is typical of thick cylinders, the fundamental, first and third radial modes, R0, R1 and R3 respectively, are grouped within a relatively small frequency band and separation of these modal frequencies is vital to the successful design of such horns [142]. It is hypothesised that the R1 and R3 modes will not focus the ultrasonic energy at the centre of the cavity and these modes will be less effective at bacterial inactivation. To verify this hypothesis, a horn tuned to the R3 mode is studied. The R3<sub>ID50</sub> mode horn will also be used in order to verify that the resulting cavitation and the predicted pressure field in the fluid cavity agree with visualisation studies.

The results of the finite element study are validated against experiments using chemiluminescence supported by photographs of the cavitation field and aluminium foil tests. It is demonstrated that despite the simplifying assumptions which neglect the complex nature of fluids undergoing cavitation, useful estimations of the pressure fields created by the two devices, and hence where cavitation is likely to occur within the fluid, are achieved.

## **4.2 Finite element models**

The FE models were created using the ABAQUS finite element package. Models were developed to simulate the pressure fields created by an ultrasonic probe and ultrasonic radial horns tuned to the R0, R1 and R3 modes. All the ultrasonic devices modelled were tuned to an operating frequency of 20 kHz. Both the radial and probe horns were made from aluminium, having a Young's modulus of 71 GN/m<sup>2</sup> and a Poisson's ratio of 0.33. The water in the cavity was modelled using acoustic elements, with density 1000 kg/m<sup>3</sup> and bulk modulus 2.09 GPa. These elements allow the pressure to be calculated from a fluid under stress.

This type of analysis has some limitations. Firstly, it is only valid up to the point of cavitation inception and is therefore only used to indicate where cavitation is most likely to occur and not to model the cavitating region. The second limitation is that the fluid cavity must be considered as stationary and therefore the models are not used directly in the design of flow-through devices. However, the models can allow comparisons between different tuned mode devices.



### 4.2.1 Probe Model

The ultrasonic probe used in these studies is the Jencons VCX 400 considered in Chapter 3. The gain in this probe is achieved by a steep reduction in cross-sectional area, however the length of the probe in contact with the fluid has a constant cross-section. The probe horn was modelled as an aluminium rod with the probe tip positioned two centimetres below the surface of the water. This ensured the probe was in the centre of the fluid cavity and also prevented foaming which can occur if the probe horn is immersed just below the fluid surface. The rod was tuned to the longitudinal mode of vibration at 20 kHz and an ultrasonic amplitude of 34  $\mu\text{m}$  was applied to the tip to represent the actual amplitude achieved by the probe. Due to the excessive run times associated with achieving a converged solution for a full 3-D model, a two-dimensional axi-symmetric model of the probe in the fluid filled cavity was created, taking advantage of symmetry. Boundary conditions were applied at the fluid edge such that it was fully constrained, to represent the fluid being enclosed in a rigid container. The probe was placed at a depth of 30 mm beneath the surface of the fluid with the container measuring 150 mm in diameter. The fluid-structure interaction was modelled by tying the nodes of the fluid to those of the wetted surface of the probe. The probe was modelled in different fluid cavities to determine the effect that the cavity depth has on the pressure field generated. The water depth between the probe tip and cavity floor was varied from  $\frac{1}{4}$  to 1 wavelength in steps of  $\frac{1}{4}$  wavelength as it is likely that if there are any effects they will occur at these depths due to resonance and/ or constructive and destructive interference. The depths of the water cavities was calculated using Equation 4-1

$$\lambda = \frac{1}{f} \sqrt{\frac{B}{\rho}} \quad (4-1)$$

where  $\lambda$  is the wavelength of the fluid, the frequency,  $f$ , is 20000 Hz, the bulk modulus for water,  $B$ , is 2.2 GPa, and the density of water,  $\rho$ , is 1000  $\text{kg/m}^3$ . This gives water cavity depths of 18.54 mm, 37.08 mm, 55.62 mm and 74.16 mm from the end of the probe tip for  $\frac{1}{4}$ ,  $\frac{1}{2}$ ,  $\frac{3}{4}$  and 1 wavelength respectively.

A steady-state dynamic finite element analysis was carried out for these depths and in each analysis the probe had a tip vibration amplitude of 34  $\mu\text{m}$ . This kind of analysis allows for the calculation of the steady-state response of a dynamic system subject to harmonic loading. In such an analysis, transient effects (those taking place in the first few cycles of

vibration) are not included as it is assumed the system is vibrating in a continuous steady manner. Models were created for two depths of water,  $\frac{3}{4}$  and 1 wavelength, such that an analysis to determine the effect of the tip vibration amplitude on acoustic pressure could be carried out. Tip amplitudes ranging from 20-100  $\mu\text{m}$  in steps of 20  $\mu\text{m}$  were examined as these are typical amplitudes of probes.

Figure 4-1 shows the calculated contour plots of the pressure field created by the ultrasonic probe immersed in four different fluid cavities of depths:  $0.25\lambda$ ,  $0.5\lambda$ ,  $0.75\lambda$  and  $1.0\lambda$ . For all cases it is observed that a large negative pressure is obtained at the probe tip which rapidly dissipates at distances further from the vibrating tip.

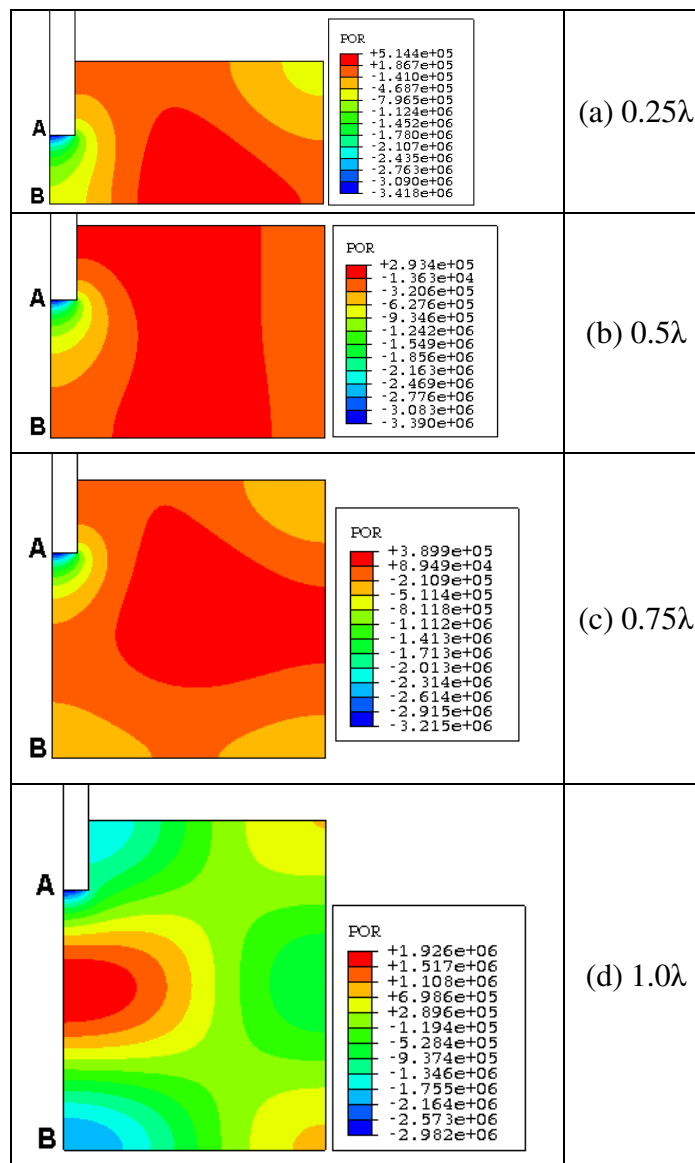


Figure 4-1 – Contour plots of the pressure generated by a 20 kHz ultrasonic probe in cavities of depth (a)  $0.25\lambda$  (b)  $0.5\lambda$  (c)  $0.75\lambda$  (d)  $1.0\lambda$ . Pressure magnitude is shown in  $\text{N/m}^2$

Figure 4-2 plots the pressure along the line A-B shown in Figure 4-1 for the four fluid depths. It can be observed that the maximum pressure amplitude in all four cases is approximately 3 MPa at the probe tip.

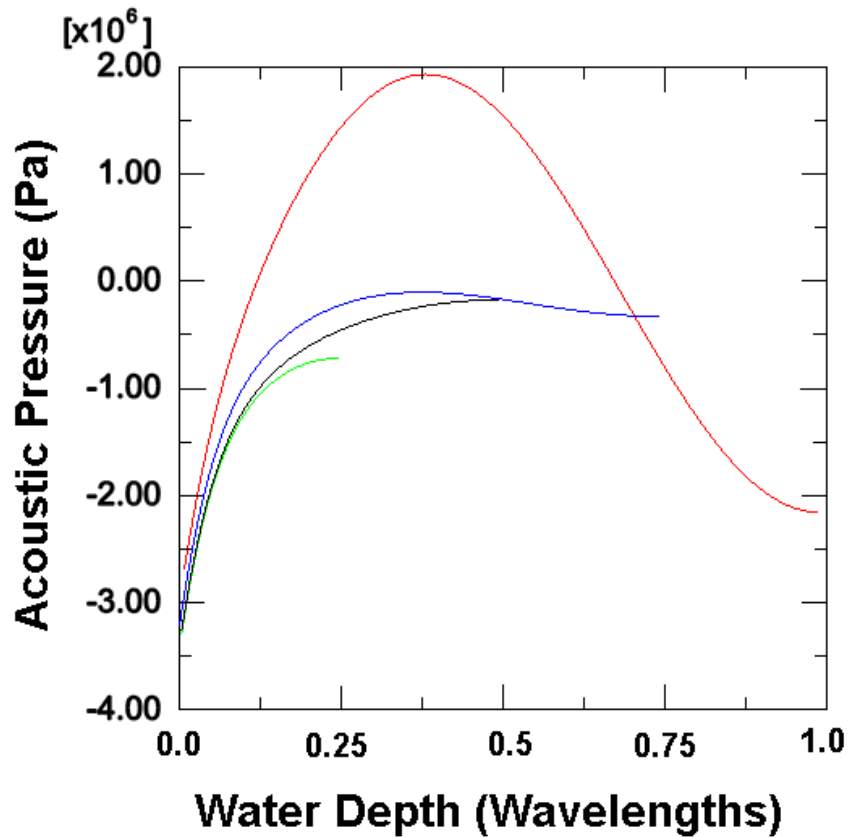


Figure 4-2 – Pressure variation through fluid cavity depth using 20 kHz probe horn for various fluid depths  $0.25\lambda$  (green),  $0.5\lambda$  (black),  $0.75\lambda$  (blue) and  $1.0\lambda$  (red)

Studies were also carried out to predict the influence of the ultrasonic amplitude at the tip of the probe on the pressure field, for fluid depths of  $1.0\lambda$  and  $0.75\lambda$ . Figure 4-3(a) and (b) show the pressure along line A-B for amplitudes ranging from 20-100  $\mu\text{m}$  for water depths of  $0.75\lambda$  and  $1.0\lambda$  respectively. It can be seen that in both cases the magnitude of the acoustic pressure increases in proportion to the ultrasonic amplitude indicating a linear relationship between the maximum pressure in the fluid cavity and the applied ultrasonic vibration amplitude. It can also be observed that at a vibration amplitude of 100  $\mu\text{m}$  that the maximum pressure at the probe tip varies significantly between the  $0.75\lambda$  and  $1.0\lambda$  case. This is due to a standing wave pattern being set up within the fluid when the fluid depth is equal to a multiple of half wavelengths. However, at low amplitudes this effect is negligible as is shown in Figure 4-2 by the small variation in maximum pressure at all fluid depths.

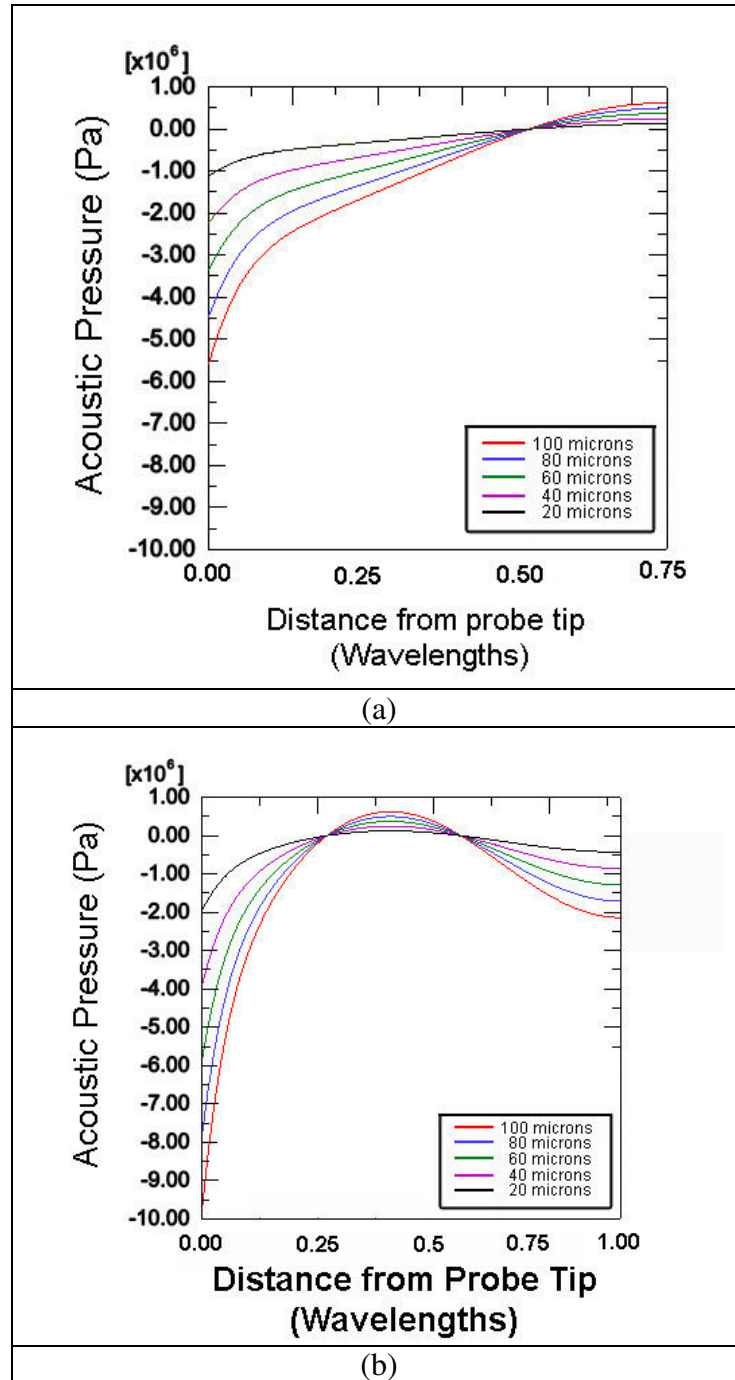


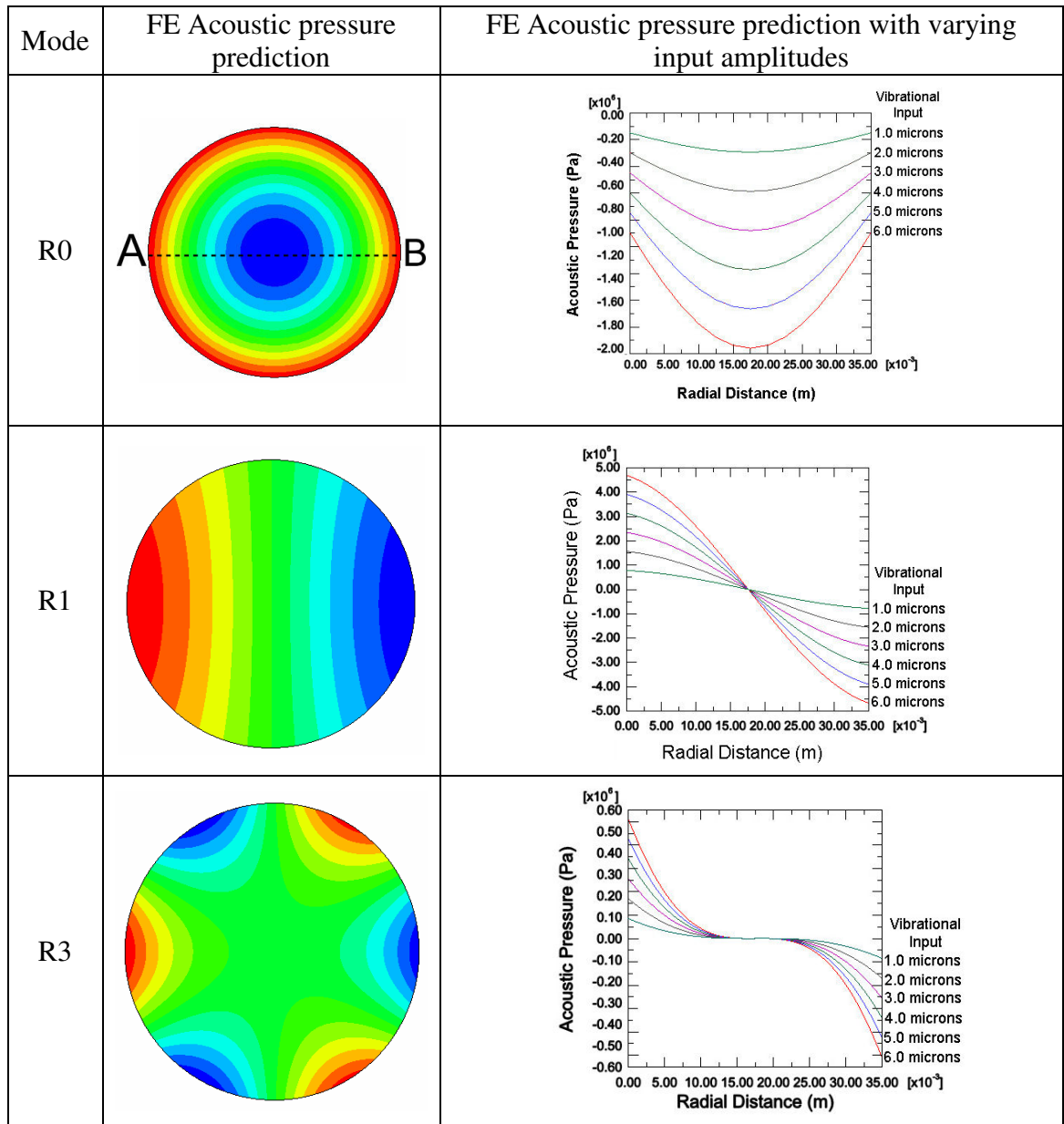
Figure 4-3 – Pressure distribution through fluid cavity for depths of (a)  $0.75 \lambda$  and (b)  $1.0 \lambda$

### 4.2.2 Radial Horn Models

The radial horn was modelled as a two dimensional disc. The radial mode frequencies were determined from the mean radius of the disc and it has been shown in the previous chapter that there is no axial variation in the modal response in the three radial modes of vibration. The acoustic elements form the fluid cavity in the centre of the radial horn and these elements were tied to the inner diameter of the radial horn so that the fluid-structure interaction was accounted for. The ultrasonic vibration excitation was applied at the outer diameter of the radial horn, simulating the transducer location in the experiments. Radial horn models were constructed such that the inner diameter and tuned frequency remained constant, whilst the outer diameter was adjusted to tune the R0, R1 and R3 modes at 20 kHz. This allowed for a comparison of the pressure fields created by the different modes of vibration when excited with the same ultrasonic amplitude for the same size of fluid cavity. Further analysis was carried out on the R0 mode radial horn to evaluate the effects of ultrasonic amplitude and inner diameter (fluid cavity dimensions) on the predicted pressure field.

Figure 4-4 shows the predicted acoustic pressure plotted along line A-B for ultrasonic amplitudes between 1 and 6  $\mu\text{m}$  in steps of 1  $\mu\text{m}$  for the R0, R1 and R3 modes. This Figure clearly shows the concentrating effect of the R0 mode radial horn. It can also be observed that the pressure throughout the fluid increases with ultrasonic amplitude but the increase is more pronounced close to the centre of the horn. It can also be observed that the R1 and R3 radial modes do not concentrate high pressure in the centre of the cavity and the highest pressures are located at the vibrating surface. If Figure 4-4 is examined closely it can be seen that the finite element model predicts that, for the same ultrasonic amplitude of the horn, the R1 mode produces a much higher pressure than the R0 and R3 modes. For a 6  $\mu\text{m}$  input amplitude the maximum pressure predicted for the R0, R1 and R3 modes is 1.9 MPa, 5.9 MPa and 0.6 MPa respectively. The finite element results for the R0 horn and probe horn, at input amplitudes in the working range, predict that pressures well above the tensile strength of tap water, which is in the region of 0.8-1.5 MPa, are excited [44]. The large pressure magnitudes predicted for the R1 radial mode is due to the diameter of the fluid cavity (35 mm) being approximately one half wavelength (36.1 mm) causing a standing wave in the fluid cavity and hence a large pressure magnitude to be observed.

Therefore the finite element simulations are predicting that the horns will operate above the cavitation threshold but the predicted pressures have not been validated at this stage.



**Figure 4-4 – Contour plot of the pressure field generated by the three radial modes of vibration R0 (top), R1 (middle) and R3 (bottom) alongside graphs showing the pressure distribution through the cavity**

It can also be seen, by comparing the results from the probe horn (Figure 4-3) and the R0<sub>ID30</sub> mode radial horn (Figure 4-4) that the ultrasonic amplitude required to reach the cavitation threshold in the fluid is much higher for the probe device. In fact, if the cavitation threshold is considered to be 0.8 MPa then cavitation can be caused by amplitudes as low as 3  $\mu\text{m}$  using the R0<sub>ID30</sub> radial horn but at least 20  $\mu\text{m}$  for the probe.

Figure 4-5 shows the results from altering the internal diameter of the R0 radial horn whilst keeping the mode of vibration and tuned frequency constant i.e. varying the size of the fluid cavity. It can be seen that for the same ultrasonic amplitude the highest fluid pressure is achieved for the largest internal diameter. However, the most uniform pressure is achieved for the smallest diameter. These results imply that for large diameters cavitation is less likely to occur at the vibrating face of the horn and therefore surface damage due to bubble collapse is less likely to occur. For small diameters, strong cavitation is likely to be more evenly distributed throughout the entire fluid cavity. This would mean the lifetime of the device may be reduced due to cavitation occurring close to the vibrating face but it may be more suitable for bacterial inactivation purposes as the entire volume of fluid would be treated more evenly.

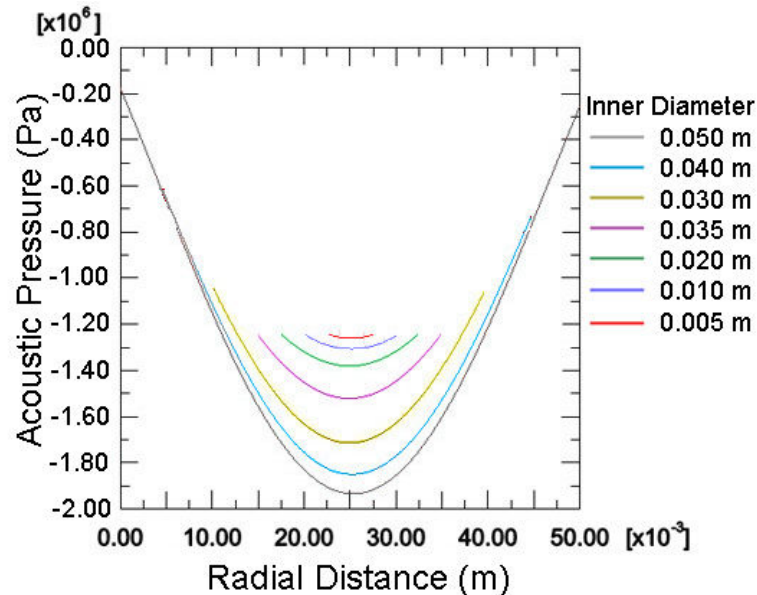


Figure 4-5 – Pressure through the fluid generated by R0 mode radial horns with varying inner diameters

## 4.3 Visualisation

### 4.3.1 Introduction

Visualisation of the cavitation field provides a means of supporting the results from the FE analysis. Three methods of visualisation were used in these studies: photographs, aluminium foil damage, and chemiluminescence. The bubble size and size of cavitation field generated by the probe horn and radial horn devices when in operation allows photographs to be taken which indicate the size and shape of the cavitation field generated.

Further, the strength of the cavitation field at specific points within the fluid can be estimated using aluminium foil. Due to the aspherical collapse of bubbles close to a surface, the immersion of aluminium foil into the cavitation field and the subsequent damage observed gives a good indication of the strength of the cavitation field. Finally, cavitation bubble collapse causes the release of free radicals which are highly reactive. The reaction between these radicals and luminol solution gives rise to an emission of blue light which can be used to indicate areas undergoing cavitation.

### **4.3.2 Methods**

A simple method to visualise the cavitation field is through photographs of the bubble clouds formed during cavitation by the different ultrasonic devices. The bubbles created during cavitation are significantly large in size and concentration to cause light to be reflected and refracted differently from that of water not undergoing cavitation, thus making it straightforward to capture the cavitation clouds created by the devices using a camera and some backlighting. A Canon Ixus 50 was used to provide the photographs.

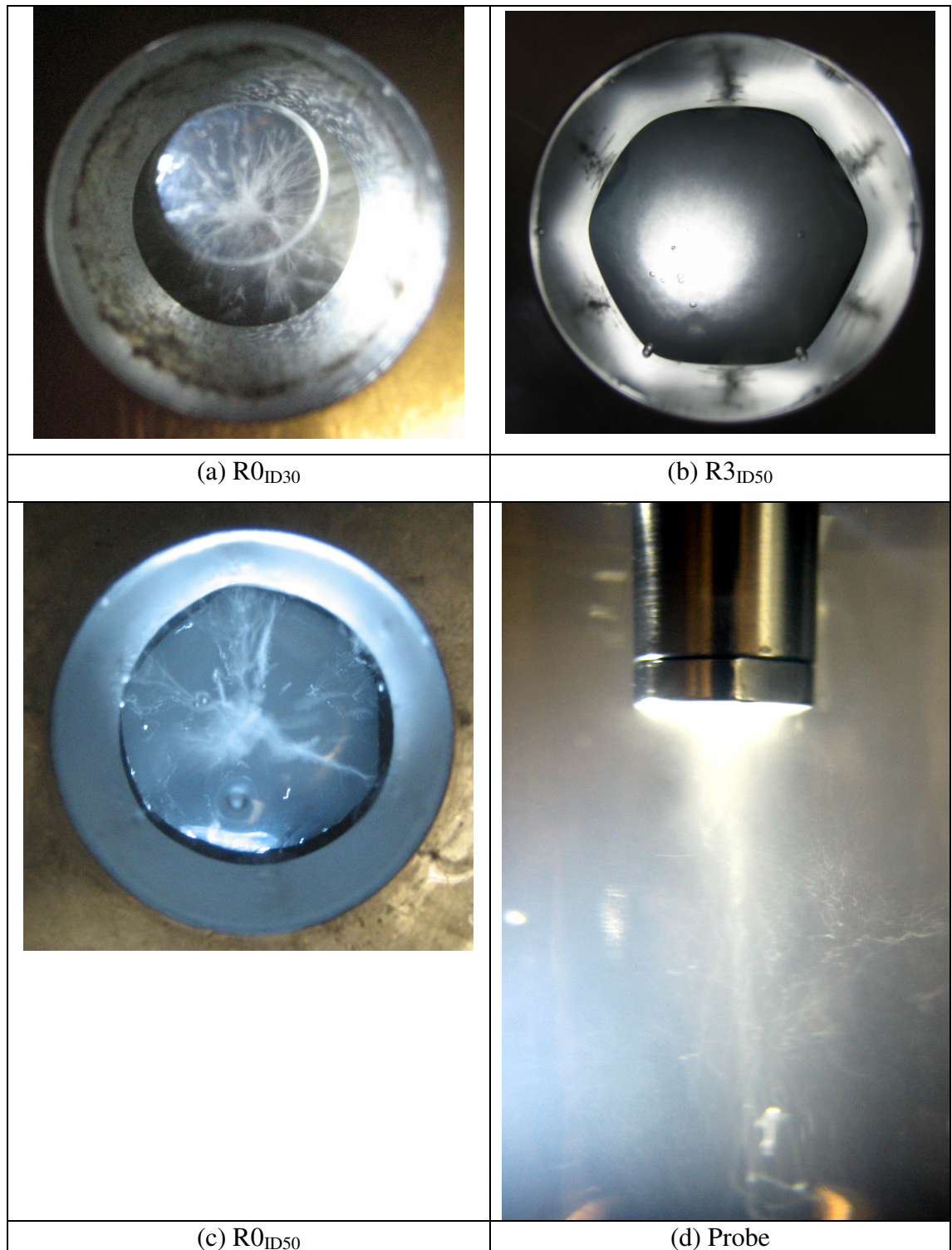
The aluminium foil test is used widely in industry where cavitation is concerned as it is cheap, simple to carry out and gives a good indication of the size, location and strength of the cavitation field. This test involves placing a strip of aluminium foil into the cavitating fluid for a set period of time before removing it and examining the pitting on the foil produced by cavitation bubble collapse. The more pitting produced, the stronger the cavitation field. Aluminium strips were cut to length such that they would fit around the inner circumference of the radial horns. For the R0<sub>ID30</sub> mode radial horn the strips were 90 mm long and 45 mm wide while the strips for the R3<sub>ID50</sub> and R0<sub>ID50</sub> mode radial horns were 156 mm long and 45 mm wide. The aluminium strips were placed carefully around the inner circumference of the horn and the cavity was filled with tap water. The aluminium strip was then subjected to cavitation for a set period of time (2, 4, 6, 8 and 10 seconds) before being removed and photographed. In the case of the R0<sub>ID30</sub> horn, tests were carried out at ultrasonic amplitudes of 1.5, 2.3, 3.8 and 7.3  $\mu\text{m}$ . The R3<sub>ID50</sub> horn was tested at amplitudes of 1.3, 1.7, 2.9 and 5.7  $\mu\text{m}$ . Finally, the R0<sub>ID50</sub> horn was tested at amplitudes of 1.8, 2.5, 3.7 and 4.8  $\mu\text{m}$ . These amplitudes were achieved using different power settings on the ultrasonic generator in combination with the booster horn.



Cavitation can cause sonochemiluminescence (SCL) through chemical reactions involving Luminol (3-aminophthalhydrazide, 97%) and hydrogen peroxide ( $\text{H}_2\text{O}_2$ ) [144-146]. The cavitation collapse of bubbles causes the release of HO free radicals which react with the Luminol solution. These free radicals are also known to have a bactericidal effect [147, 148]. Hydrogen peroxide is used as an oxidiser and enhances this reaction. Solutions were made using the following: 0.1 g of Luminol ( $\text{C}_8\text{H}_7\text{N}_3\text{O}_2$ ), 0.5 g of ammonium carbonate ( $(\text{NH}_4)_2\text{CO}_3$ ), 4 g of sodium carbonate ( $\text{Na}_2\text{CO}_3$ ) and 24 g of sodium bicarbonate ( $\text{NaHCO}_3$ ) dissolved in 1 litre of distilled water ( $\text{H}_2\text{O}$ ). 25 ml of 6% hydrogen peroxide ( $\text{H}_2\text{O}_2$ ) was diluted in 1 litre of distilled water. The two solutions were then mixed in equal quantities to achieve the final solution. It is known that the intensity of cavitation induced sonochemiluminescence is dependant on the pH of the solution [146], with the greatest intensity observed at a pH of 12. Two pH levels were used in these tests; pH 9.5 and pH 12. The pH was altered by adding Sodium Hydroxide ( $\text{NaOH}$ ) to the working solution. This provided an intensity that could easily be captured by a digital camera on a long exposure setting in a dark room. All solutions were used within 12 hours of preparation. The solution was poured into the horn and photographs of the luminescence were taken using a digital camera (Canon Eos 350D, exposure: 4-30 secs, F/5.6). The probe horn was partially immersed in a clear beaker filled with luminol solution and photographs were taken using the same settings as those for the radial horn.

### 4.3.3 Results

In an attempt to visualise the cavitation field produced by the radial horn, digital images were taken using white backlighting. Using a Canon Ixus 50 digital camera, it was possible to capture pictures of the bubble clouds generated. The fluid used was tap water and backlighting was provided by a torch. It can be seen from Figure 4-6 that the  $\text{R0}_{\text{ID}30}$  mode radial horn creates a bubble cloud in the centre of the fluid volume with streamers extending to the outer surface. This is expected due to the focussing effect of the radial horn creating a low pressure area in the centre of the horn cavity where cavitation can occur. It can be observed that the  $\text{R3}_{\text{ID}50}$  mode radial horn creates cavitation close to the inner surface of the horn with no cavitation taking place in the centre of the cavity. The cavitation-free zone creates a hexagonal shape whose corners are at the R3 mode nodes. The cavitating regions are concentrated at the 6 anti-nodes. The probe horn creates a cone-like structure of cavitation bubbles below the probe tip consistent with that reported by Mousatov [149].

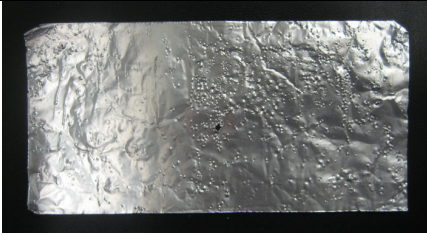
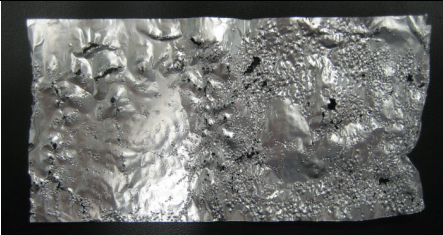
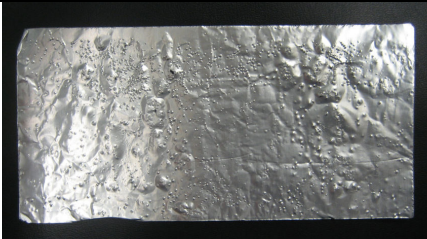
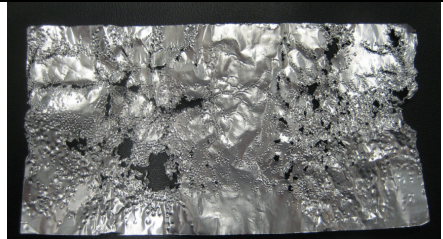
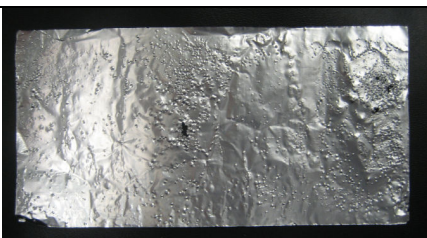
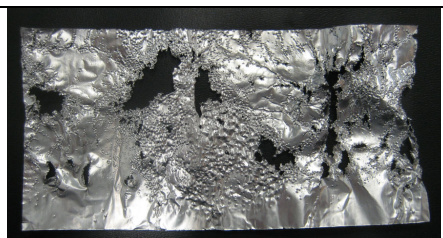



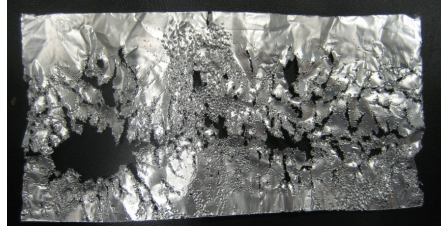


**Figure 4-6 – Photographs of the cavitation field generated by (a) the R0<sub>ID30</sub> radial mode horn, (b) the R3<sub>ID50</sub> mode radial horn, (c) the R0<sub>ID50</sub> horn and (d) the probe horn**

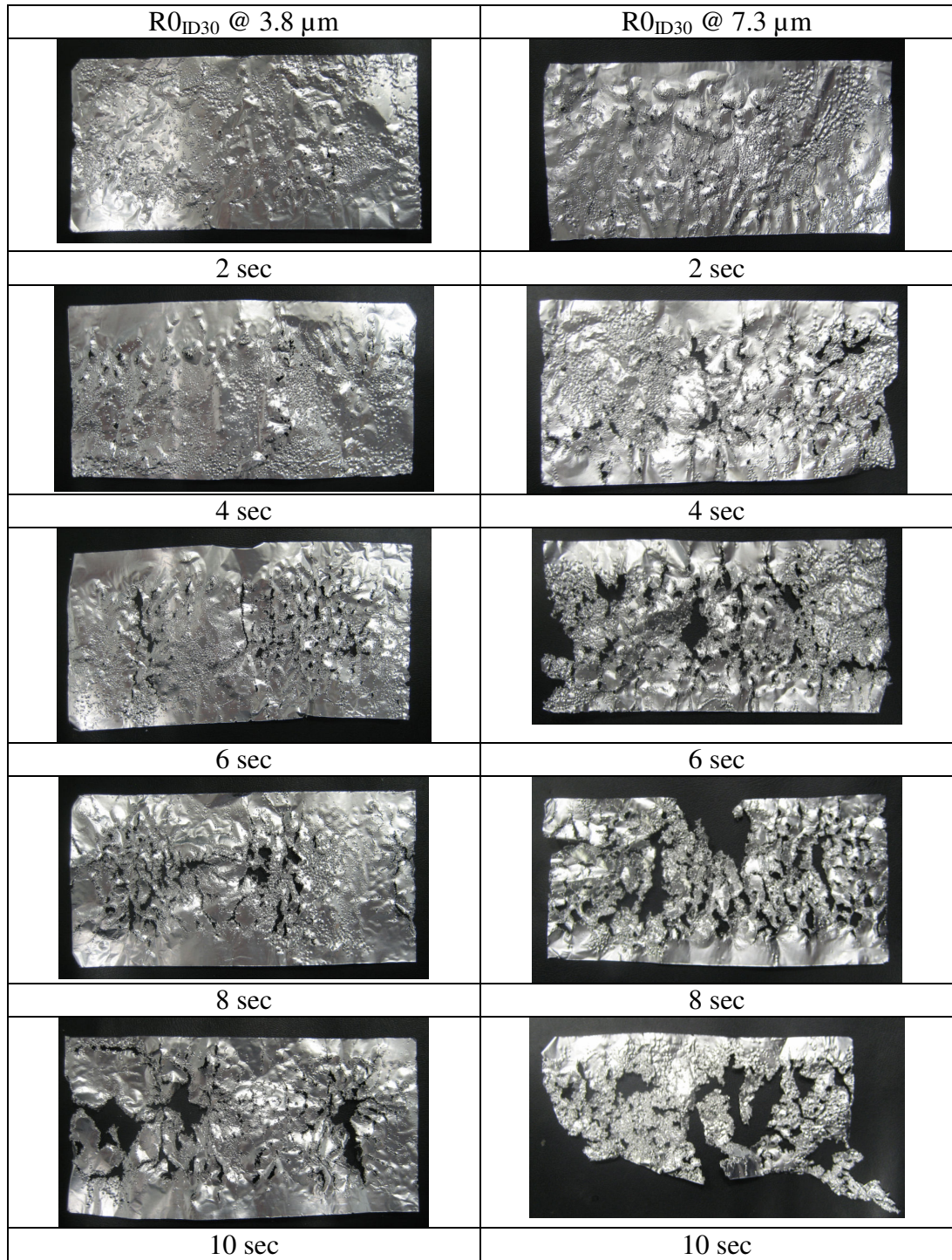
Figure 4-7 and Figure 4-8 show the results from the aluminium foil tests using the R0<sub>ID30</sub> mode radial horn and the R0<sub>ID50</sub> mode radial horn respectively at the various amplitudes. It can be clearly observed that pitting damage increases with exposure time and with

ultrasonic amplitude. These Figures also show that the cavitation field generated by the  $R0_{ID30}$  horn extends to the extremities of the cavity and that the cavitation field is uniform in strength i.e. in general, the aluminium foil is pitted everywhere on the strip with no discernable areas of greater or lesser pitting. Figure 4-9 shows the results from the aluminium foil tests using the  $R3_{ID50}$  mode radial horn. Again, it can be clearly seen that the pitting damage increases with exposure time and ultrasonic amplitude. However, these pictures also show that the pitting damage is not uniform around the circumference of the  $R3_{ID50}$  horn. It can be observed that there are six distinct regions where there is severe cavitation damage and another six regions where there is relatively little or no cavitation damage. These regions of pitting damage form lines on the foil which correspond to the anti-nodes of the  $R3_{ID50}$  mode of the horn.





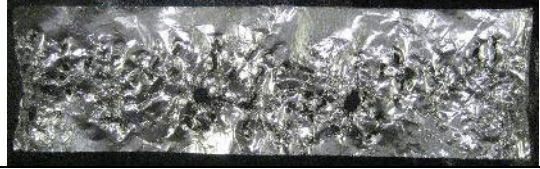
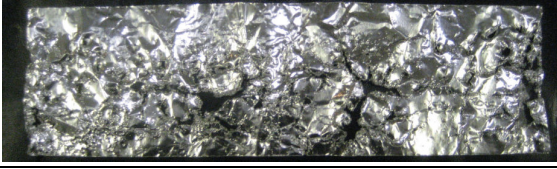


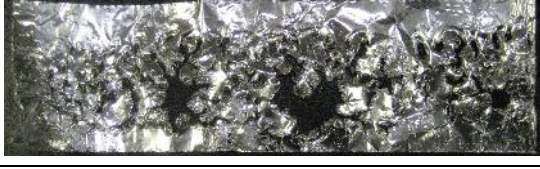



R0 <sub>ID30</sub> @ 1.5 $\mu$ m	R0 <sub>ID30</sub> @ 2.3 $\mu$ m
	
2 sec	2 sec
	
4 sec	4 sec
	
6 sec	6 sec
	
8 sec	8 sec
	
10 sec	10 sec



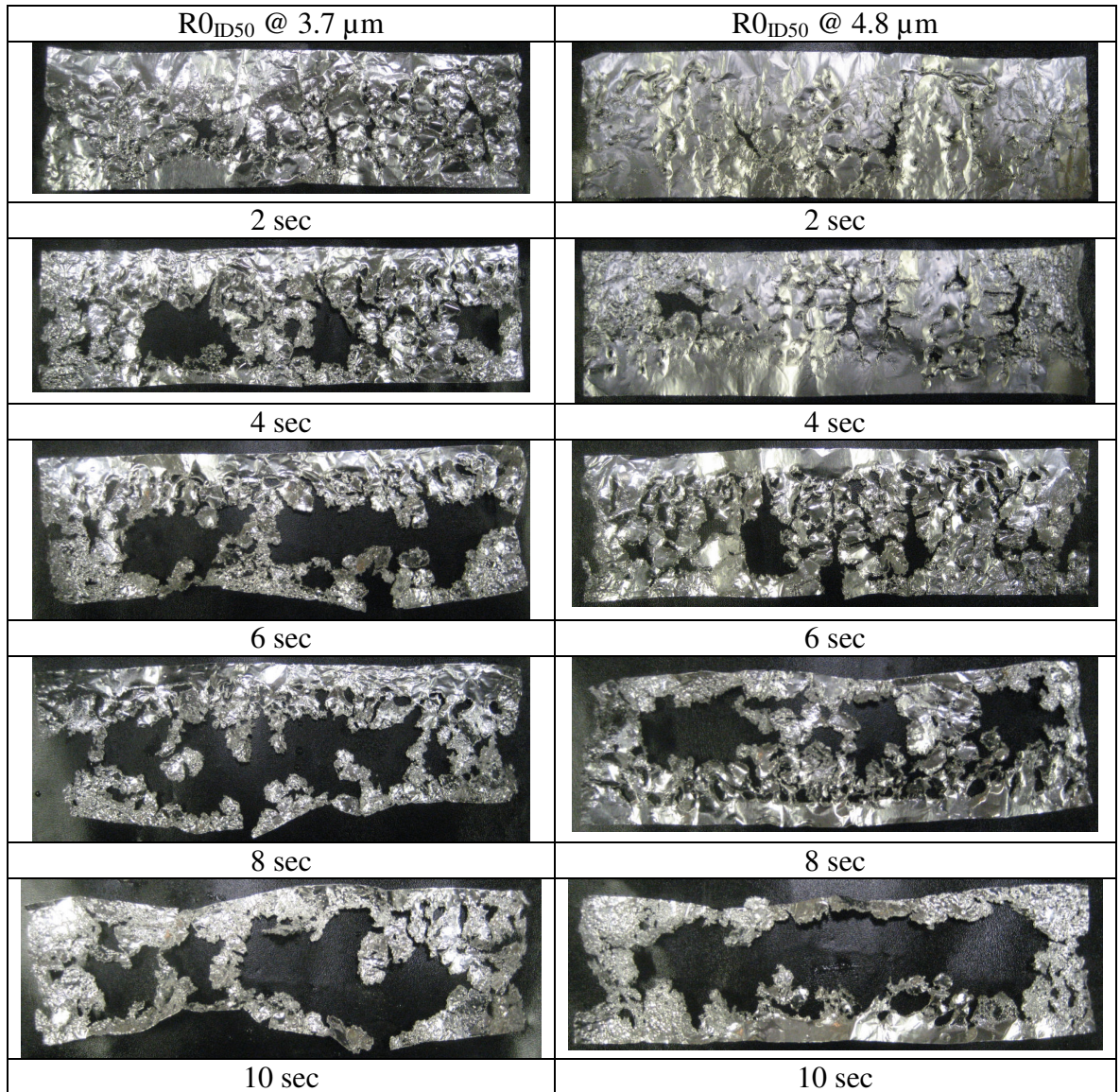


**Figure 4-7 – Aluminium foil specimens subjected to cavitation by R0<sub>ID30</sub> mode radial horn with 0.5 gain booster attached for 2 s (top row), 4 s (2<sup>nd</sup> row) 6 s (3<sup>rd</sup> row), 8 s (4<sup>th</sup> row) and 10 s (bottom row) at 1.5, 2.3, 3.8 and 7.3  $\mu\text{m}$  ultrasonic amplitudes**

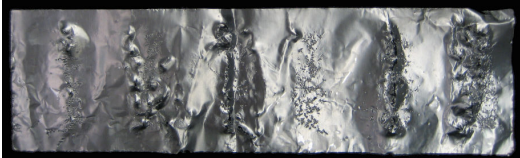


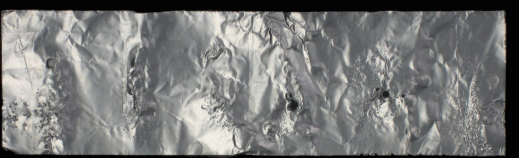
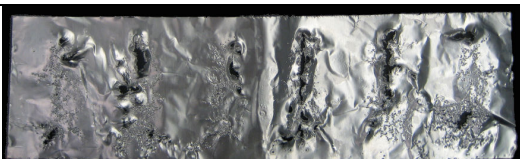

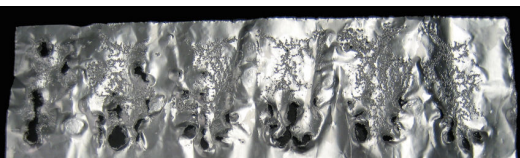
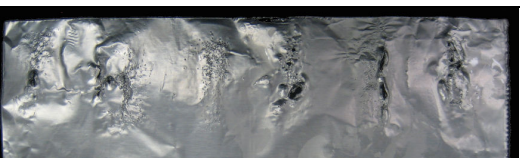
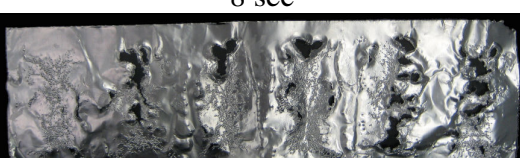
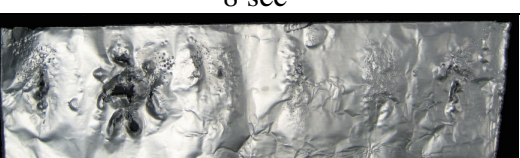


R0 <sub>ID50</sub> @ 1.8 μm	R0 <sub>ID50</sub> @ 2.3 μm
	
2 sec	2 sec
	
4sec	4sec
	
6 sec	6 sec
	
8 sec	8 sec
	
10 sec	10 sec

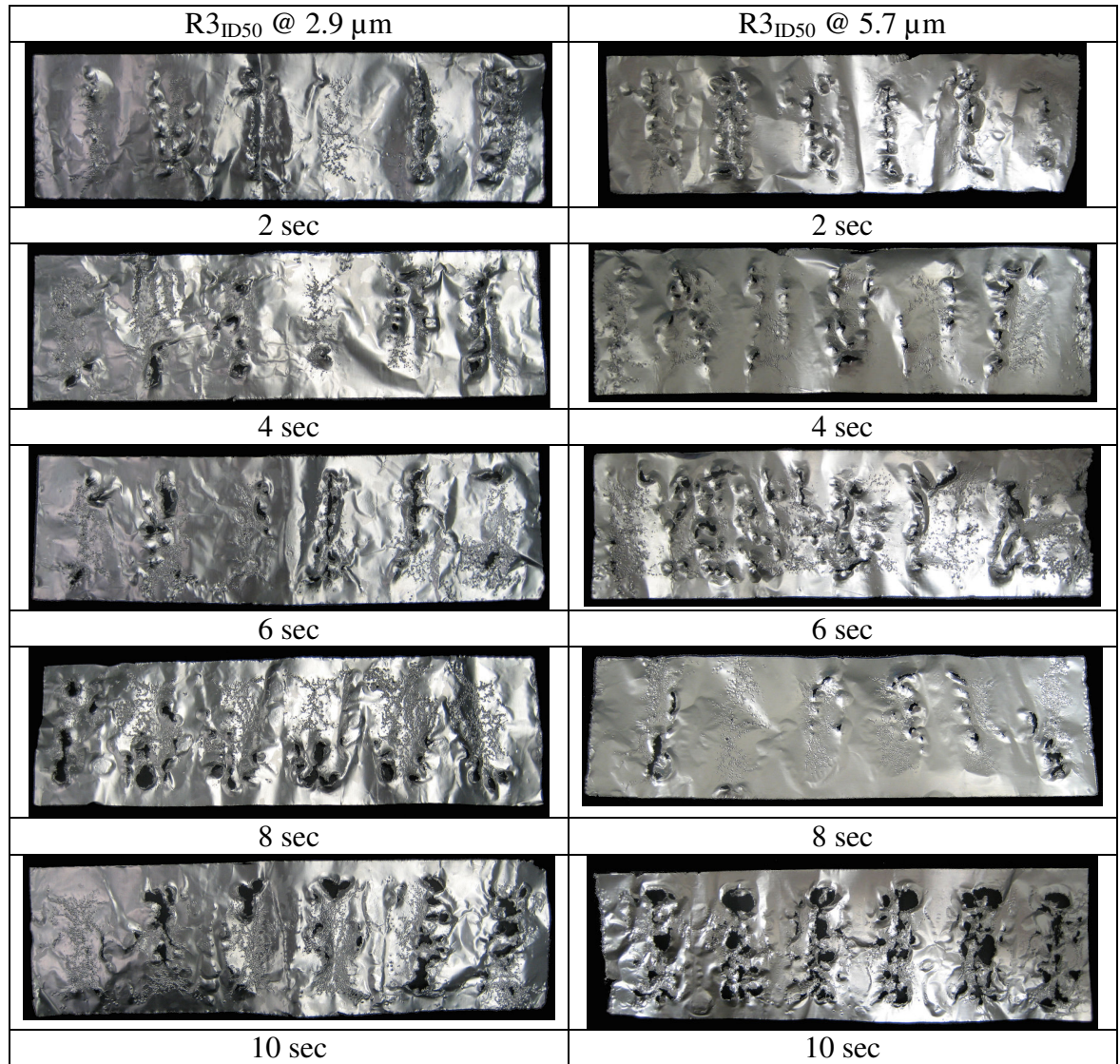




**Figure 4-8 – Aluminium foil specimens subjected to cavitation by  $R0_{ID50}$  mode radial horn for 2 s (top row), 4 s (2<sup>nd</sup> row) 6 s (3<sup>rd</sup> row), 8 s (4<sup>th</sup> row) and 10 s (bottom row) at 1.8, 2.5, 3.7 and 4.8  $\mu\text{m}$  ultrasonic amplitudes**

R3 <sub>ID50</sub> @ 1.3 μm	R3 <sub>ID50</sub> @ 1.7 μm
	
2 sec	2 sec
	
4 sec	4 sec
	
6 sec	6 sec
	
8 sec	8 sec
	
10 sec	10 sec

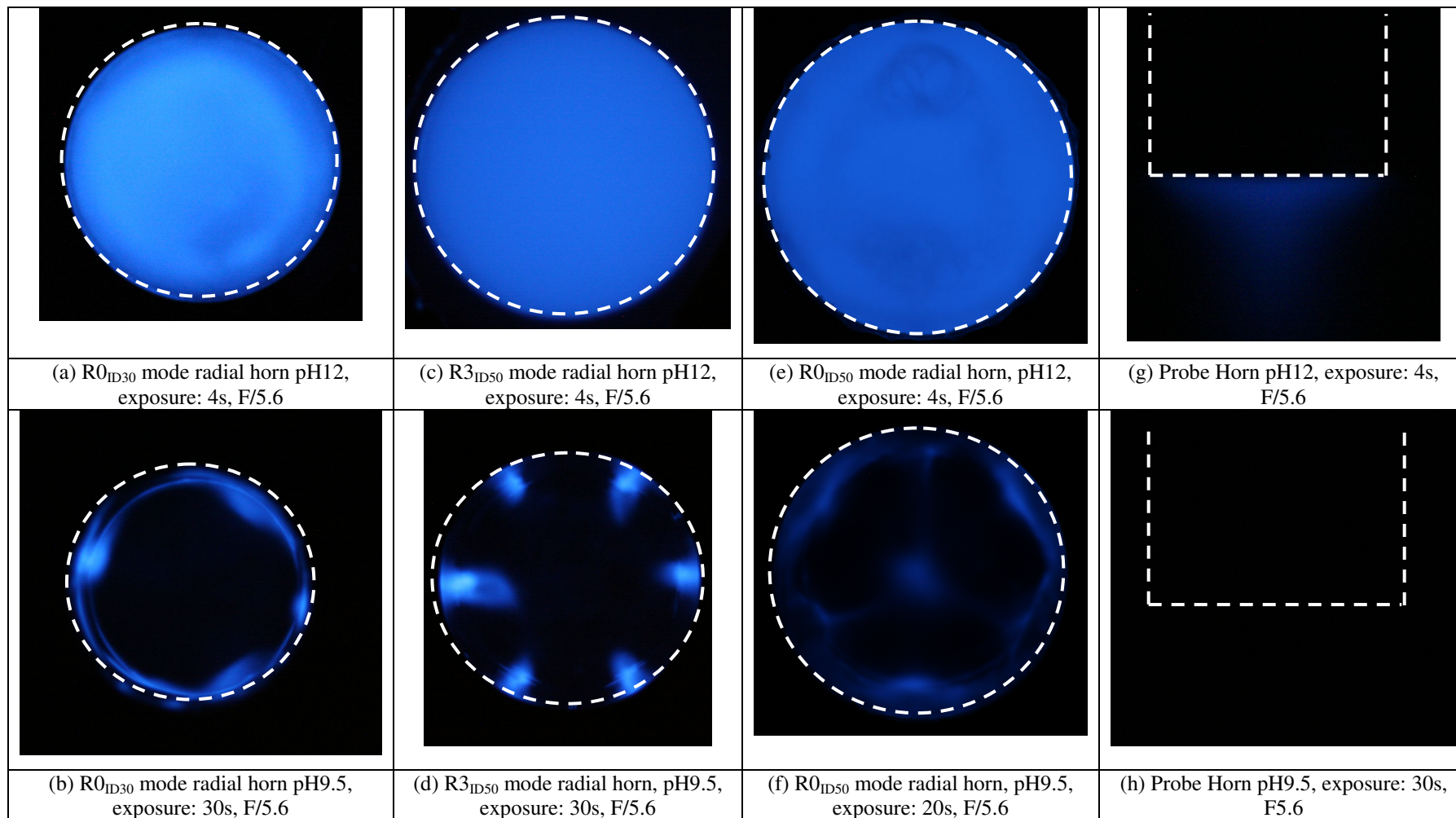




**Figure 4-9 – Aluminium foil specimens subjected to cavitation by R3<sub>ID50</sub> mode radial horn with 2.0 gain booster attached for 2 s (top row), 4 s (2<sup>nd</sup> row) 6 s (3<sup>rd</sup> row), 8 s (4<sup>th</sup> row) and 10 s (bottom row) at 1.3, 1.7, 2.9 and 5.7  $\mu\text{m}$  ultrasonic amplitude**

Applying the chemical method of visualisation, photographs of the Sonochemiluminescence of both the radial and probe horns can be observed in Figure 4-10. It can be seen that the probe device gives a cone like field of luminescence at pH 12, similar to that described by other researchers [149, 150] but exhibits no luminescence at the lower pH 9.5. This field can be more clearly seen in Figure 4-11, which is the same image as Figure 4-10 (g) with the brightness levels adjusted. It can also be seen that the R0<sub>ID30</sub> mode radial horn produces an intense SCL field close to the vibrating face at the lower pH whilst an intense luminescence field over the entire area is produced at the higher pH. The R0<sub>ID50</sub> mode radial horn again produces a strong luminescence throughout the

entire volume at pH 12. At pH 9.5 this horn produces luminescence at the edges of the volume, similar to the results for the  $R0_{ID30}$  mode horn. However, there is also a visible luminescence from the centre of the volume with lines extending from the centre to the extremities of the cavity. The  $R3_{ID50}$  horn also exhibits a bright luminescence at pH 12 while at pH 9.5 six distinct areas of light can be observed equally spread over the circumference of the inner cavity.



**Figure 4-10 – Photographs of chemiluminescence of luminol solution for pH12 [(a), (c), (e), (g)] and pH9.5 [(b), (d), (e), (h)] for the R0<sub>ID30</sub> mode radial horn [(a), (b)], the R3<sub>ID50</sub> mode radial horn [(c), (d)], the R0<sub>ID50</sub> mode radial horn [(e), (f)] and the probe horn [(g), (h)]**



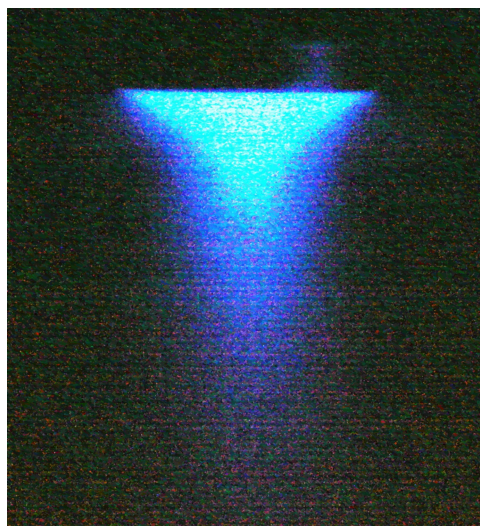


Figure 4-11 - Chemiluminescence of the probe horn at pH12 with adjusted brightness

#### 4.3.4 Discussion

From the literature, strong luminescence at the areas of strong cavitation is expected. Thus it was predicted that an area of luminescence at the centre of the R0 horns should be observed. Luminescence was observed in the centre of the R0<sub>ID50</sub> horn but not the R0<sub>ID30</sub> horn. Both radial horns displayed a luminescence at the outer edge of the fluid volume. It is proposed that the sonochemiluminescence observed at the outer edge of the fluid volume in Figure 4-10 for the R0<sub>ID30</sub> and R0<sub>ID50</sub> radial horns at pH 9.5 is due to chemical reactions taking place involving the luminol solution and the aluminium horn. Kulmala et al. [151] have shown that chemiluminescence of luminol solutions can occur through reactions with aluminium. Kumala et al. argued that the high pH of the solution broke down the microscopic aluminium oxide layer which prevents any further oxidation of aluminium and thus allowed the solution to come in contact with the aluminium metal and react chemically with it. This is not the case here, since no emission of light is observed when the radial horn is not vibrating. However, breakdown of this layer will be enhanced by the aspherical collapse of cavitation bubbles near a solid boundary which causes high speed jets to be formed and is known to cause the breakdown of oxide layers on surfaces. In fact this is the primary function for ultrasonic cleaning baths. The observations from the aluminium foil test using the R0<sub>ID30</sub> and R3<sub>ID50</sub> horn strongly support this since cavitation damage is observed on the foil strips. Also, the chemiluminescence results from the R0<sub>ID50</sub> horn at pH 9.5 clearly show an area of luminescence in the centre of the fluid cavity, this indicates that this mode does indeed have a strong cavitation field at the centre of the fluid volume. It may be that the small inner diameter of the R0<sub>ID30</sub> mode radial horn prevents

this feature from being captured by the SCL technique. The results for all the radial horns at the higher pH show an intense luminescence field throughout the fluid. This is caused by the luminol solution reacting with OH radicals produced during bubble collapse. Although there is a strong cavitation focus in the centre, there are also streamers and bubble collapse is happening throughout the fluid which causes the entire volume to glow.

It can be seen that the cavitation fields of both the radial and probe horns are quite different. The probe horn has its cavitation field located in a cone structure at the tip and it has been shown this area is also chemically active. The radial horn, however, focuses the cavitation field in the centre of the horn away from the vibrating face yet is very chemically reactive throughout the whole volume.

In assessing the effectiveness of the booster, it can be observed that by comparing the aluminium foil tests there is a noticeable effect on cavitation pitting when used in either the 0.5 gain or 2.0 gain configuration. Figure 4-12 shows the damage caused to the strip of aluminium foil in the R0<sub>ID30</sub> mode radial horn cavity after 10 s for vibration amplitudes of 1.5, 2.3, 3.8 and 7.3  $\mu\text{m}$ . It can be seen that there is significantly less damage caused to the foil when the ultrasonic amplitude is small but damage increases significantly as greater ultrasonic amplitude is applied. This indicates that the amplitude of the radial horn is the primary factor in the strength of cavitation field generated and that a booster horn may be used successfully to adjust the range of amplitudes available.

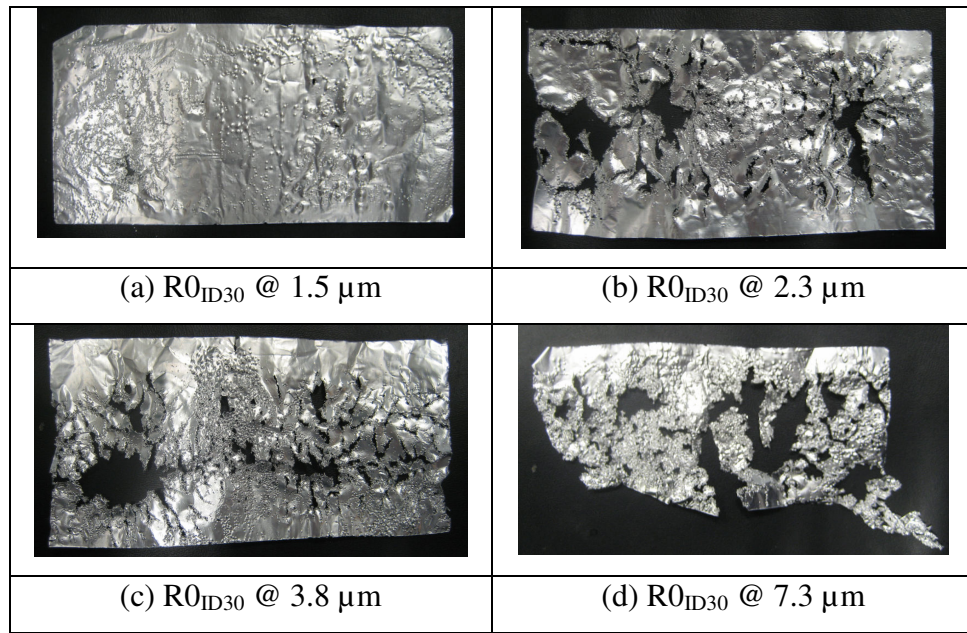
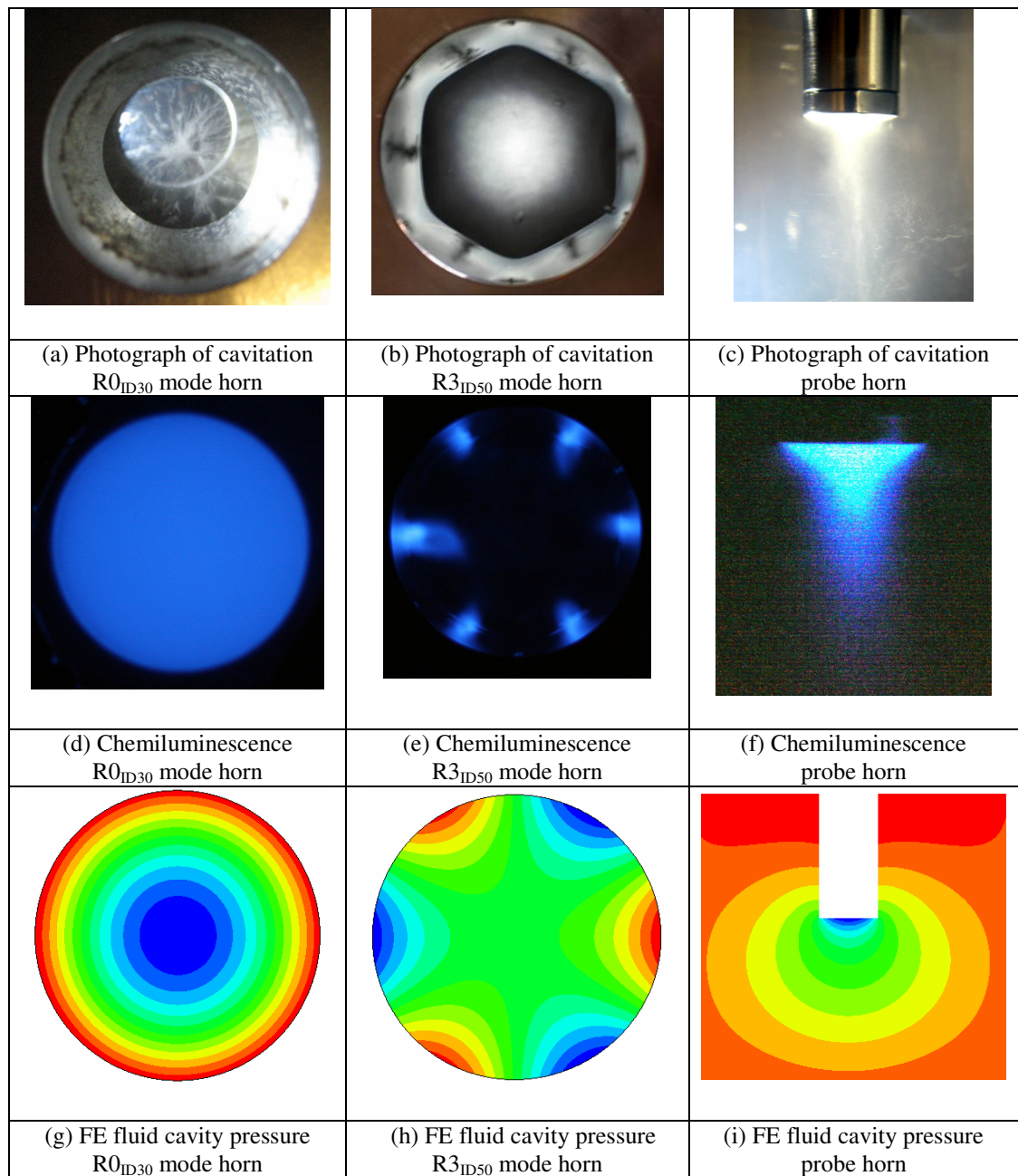


Figure 4-12 – Comparison of aluminium foil tests using the R0<sub>ID30</sub> horn at 1.5, 2.3, 3.8 and 7.3 μm after 10s sonication

#### 4.4 Model Verification

Figure 4-13 summarises the results from the visualisation study and the FE model of the fluid cavity. As discussed previously, it can be observed from the photographs in the first row that the R0<sub>ID30</sub> mode horn creates a focussed bubble field in the centre of the fluid cavity away from the vibrating face, the R3<sub>ID50</sub> mode horn produces a hexagonal volume of fluid in the centre which is not undergoing cavitation, and the probe horn creates a conical cavitation field close to the vibrating tip.



**Figure 4-13 – Comparison of photographs, chemiluminescence and FEA predictions for the R0<sub>ID30</sub> mode radial horn, the R3<sub>ID50</sub> mode radial horn and the probe horn**

These patterns of cavitation activity are confirmed by the chemiluminescence of luminol, shown in the second row of Figure 4-13. The R0<sub>ID30</sub> mode radial horn produces a uniform light output throughout the fluid in the cavity, indicating that there is cavitation throughout the fluid volume and not only at the centre, whilst the R3<sub>ID50</sub> radial horn produces six distinct light points known to be at the anti-nodes of the horn mode shape. The probe device creates a conical volume of light output in the fluid. There is evidence [151] that a

chemiluminescent reaction with luminol can take place if it is exposed to aluminium. It is likely that the chemiluminescence close to the horn inner surface is caused by this reaction.

The third row of Figure 4-12 shows the predicted pressure fields in the fluid cavity for all three devices from the FE models. Areas of high pressure magnitude are displayed in blue and red, red indicates a positive pressure while blue indicates a negative one. It can be seen that the predicted pressure fields correlate well with the experimentally observed cavitation fields using photographs and chemiluminescence. In the case of the R0<sub>ID30</sub> and R3<sub>ID50</sub> radial horns there is close correlation between the locations of the observed cavitation fields and the FE predicted locations of high pressure magnitude. However, the results from the probe horn study indicate that although the finite element model predicts high pressure at the probe tip, the pressure field close to the tip is dome shaped rather than cone shaped as observed in experiments. Moussatov [149] argues that the formation of a cone shaped bubble field lies in the primary Bjerknes forces and high pressure zones can actually repel bubbles, thus it is not surprising that the predicted pressure field does not exhibit a cone like structure. The primary Bjerknes forces are radiation forces caused by bubbles being acted upon by a sound field and are the most significant force after buoyancy. Translational forces can be produced by bubble oscillations coupling with non-zero acoustic pressure gradients. The pressure gradients set up within the fluid due to the acoustic field cause bubbles which are smaller or larger than resonance to move toward the anti-node and node respectively. Bubbles smaller than the resonance size, 120  $\mu\text{m}$  at 20 kHz, are normally attracted to the anti-nodes of the pressure field. However, at high amplitudes, it is possible for the direction of the primary Bjerknes forces to change causing these areas to become repulsive zones. Thus bubbles are repelled from this area and pass round it. Further from the probe tip, the pressure level reduces and the radial diameter of the repulsive zone decreases to the point where the direction of the primary Bjerknes forces changes from repulsive to attractive causing the formation of the cone like structure [149].

## **4.5 Conclusions**

The pressure fields created by several different ultrasonic devices operating in water have been calculated using the finite element method. The shape of the pressure fields is shown to be consistent with evidence in the published literature for probe horns and is further confirmed by visualisation studies using photographs, chemiluminescence and aluminium



foil. The parametric studies carried out using FEA show that the pressure field created is dependant on the shape of the fluid cavity, applied vibration amplitude and mode of vibration. It has been shown that for the  $R0_{ID30}$  mode radial horn that there is a concentration effect and the pressure obtained in the centre of the fluid cavity is much greater than that obtained close to the vibrating surface. It has also been shown that as the inner diameter of the radial horn decreases, the pressure field becomes more uniform, though the maximum pressure obtained is lower compared to larger diameters for the same input vibration amplitude. Furthermore, the aluminium foil tests have shown that the  $R0_{ID30}$  mode horn causes significant damage even close to the vibrating face where the lowest pressure has been predicted. Meanwhile the  $R3_{ID50}$  mode radial horn leaves significant areas of the aluminium foil undamaged due to the locations of the nodes of the R3 mode. Thus, were a R3 mode radial horn to be used for bacterial inactivation, it could be expected that significant portions of the fluid would go untreated. It has also been shown that the cavitation field of the probe horn is only effective close to the probe tip. It is concluded that for use in bacterial inactivation, R0 mode radial horns with small diameter should be used as more of the fluid will be treated although it should be noted that the lifetime of the device may be reduced due to more cavitation damage occurring at the vibrating surface of the horn.

---

## Chapter 5 – Bacterial Inactivation under No Flow Conditions

---

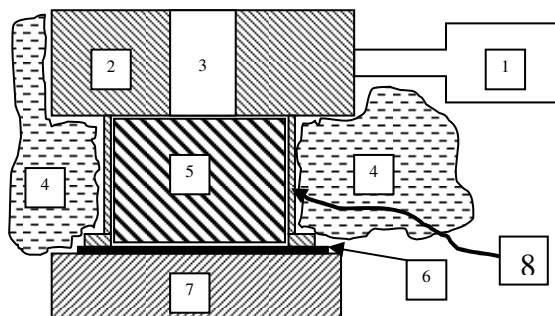
### 5.1. Introduction

Ultrasonic treatment alone takes a long time to inactivate bacteria sufficiently to be useful in most flow processes [29]. Consequently there have been only a few studies researching the use of ultrasonics as a bactericidal technology in flow-through systems [29, 111, 138, 139]. These studies have concentrated on adapting a fluid system to incorporate an ultrasonic probe with the flow rates being very low. The ultrasonic probe may not be ideal for flow-through devices, even for very low flow-rates, as the cavitation field is concentrated around the tip of the probe and not distributed across the flow. Also, at large amplitudes the probe device creates a permanent layer of gas at the tip thus making additional energy input to the fluid extremely difficult if not impossible. This chapter investigates the use of a radial mode ultrasonic horn, which could be more readily adapted as a flow through bacterial inactivation device. Initially no-flow conditions were investigated to ascertain the effectiveness of these devices on *Escherichia coli* K12 and *Staphylococcus aureus* 24 before moving onto the more complex flow conditions. The performance of the radial horn designed here is compared with an ultrasonic probe in order to assess its effectiveness across a number of criteria. These include the power intensity ( $\text{W}/\text{cm}^2$ ) and power density ( $\text{W}/\text{cm}^3$ ) as well as the bacterial inactivation rate.

### 5.2. Microbiological Methods

During the microbiological tests a sterile technique was used throughout. The radial horn was mounted on an aluminium base with the fluid sealing provided by a rubber gasket. The main vibratory action is through the horn with the tuned cylinder acting simply as part of the mounting, thus there will be little inactivation of bacteria in the mounting structure. In order to observe the bacterial efficacy of the horn it was necessary to have as little fluid as

possible in the tuned cylinder mounting section; this was achieved by inserting a loose fitting plastic cylinder into the tuned cylinder cavity (Figure 5-1).



**Figure 5-1 – Sketch of experimental set-up. (1) 20 kHz Ultrasonic Transducer, (2) Radial Horn, (3) Radial horn cavity (volume of fluid containing bacteria), (4) Ice packing, (5) Plastic insert, (6) Rubber gasket, (7) Aluminium mounting flange, (8) Tuned mounting cylinder**

In order to assess the efficacy of the devices being tested it is required to know the number of viable bacteria at set times during the test. There are a number of methods to achieve this, each with their own advantages and drawbacks. The direct microscopic count method involves taking a sample of the media and placing it in a counting chamber over which a glass slide with imprinted grid is placed. The volume within each grid square is precisely known and the cells in each grid square can be counted using a microscope, thus allowing an accurate estimate of the bacterial concentration within the fluid. This is a quick way of determining the bacterial concentration, however its drawbacks mean it is unsuitable for this work. The direct microscopic count method does not distinguish viable cells from dead cells making it impossible to determine the efficacy of the devices used. In order to distinguish between viable and dead cells, a viable cell count method must be used.

The traditional method of counting viable cells is known as the pour plate method or spread plate method. In the pour plate method a small sample (typically 0.1-1 ml) of the liquid is pipetted onto a sterile Petri dish into which is poured sterile molten agar and mixed well. Agar is a gelatinous substance that acts as a solid nutrient for the growth of cells. The agar plate is then incubated and the number of colonies produced is counted. From this the bacterial concentration of the fluid can be determined. The spread plate method is similar, however it uses agar which has already set. A sample of the fluid is pipetted onto the set agar and spread evenly over the surface of the agar using a sterile glass spreader. Typically no greater than 0.1 ml of fluid is used since the fluid is required to soak into the agar and greater volumes tend not to fully soak in, leaving excess fluid on

the surface of the agar which causes problems when colonies begin to form. The plate is then incubated and the resulting colonies counted. Both of these methods make the assumption that a single viable bacterial cell will form a single colony. This may not be the case due to bacterial cells clumping together, thus several cells will create a single colony resulting in an artificially low concentration being observed. In order to minimise this problem, serial dilutions are usually made and plated out, with the optimum dilution being one which does not produce too few or too many colonies that can be counted. Further, the pour plate method will require the bacteria in the sample to briefly withstand the temperature of molten agar (45-60 °C) and so the spread plate method is more popular with microbiologists since these temperatures could cause bacterial inactivation and give an artificially low cell count. Despite these drawbacks, this method is highly sensitive and accurate and a modified version of the spread plate method is used in these microbiological tests.

There is also an optical method for determining viable cell numbers based on the turbidity of cell suspensions. A fluid medium with suspended bacterial cells looks cloudy because the cells scatter light passing through the suspension. The scattering of light is directly proportional to the number of viable cells within the suspension. By passing an incident light source through the medium and measuring the amount of unscattered light it is possible to determine the bacterial concentration in the fluid. The unscattered light is measured in photometer units and thus a standard curve which relates these units to the bacterial concentration must be determined using the viable count methods described above. This is an extremely fast way to determine the concentration of viable cells within a suspension once the standard curve has been ascertained. Unfortunately, the sensitivity of this method is poor and cell concentrations must be greater than  $10^7$  for the method to give accurate results [152]. The concentrations used in these experiments and the requirement for accurate results make this method inappropriate for these tests.

*E. coli* K12 and *S. aureus* 24 were provided by IBLS (Institute of Biomedical and Life Sciences) at the University of Glasgow for these experiments. These bacteria are ideal laboratory strains as both are non-pathogenic, easy to cultivate and do not require special conditions to grow, while at the same time they are structurally similar to the pathogenic bacteria found in contaminated water and liquid food products. The bacteria were inoculated into trypticase soy broth and incubated at 37 °C in a shaker at 150 rpm until

concentrations of  $10^8$ - $10^9$  CFU/ml were achieved. Since each bacterial culture is unique and the conditions in which they are grown vary slightly from batch to batch it is impossible to determine the exact concentration before a test begins. Thus it is necessary to use similar growth conditions which will yield a close range of concentrations which can be used in the tests. The bacteria were then allowed to rest at room temperature for 1 hour before the solution was poured into the radial horn cavity. Because ultrasonic vibrations can cause large increases in temperature in the fluid inside the horn, the device was placed in a bath of iced water to maintain a low temperature throughout the tests ( $<10$  °C). This ensured that only inactivation due to cavitation was observed and the contribution from thermal mechanisms was negligible. 0.5 ml samples were removed aseptically from the horn by pipetting at 30 s intervals over 5 min. The samples were placed in sterile universals before being serially diluted and plated on trypticase soy agar. Serial dilutions were made to  $10^8$  and then 0.01 ml spots of each dilution were plated, in triplicate. The plates were then incubated at 37 °C for 16 hours before being removed and the resulting colonies counted. Experiments were carried out in duplicate to ensure repeatability. For the radial horn, tests comparing the effect of power input were carried out at 400 W and 600 W. The probe device operated at its maximum output of approximately 400 W during testing.

It is known that for probe type devices their efficacy is dependant on the sonicated volume and the shape of the sonication cell [153]. However, in order to make a comparison between the devices, the probe device was placed in the same fluid volume as the radial horn cavity. During the experiments, the probe was held in the centre of this volume at a depth such that foaming did not occur and the probe did not touch the bottom of the sonication cell.

Tests were also carried out at two different concentration levels in order to observe if the bacterial inactivation rate was affected by initial bacterial concentrations. This was carried out for the R0 and R3 radial horns at amplitudes of 7.362 and 5.714  $\mu\text{m}$  and for the probe horn at 34.22  $\mu\text{m}$ . Bacterial concentrations of  $2\text{-}3 \times 10^9$  CFU/ml and  $4\text{-}6 \times 10^6$  CFU/ml were used for this experiment.

In order to compare the devices, a set of criteria must be chosen. The radial and probe devices are quite different and have different ideal setups thus it is proposed that the

devices should be compared in a manner consistent with other published studies [109, 131, 154]. Thus, the power input of both devices was measured. The probe device was connected to a generator that displayed the power input in Watts, however the generator for the radial horn had no such feature and thus power input was estimated through calorific methods [132]. It was assumed that all the ultrasonic energy was eventually converted into heat, thus producing a rise in the bulk temperature of the horn and fluid contained within. This rise in temperature can be related to the energy input through;

$$E = (m C_p \Delta T)_{horn} + (m C_p \Delta T)_{fluid} \quad (5-1)$$

Where  $m$  is the mass being sonicated,  $C_p$  the specific heat capacity and  $\Delta T$  the temperature rise in Kelvin. The power input,  $P$ , can then be calculated using;

$$E = P t \quad (5-2)$$

Where  $t$  is the time taken to achieve the temperature rise in seconds.

Experiments were carried out under “no ice” conditions by filling the fluid cavity with water, applying the ultrasonic vibrations and measuring the increase in temperature using a thermometer at 30 s intervals over a period of 5 min in order to determine the power input to the system. This was carried out for all the devices, configurations and power levels used in the microbiological experiments.

There are two main criteria used when comparing ultrasonic tests; the ultrasonic intensity and power density. Ultrasonic intensity is defined in the literature in units of Watts per square centimetre ( $\text{W}/\text{cm}^2$ ) of horn working surface [109, 131] and power density as Watts per cubic centimetre ( $\text{W}/\text{cm}^3$ ) of the sonicated volume [131]. In this study, both are presented for comparative purposes. For consistency, the intensity measurements for the probe horn were carried out in the same sonicated volume as the radial horn.

### **5.3. Results**

Figures 5-2 – 5-4 show the results from the temperature tests in order to determine the power from the various ultrasonic horn devices and set-ups for the  $R0_{ID30}$ ,  $R3_{ID50}$  and  $R0_{ID50}$  horns. It can be seen that in all cases the relationship between the increase in temperature and the length of time ultrasonic vibrations were applied is linear. A line of best fit has been applied to the data points and the power input to the system is estimated from equations 5-1 and 5-2 and the results of this are shown in Table 5-1.

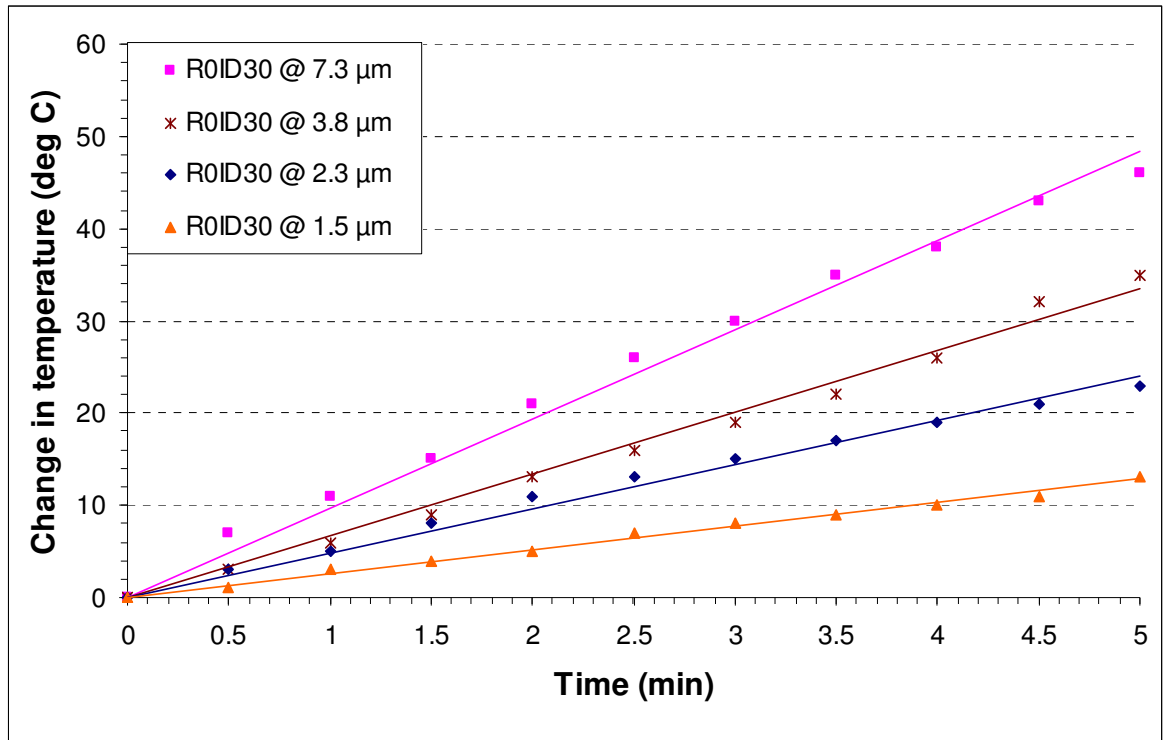


Figure 5-2 – Temperature increase of R0<sub>ID30</sub> mode radial horn and liquid at different input vibration amplitude

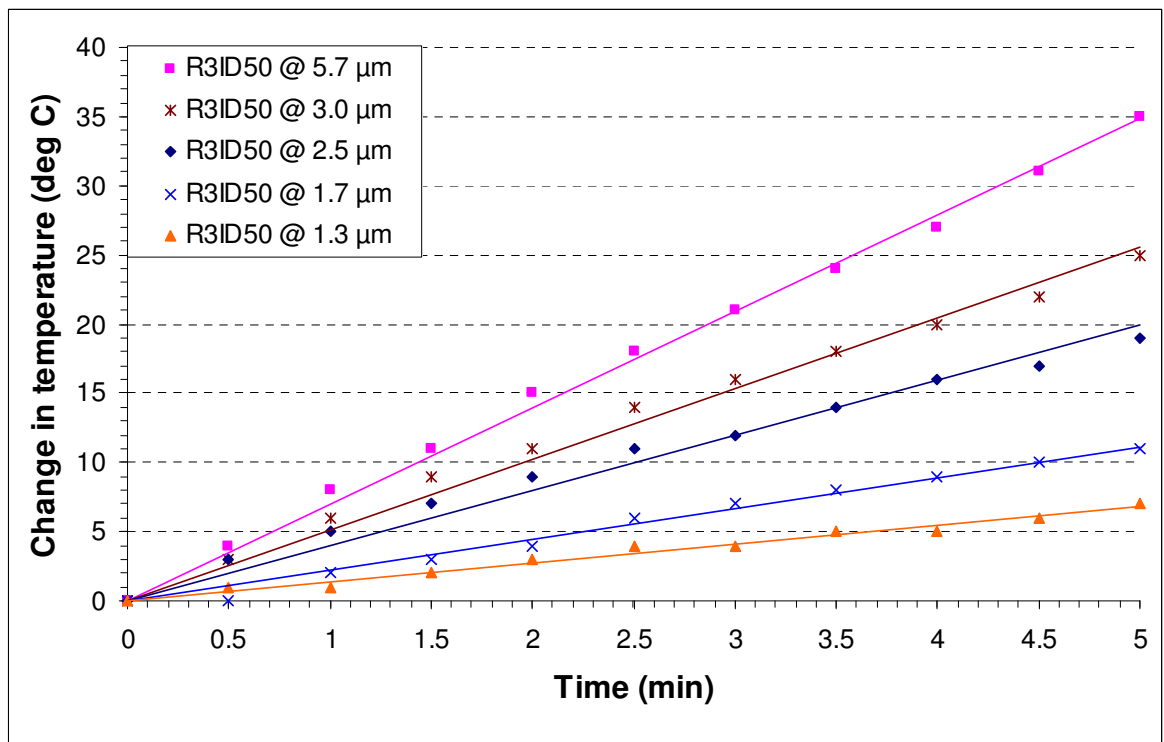
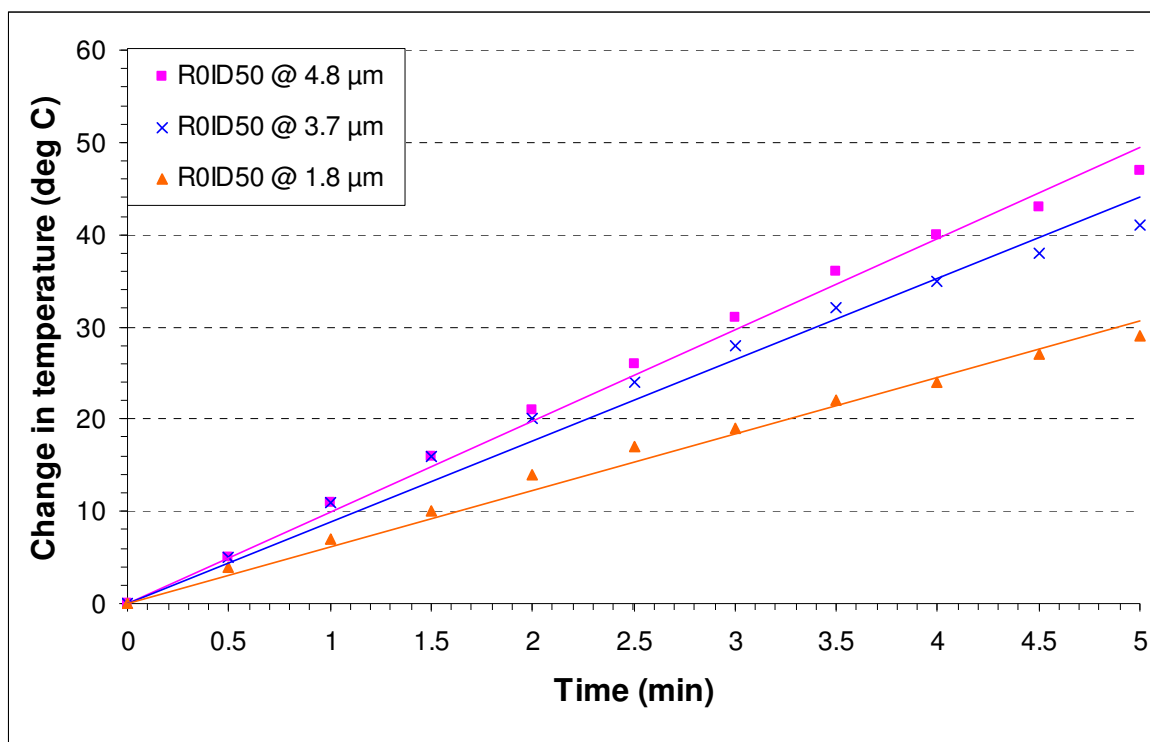


Figure 5-3 – Temperature increase of R3<sub>ID50</sub> mode radial horn and liquid at different temperatures and power levels, with and without the booster horn



**Figure 5-4 – Temperature increase of R0<sub>ID50</sub> mode radial horn and liquid at different input vibration amplitude**

Table 5-1 shows the power consumption (W), ultrasonic intensity  $I_1$  ( $\text{W}/\text{cm}^2$ ) and power density  $I_2$  ( $\text{W}/\text{cm}^3$ ) of the R0<sub>ID30</sub>, R3<sub>ID50</sub>, R0<sub>ID50</sub> and probe horns at the ratings used during the microbiological tests. It can be observed that the radial horns draw between 150 and 325 W when operating at 1.3  $\mu\text{m}$  and 7.3  $\mu\text{m}$  respectively while the probe device draws 380-400 W, close to its maximum capacity. The intensity of the radial devices varies from 0.8-9.2  $\text{W}/\text{cm}^2$  between 1.3-7.3  $\mu\text{m}$  respectively whilst the probe device operates at over 300  $\text{W}/\text{cm}^2$ . This large variation in intensity is due to the difference in horn surface area. The probe surface area is calculated as the area of the probe tip whereas the radial horn surface area is calculated as the product of the inner circumference and the depth of the cylinder. Comparisons of intensity are usually carried out for different probe designs due to the similar sizes, designs and cavitation fields created, however, due to the large difference in physical size of the radial horn and probe, as well as the differences already outlined in the cavitation field created, the measure of ultrasonic intensity as a method for comparison seems weak. A more sensible criterion is that of power density, whereby the power input to the fluid cavity is determined. This criterion eliminates the problems associated with trying to compare devices with vastly different surface areas and cavitation fields. Table 5-1 shows that using this criterion the radial horns operate at between 0.6 and 14.8  $\text{W}/\text{cm}^3$  for



1.3  $\mu\text{m}$  (R0<sub>ID50</sub> horn) and 7.3  $\mu\text{m}$  (R0<sub>ID30</sub> horn) vibration input amplitudes respectively while the probe device operates at 12.6 W/cm<sup>3</sup> at 34.2  $\mu\text{m}$ .

Horn	Inner Diameter (mm)	Ultrasonic amplitude ( $\mu\text{m}$ )	Power (W)	I <sub>1</sub> (W/cm <sup>2</sup> )	I <sub>2</sub> (W/cm <sup>3</sup> )
R0 <sub>ID30</sub>	30	7.3	325	9.2	14.8
R0 <sub>ID30</sub>	30	3.8	248	7.0	11.2
R0 <sub>ID30</sub>	30	2.3	162	4.6	7.4
R0 <sub>ID30</sub>	30	1.5	92	2.6	4.2
R3 <sub>ID50</sub>	50	5.7	280	4.0	3.2
R3 <sub>ID50</sub>	50	3.0	200	2.8	2.3
R3 <sub>ID50</sub>	50	2.5	152	2.2	1.7
R3 <sub>ID50</sub>	50	1.7	88	1.2	1.0
R3 <sub>ID50</sub>	50	1.3	56	0.8	0.6
R0 <sub>ID50</sub>	50	4.8	227	3.2	2.6
R0 <sub>ID50</sub>	50	3.7	198	2.8	2.2
R0 <sub>ID50</sub>	50	1.8	150	2.1	1.7
	<b>Tip Diameter (mm)</b>				
Probe	13	34.2	380-400	301	12.6

**Table 5-1 – Power and intensities of the radial horns and probe device in the configurations used in these studies**

In determining the bacterial efficacy of the ultrasonic devices used in these studies, several tests were carried out. Figure 5-5 shows the results from using the R3<sub>ID50</sub> radial mode horn at ultrasonic amplitudes of 1.3, 1.7, 2.5, 3.0 and 5.7  $\mu\text{m}$  using *E. coli* K12. The booster horn described in Chapter 3 was used in the 0.5 gain and 2.0 gain configurations in an attempt to provide a greater variation in amplitudes which the horn could operate in and thus provide a better view of the relationship between amplitude and bacterial efficacy. The error bars in the Figure show the spread of results from the several tests carried out to ensure repeatability. The results have been plotted on an ordinate of sonication time in minutes and an abscissa of % survival on a logarithmic scale. It can be seen that in all cases the % survival is consistent with first order death kinetics and a line of best fit has been applied to the data. From these results the D-values can be obtained for each of the different cases. The D-value is defined as the length of time it takes to reduce the viable bacterial count by one log. Using the line of best fit the D-values for the R3<sub>ID50</sub> radial horn are determined. The D-values for the tests carried out are found to vary between 2.2 and 12.7 min (Table 5-2).

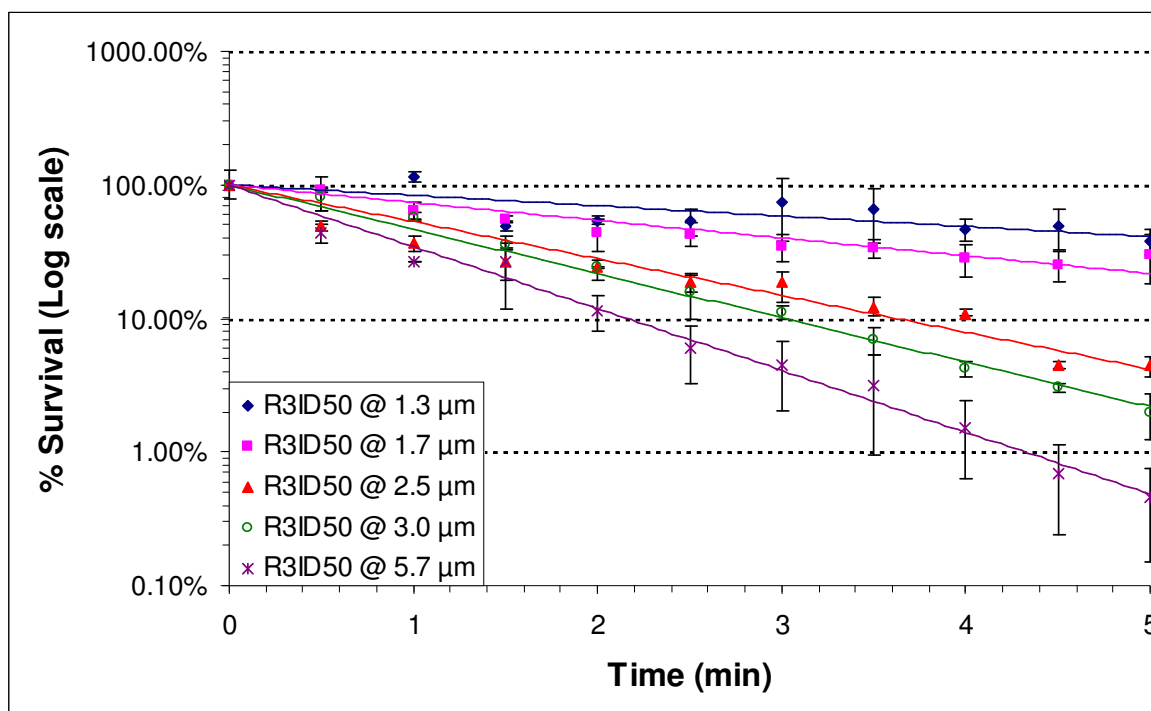


Figure 5-5 – Bacterial inactivation using the R3<sub>ID50</sub> radial horn at vibration input amplitudes of 1.3, 1.7, 2.5, 3.0 and 5.7  $\mu\text{m}$  using *E. coli* K12

Horn	Ultrasonic amplitude ( $\mu\text{m}$ )	D-Value (min)
R3 <sub>ID50</sub>	5.7	2.2
R3 <sub>ID50</sub>	3.0	3.0
R3 <sub>ID50</sub>	2.5	3.6
R3 <sub>ID50</sub>	1.7	7.5
R3 <sub>ID50</sub>	1.3	12.7

Table 5-2 – D-values for R3 mode radial horn

Figure 5-6 shows a similar analysis carried out with the R0<sub>ID30</sub> mode radial horn again using *E. coli* K12 as the test organism. The booster was used in the 0.5 and 2.0 gain configurations to provide ultrasonic amplitudes of 1.5, 2.3, 3.8 and 7.3  $\mu\text{m}$ . Again, D-values are determined using the line of best fit for the data and are shown in Table 5-3. It was found that the D-values for this horn varied between 1.5 and 12 min.

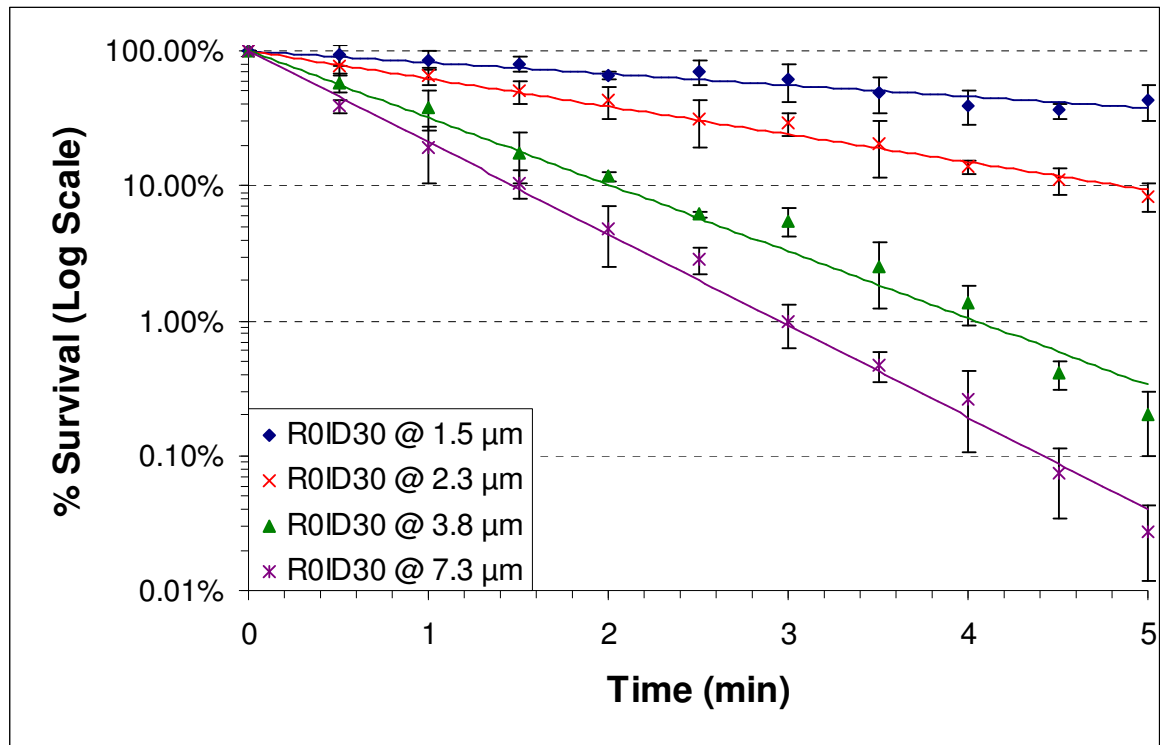


Figure 5-6 – Bacterial inactivation using the R0<sub>ID30</sub> radial horn at vibration input amplitudes of 1.5, 2.3, 3.8 and 7.3  $\mu\text{m}$  using *E. coli* K12

Horn	Ultrasonic Amplitude ( $\mu\text{m}$ )	D-value (min)
R0 <sub>ID30</sub>	7.3	1.5
R0 <sub>ID30</sub>	3.8	2.0
R0 <sub>ID30</sub>	2.3	4.9
R0 <sub>ID30</sub>	1.5	12

Table 5-3 – D-values for R0<sub>ID30</sub> mode radial horn

Figure 5-7 shows the results of the analysis carried out with the R0<sub>ID50</sub> mode radial horn. Microbiological tests using *E. coli* K12 were carried out at vibration amplitudes of 1.8, 3.7 and 4.8  $\mu\text{m}$ . D-values are given in Table 5-4. The minimum and maximum D-values are found to be 1.3 and 4.5 min respectively.

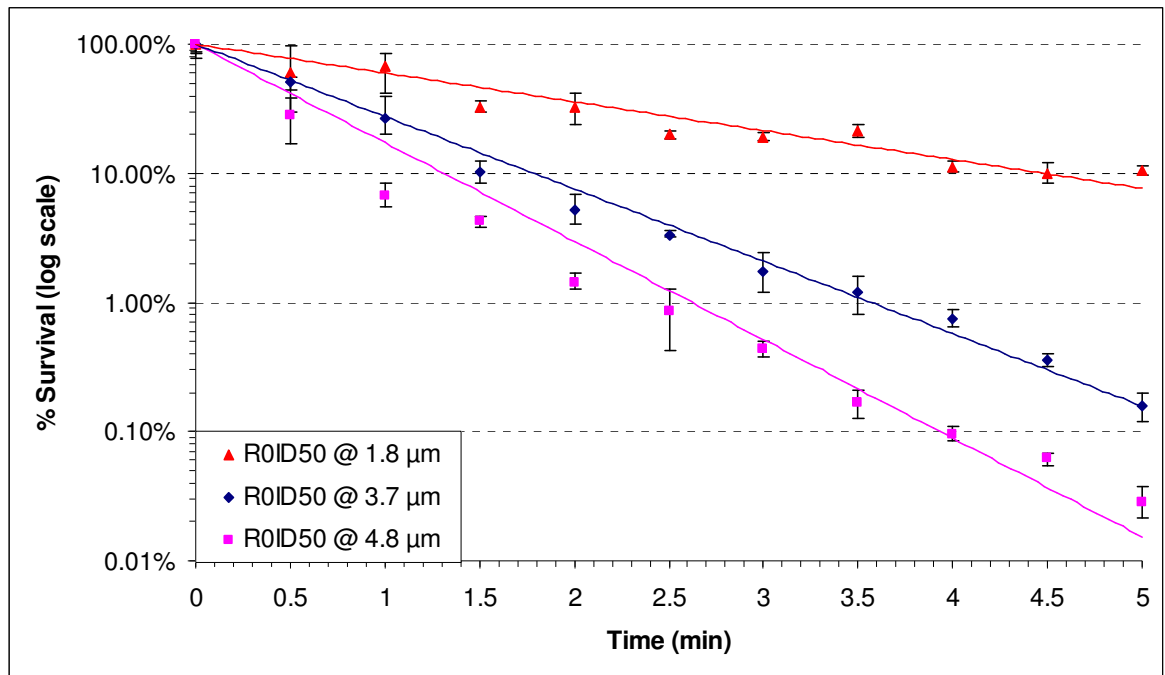


Figure 5-7 - Bacterial inactivation using the R0<sub>ID50</sub> radial horn at vibration input amplitudes of 1.8, 3.7 and 4.8  $\mu\text{m}$  using *E. coli* K12

Horn	Vibration Input ( $\mu\text{m}$ )	D-value (min)
R0 <sub>ID50</sub>	4.8	1.3
R0 <sub>ID50</sub>	3.7	1.8
R0 <sub>ID50</sub>	1.8	4.5

Table 5-4 – D-values for R0<sub>ID50</sub> mode radial horn

Figure 5-8 shows a comparison of the results for the R0<sub>ID30</sub>, R3<sub>ID50</sub>, R0<sub>ID50</sub> and probe horn at a power density level of 14.8, 3.2, 2.6, 12.6 W/cm<sup>3</sup> respectively. It can be seen that in all cases the radial horns perform better than the probe horn.

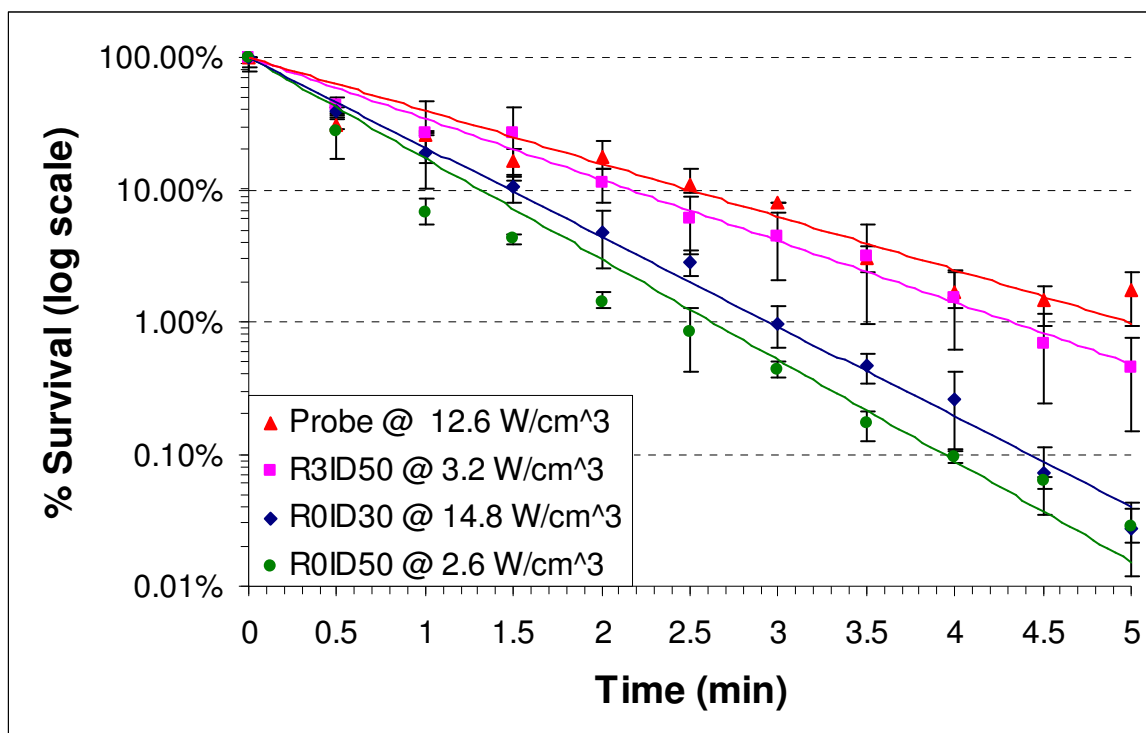


Figure 5-8 – Bacterial efficacy of the R0<sub>ID30</sub>, R3<sub>ID50</sub>, R0<sub>ID50</sub> and probe horns at an intensity level of 14.8, 3.2, 2.6 and 12.6 W/cm<sup>3</sup> respectively using *E. coli* K12

Figure 5-9 shows the effect of initial bacterial concentration on the bacterial efficacy of the R0<sub>ID30</sub>, R3<sub>ID50</sub> and probe horn for *E. coli* K12. It can be seen that in the case of both radial horns, a greater D-value is obtained at lower initial concentrations while the opposite is true for the probe horn. Initial concentrations for all cases are shown in Table 5-5.

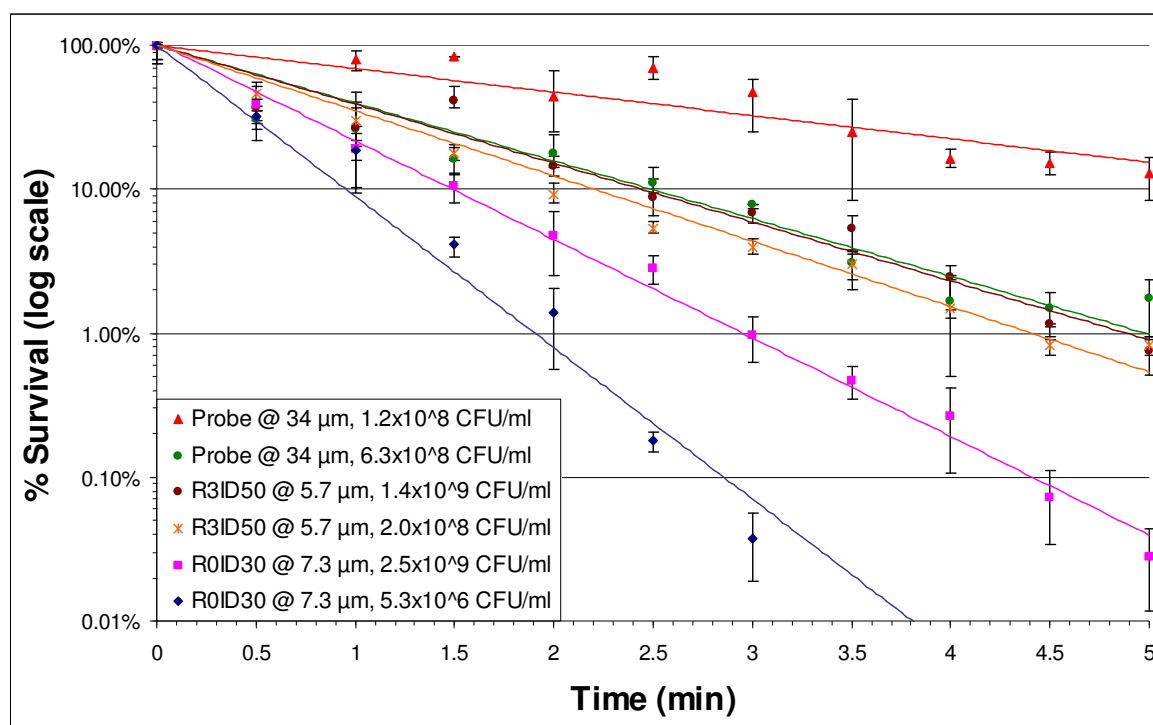


Figure 5-9 –Effect of initial concentration on bacterial efficacy of the R0<sub>ID30</sub>, R3<sub>ID50</sub> and probe horn on *E. coli* K12

Device	Vibration Input (μm)	Initial Concentration CFU/ml
R0 <sub>ID30</sub>	5.7	$5.3 \times 10^6$
R0 <sub>ID30</sub>	5.7	$2.5 \times 10^9$
Probe	34	$1.2 \times 10^8$
Probe	34	$6.3 \times 10^8$
R3 <sub>ID50</sub>	7.3	$2.0 \times 10^8$
R3 <sub>ID50</sub>	7.3	$1.4 \times 10^9$

Table 5-5 – Initial Concentrations

Figures 5-10 and 5-11 show the results from using the R3<sub>ID50</sub> radial horn to inactivate *S. aureus* 24. Figure 5-10 shows the results from an analysis carried out between 0 and 5 min where samples were taken every 30 s while Figure 5-11 shows the results from an analysis carried out between 0 and 30 min with samples taken at 5 min intervals.

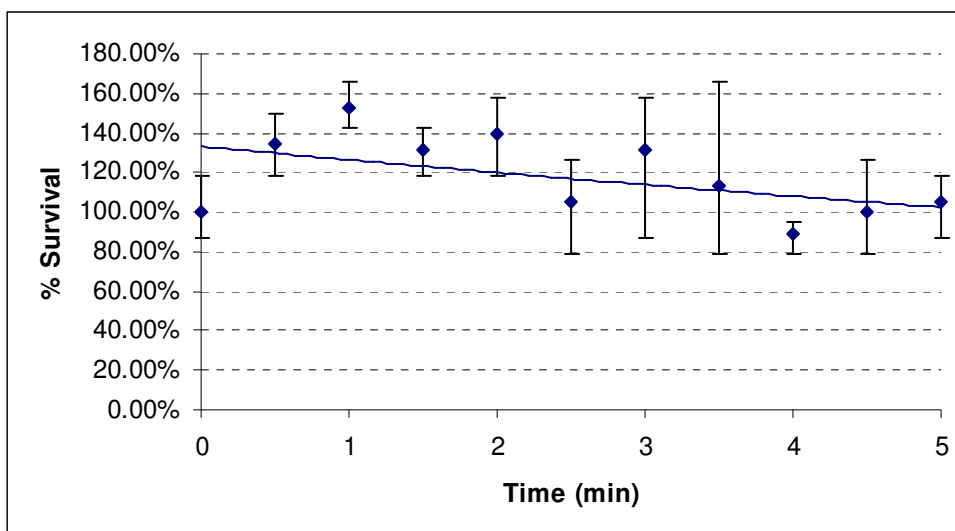


Figure 5-10 – Bacterial efficacy of the R3<sub>ID50</sub> mode radial horn on *S. aureus* 24 for exposure times up to 5 min, samples taken at 30 s intervals

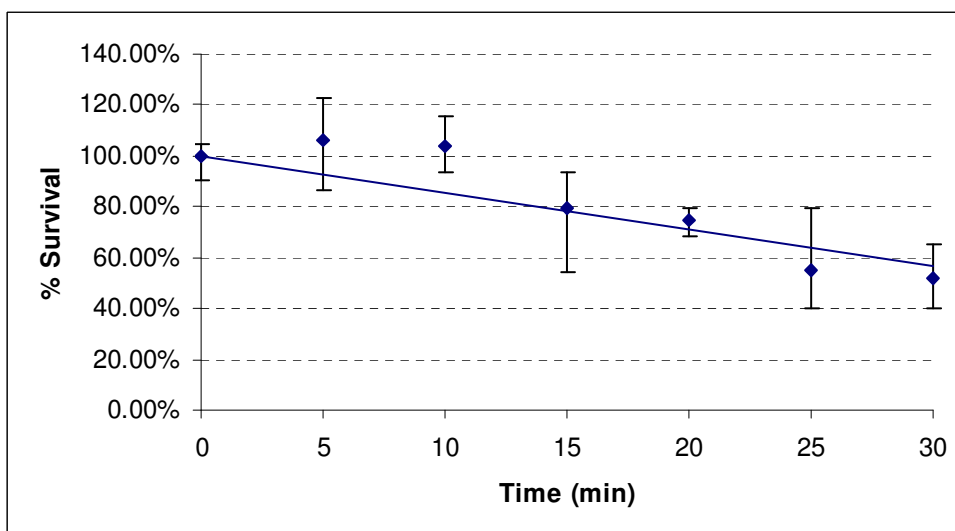


Figure 5-11 - Bacterial efficacy of the R3<sub>ID50</sub> mode radial horn on *S. aureus* 24 for exposure times up to 30 min, samples taken at 5 min intervals

## 5.4. Discussion

Using the comparison criteria set out in section 5.2, Table 5-6 shows the power input, intensity and power density associated with both the radial horn and probe device at the power levels used during this study. This table clearly shows that at similar power levels the probe horn has a much higher ultrasonic intensity ( $\text{W}/\text{cm}^2$ ) due to the small area over which this power is distributed. The radial horns, having a much larger contact surface area, have a much lower intensity level. The power density ( $\text{W}/\text{cm}^3$ ) of the R0<sub>ID30</sub> radial horn and probe device is closely matched due to the same volume of liquid being used

throughout the tests and the power of both devices being similar. The increase in volume for the R3<sub>ID50</sub> and R0<sub>ID50</sub> horns causes the power density to reduce significantly making direct comparisons difficult. It is also difficult to compare this work directly to previous studies in this field as all the studies concerning strains of *E. coli* have been carried out at significantly lower power levels. Studies by Allison (20 kHz, 60W) [106], Hua (20 kHz, 80-140W) [154], and Phull (20 kHz, 50W) [108], investigated the ultrasonic treatment of *E. coli* suspensions.

A new variable is defined here in order to make comparisons between different devices operating at different power levels. In any industrial application of this technology there are two major factors that are of primary importance. First, the power input to a system is of critical importance due to the financial implications; more power means higher cost. Second, the D-value of the system in use is vital because of the importance of reducing bacterial levels to acceptable levels. Thus, such systems will ideally have a low power consumption and a low D-value. Assuming both power and D-value have equal merit then multiplying one by the other gives a number that can be used to compare different systems. This factor should be as small as possible since both power and D-value are desired to be small. Combining the results from Tables 5-1 - 5-4 into a single table and arranging it according to D-value from low to high, Table 5-6 is obtained. This table also shows the multiple of D-value and input power.

Horn	Amplitude (μm)	D-Value (min)	Power (W)	D-value*power (W*min)
R0 <sub>ID50</sub>	4.8	1.3	227	295
R0 <sub>ID30</sub>	7.4	1.5	326	489
R0 <sub>ID50</sub>	3.7	1.8	198	356
R0 <sub>ID30</sub>	3.8	2.0	248	496
R0 <sub>ID30</sub>	2.3	2.2	163	358
R3 <sub>ID50</sub>	5.7	2.2	281	618
R3 <sub>ID50</sub>	3.0	3.0	201	603
R0 <sub>ID50</sub>	1.8	3.3	140	462
R3 <sub>ID50</sub>	2.5	3.6	152	547
R0 <sub>ID50</sub>	1.8	4.5	150	675
R0 <sub>ID30</sub>	2.3	4.9	128	627
R3 <sub>ID50</sub>	1.7	7.5	88	660
R0 <sub>ID30</sub>	1.5	12.0	92	1104
R3 <sub>ID50</sub>	1.4	12.7	56	711

**Table 5-6 – D-values and input powers for all configurations**



Plotting the D-values against the power input, it is possible to see a correlation between these two parameters. Figure 5-12 shows this data with the D-values plotted on the ordinate and the Power input on the abscissa.

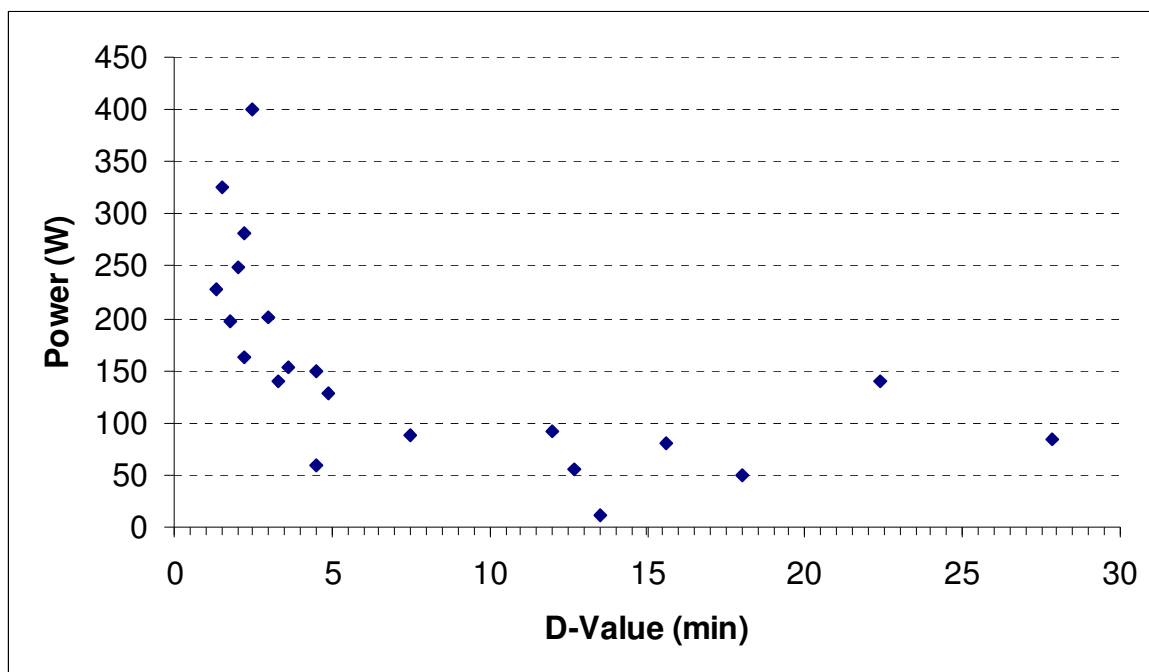


Figure 5-12 – Relationship between the D-value and power input

To determine how these results compare to those studies already published, the efficiency factor is determined for the studies by Allison (20 kHz, 60W) [106], Hua (20 kHz, 80-140W) [154], and Phull (20 kHz, 50W) [108]. Allison carried out experiments on *E. coli* HB101 using a probe horn between power levels of 0-60 W at intervals of 12 W. This study found D-values of 13.5 and 4.5 min for power inputs of 12 and 60 W. Hua carried out tests on an unspecified strain of *E. coli* using a 20 kHz probe device at input powers of 80, 85 and 140 W. This study found the D-values to be 15.62, 27.82, 22.39 min respectively. Phull examined an unspecified strain of *E. coli* using a 20 kHz VC-50 probe device at a power input of 50 W and found the D-value to be approximately 18 min. These studies showed that, at the power levels used, the D-values ranged from 5 to around 30 min. Tabulating these studies to conform to Table 5-6, adding the results of Allison, Hua and Phull and ordering these results in relation to the merit factor defined above from best to worst, it is possible to compare the results from the different devices and studies. This is shown in Table 5-7.

Horn	Amplitude ( $\mu\text{m}$ )	D-Value (min)	Power (W)	D-value*power (W*min)
Allison – Low Power		13.5	12	162
Allison – High Power		4.5	60	270
R0 <sub>ID50</sub>	4.8	1.3	227	295
R0 <sub>ID50</sub>	3.7	1.8	198	356
R0 <sub>ID30</sub>	2.3	2.2	163	359
R0 <sub>ID50</sub>	1.8	3.3	140	462
R0 <sub>ID30</sub>	7.4	1.5	325	489
R0 <sub>ID30</sub>	3.8	2	248	496
R3 <sub>ID50</sub>	2.5	3.6	152	547
R3 <sub>ID50</sub>	3	3	201	603
R3 <sub>ID50</sub>	5.7	2.2	281	618
R0 <sub>ID30</sub>	2.3	4.9	128	627
R3 <sub>ID50</sub>	1.7	7.5	88	660
R0 <sub>ID50</sub>	1.8	4.5	150	675
R3 <sub>ID50</sub>	1.3	12.7	56	711
Phull		18	50	900
R0 <sub>ID30</sub>	1.5	12	92	1104
Hua – Low Power		15.6	80	1248
Hua – Medium Power		27.8	85	2363
Hua – High Power		22.4	140	3136

Table 5-7 – Comparison of studies

Table 5-7 shows that the results obtained are similar to those found by other studies. It also shows that the probe horn used in these studies has a better efficiency than those used by Hua and Phull. This may be due to better transducer technology being used and as such gains in efficiency could be expected. It can be seen that the R0<sub>ID50</sub> horn is more efficient than either the R3<sub>ID30</sub> horn or the probe horn.

Figure 5-8 shows the survival of *E. coli* K12 during treatment with the R0<sub>ID30</sub>, R3<sub>ID50</sub>, R0<sub>ID50</sub> radial horns and probe horn. It can be seen that the radial horn, operating at significantly lower amplitude than the probe device, produced improved bacterial

inactivation. In fact, the R0<sub>ID30</sub> radial horn provided an additional 0.3 log reduction in viable bacterial cells after exposure for 5 min. It is suggested that this is as a result of the focussing of the cavitation field provided by the radial horn. It can also be observed that 600 W power to the radial horn resulted in an additional 0.5 log reduction in bacterial numbers compared to 400 W using the same system.

Although there have been studies into the effect of initial bacterial concentration on the inactivation kinetics using other mechanisms such as heat, pressure and UV radiation [155, 156, 157] there has been no published work to determine if this effect is present during ultrasonic processing. The effect of the initial bacterial concentration on the inactivation efficiency of the R0<sub>ID30</sub> and R3<sub>ID50</sub> radial horns as well as the probe horn can be seen in Figure 5-9. For both radial horns, a greater bacterial inactivation was observed for the lower concentration of *E. coli* K12, with a 2 log reduction in viable bacteria taking approximately 3 min compared to 4 min for the greater concentration using the R0<sub>ID30</sub> horn. The error bars show the spread of the results obtained during testing and represent the minimum and maximum values obtained. These results are consistent with those found in [155, 156, 157] where a larger initial concentration causes an increase in the D-value. This could be caused by a greater bacterial clumping of cells as the concentration increases which provides some protection for the inner bacterial cells within the clump. However, Figure 5-9 shows the opposite holds for the probe device and that larger initial concentrations cause a decrease in the D-value. The cause of this has yet to be elucidated.

Figure 5-10 and Figure 5-11 show the results from using the R3<sub>ID50</sub> radial horn to inactivate the bacteria *S. aureus* 24. It can be seen from these Figures that there is no significant reduction in viable bacteria after 5 min exposure to ultrasonic vibration. In fact, bacteria numbers are shown to increase to 160 % of the original concentration after 1.5 min only reducing back to 100 % after 5 min sonication. It is likely the increase in cell counts is due to bacterial de-clumping being caused by the ultrasonic vibrations. After 30 min sonication the viable cell count was found to reduce by approximately 0.5 log, indicating this bacteria is more resistant to the sonication treatment. This is likely to be caused by the physical structure of the bacteria. *S. aureus* is a gram positive organism and as such has a much thicker cell wall compared to *E. coli* K12. Also, it is spherical in shape thus giving it inherent structural strength unlike the *E. coli* K12 cells which are rod shaped.

### **5.5. Conclusions**

In this study, for a probe device operating at approximately 400 W, a 2 log reduction in viable cells can be achieved within 5 min, giving a D-value of approximately 2.5 min. It was also shown that an ultrasonic device vibrating in a radial mode that is operating at approximately the same power level and frequency as the probe device had a lower D-value, of approx 2 min. Although this is still too long a time scale to be incorporated into a flow-through device, it is possible that combining ultrasound with other bactericidal technologies, such as temperature, pressure and chlorine, to provide enhanced inactivation rates, will be even more effective using this radial device than traditional probe designs, especially since the radial horn is more easily adaptable to flow-through processes. Further increases in amplitude will likely lead to the reduction of the D-value however, the relationship between power drawn and amplitude is non-linear and there will be a point where it is not economically viable to simply increase the power, thus it is envisaged that this technology should be used in combination with other methods of bacterial inactivation. Using several methods of inactivation is beneficial because bacteria are less likely to evolve resistances to several different methods at the same time. Also, given that the cavitation field is focussed in the centre of the horn, away from the working surface, a greater reduction in cavitation damage to the device is observed as compared to probe devices which require titanium tips in order to maintain a good working life.

It has been found that the bacterial inactivation rate using the radial horns is dependant on the initial bacterial concentration. Larger initial concentrations are found to cause an increase in the D-value. However, the opposite was found for the probe horn.

In general, there appears to be a correlation between the input power and the D-value. More data points are required to determine accurately the nature of this relationship and it is likely that the relationship will vary with different bacteria; however it is useful to note that a correlation appears to exist and may assist in further studies.

Experiments using *S. aureus* as the test bacteria yielded poor inactivation results. This bacteria is highly resistant to the sonication process and excessively long treatment times are required in order to inactivate this bacteria. A single log reduction would take in the order of hours rather than minutes.

A merit factor has been defined as the D-value multiplied by the power input and has allowed for the comparison of different published studies using different devices at different power inputs. The radial horn devices are found to compare very favourably to the studies by Allison [106], Hua [154] and Phull [108] using this parameter.

---

## Chapter 6 – Preliminary Study of Bacterial Inactivation under flow conditions

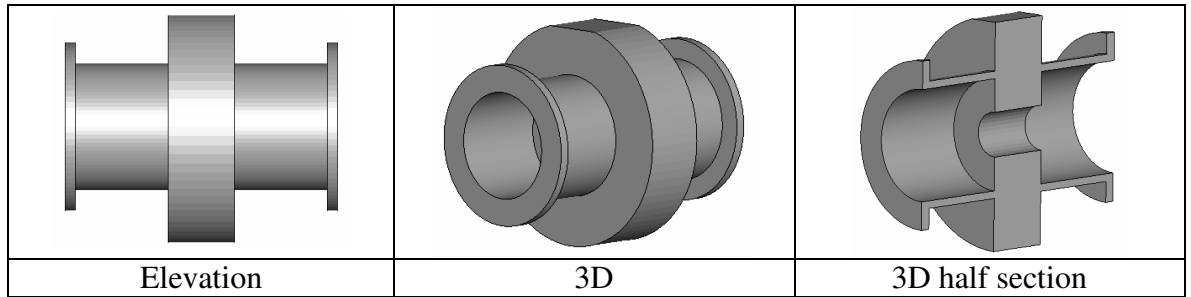
---

### **6.1 Introduction**

It has been demonstrated in the previous chapter that using a radial mode ultrasonic horn to effect bacterial inactivation is successful and more effective than the traditional probe type device. Expanding upon these encouraging results, it is of interest to develop the system further to investigate the effectiveness of using a radial horn for bacterial inactivation under flow conditions. To this end, a R0 mode radial horn based on the R0<sub>ID30</sub> design is constructed to accommodate a continuous flow. This horn was designed using finite element analysis and experiments on the bacterial efficacy of the horn were carried out using *E. coli* K12 and *S. aureus* 24 organisms in a continuous flow setting. This chapter reports the preliminary results of such a system.

### **6.2 Adaptation of Horn Design**

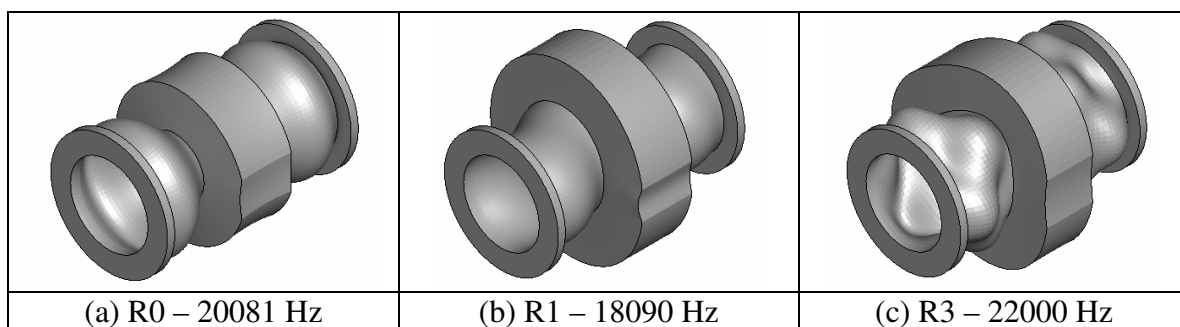
In order to carry out tests using a continuous flow system the radial horn design had to be modified to allow for this. The main horn section of the design remained as it has been proven to work well and keeping this section constant will allow for comparisons to be made between flow and no flow conditions. The easiest way for the design to allow a flow is to have a support pipe/ flange section at each side of the horn and it has already been shown that these sections can be designed not to hinder the vibratory motion of the horn section. Thus the design shown in Figure 6-1 was envisaged and analysed in ABAQUS before being manufactured.



**Figure 6-1 – Flow through design for the radial horn**

A modal analysis and steady state response analysis were carried out in ABAQUS to assess the viability of the design in terms of both modal characteristics and stresses generated during operation. The horn is to be made from Aluminium 1050 having Young's modulus of  $69 \times 10^9 \text{ N/m}^2$  and density  $2700 \text{ kg/m}^3$ . The design for a radial horn operating in the R0 mode at 20 kHz shown in Chapter 3 provides a good basis from which the initial dimensions of this design can be determined. Once the modal parameters have been determined from the initial dimensions, the horn can be scaled, if required, such that the R0 mode occurs at 20 kHz.

Figure 6-2 shows the results from a modal analysis using ABAQUS for a horn with internal and external diameters of 30 and 157 mm and length 45 mm. The pipe support sections are 63 mm long with internal and external diameters of 75 and 85 mm respectively. The flange is 14 mm long and has inner and outer diameters of 75 mm and 113 mm respectively. It can be seen that the R0, R1 and R3 modes occur in close proximity but that the device is tuned to 20081 Hz in the R0 mode with the R1 and R3 modes occurring at approximately 2000 Hz below and above this tuned frequency. This is sufficient to prevent modal coupling of the modes from occurring during operation. It can also be seen that for the R0 mode the pipe support sections also vibrate in the R0 mode and are attached at the nodal planes of the horn, this ensures that the vibratory motion of the pipe supports does not affect the vibratory motion of the horn. This horn was manufactured for use in the microbiological tests.



**Figure 6-2 – Deformed mode shapes for the radial horn flow through device (a) R0, (b) R1, and (c) R3 modes**

### 6.3 Methods and materials

Experiments were carried out by creating a continuous flow loop and taking samples at prescribed intervals from which the bacterial concentration can be obtained using the microbiological methods described in the previous chapter. Figure 6-4 shows a schematic of the experimental set up. It can be seen from this diagram that the R0 mode flow horn is mounted vertically and has a loose fitting plastic insert at both ends (shown in pink). These inserts allow the fluid to be delivered to the central area of the horn where it has been shown in the previous chapters that maximum cavitation takes place. These inserts have flanges which are used to connect them to the device. Fluid sealing is provided through a rubber gasket between the flange of the device and the flange of the plastic insert. The plastic inserts have been manufactured such that a fluid can be injected through the centre by means of an attached tube. The transducer is attached to the horn by a machined flat and screw thread. 500 ml of bacteria laden broth is held in a bottle and a pump is used to move the broth from this bottle into the bottom of the R0 mode flow horn. It is pumped up through the horn where it is treated by sonication in the central volume. Continuing to pump fluid into the horn forces the fluid in the central cavity to move up through the second insert where it is transported to a copper heat exchanger by a rubber tube. The fluid moves through the heat exchanger before being forced back into the original bottle containing the bacteria laden broth. The bottle, horn and heat exchanger are all placed in a bath of iced water to ensure that thermal effects are eliminated. The temperature of the fluid was measured using a thermometer and found to be less than 10 °C at all points during testing. Samples were removed aseptically from the bottle at regular intervals to be diluted and plated to determine the bacteria concentration in the fluid. This was done at intervals of 5 min up to 30 min sonication. Tests were carried out in quadruplicate to check



for repeatability. Initial tests in duplicate indicated an unusually large spread and a further two tests were therefore carried out to provide more data. Tests were carried out using *E. coli* K12 and *S. aureus* 24 for a flow rate of 110 ml/min, the slowest possible using the pump, at vibration input amplitudes of 2.3 and 7.6  $\mu\text{m}$ . At this flow rate, for the volume of fluid used, taking samples at 5 min intervals meant that all the fluid would be subject to sonication for 17.2, 34.74, 52.11, 69.48, 86.85 and 104.21 s for 5, 10, 15, 20, 25 and 30 min samples respectively.

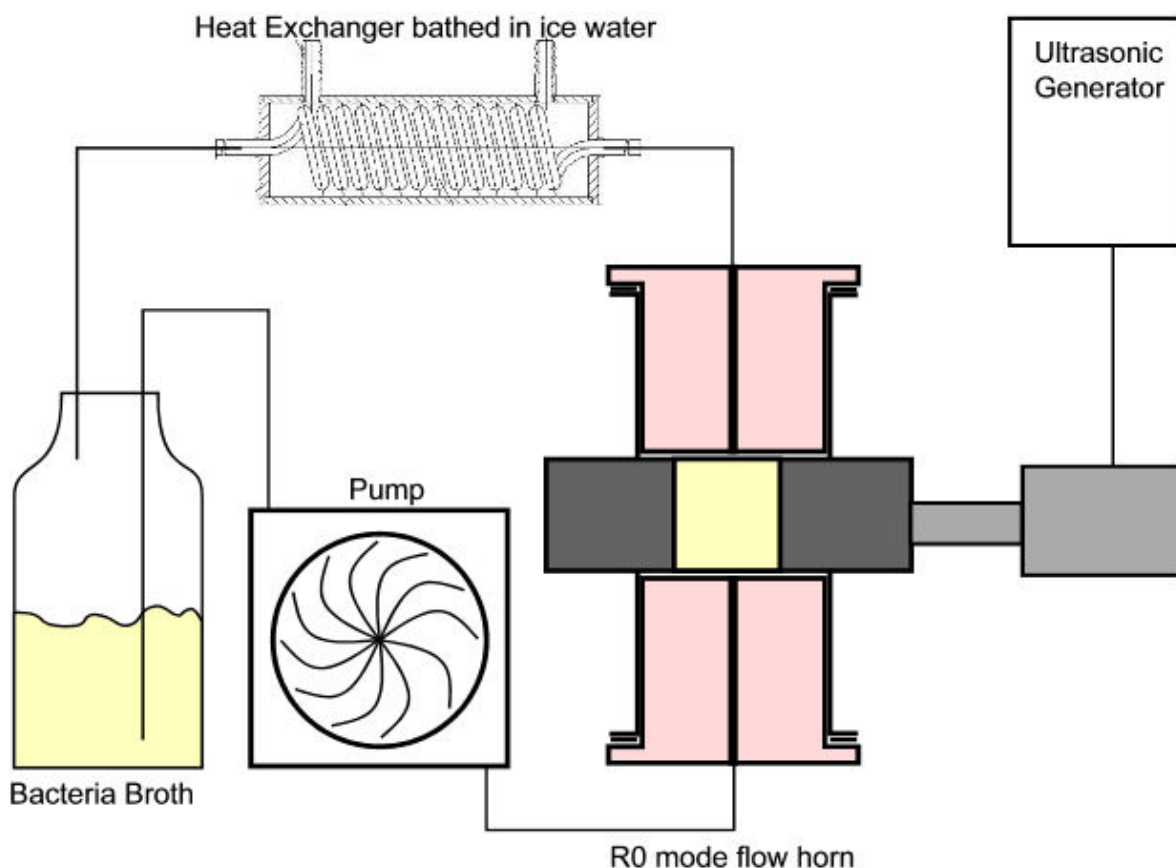


Figure 6-3 – Continuous flow experimental arrangement

## 6.4 Results

Figure 6-4 and Figure 6-5 show the results from the microbiological tests using *E. coli* K12 and *S. aureus* 24 respectively. Tests using *E. coli* K12 were carried out at 2.3 and 7.6  $\mu\text{m}$  with the horn directly connected to the transducer; the booster horn was not used in these tests. It can be observed that there is considerable spread in the results with significant overlap occurring between results for the two vibration amplitudes. The averaged results indicate a small change in the inactivation rate at the different configurations with quicker inactivation occurring at the higher amplitude. Using *S. aureus* 24, even at the 7.6  $\mu\text{m}$  over

30 min there is no sign of inactivation taking place with average bacteria concentrations actually increasing.

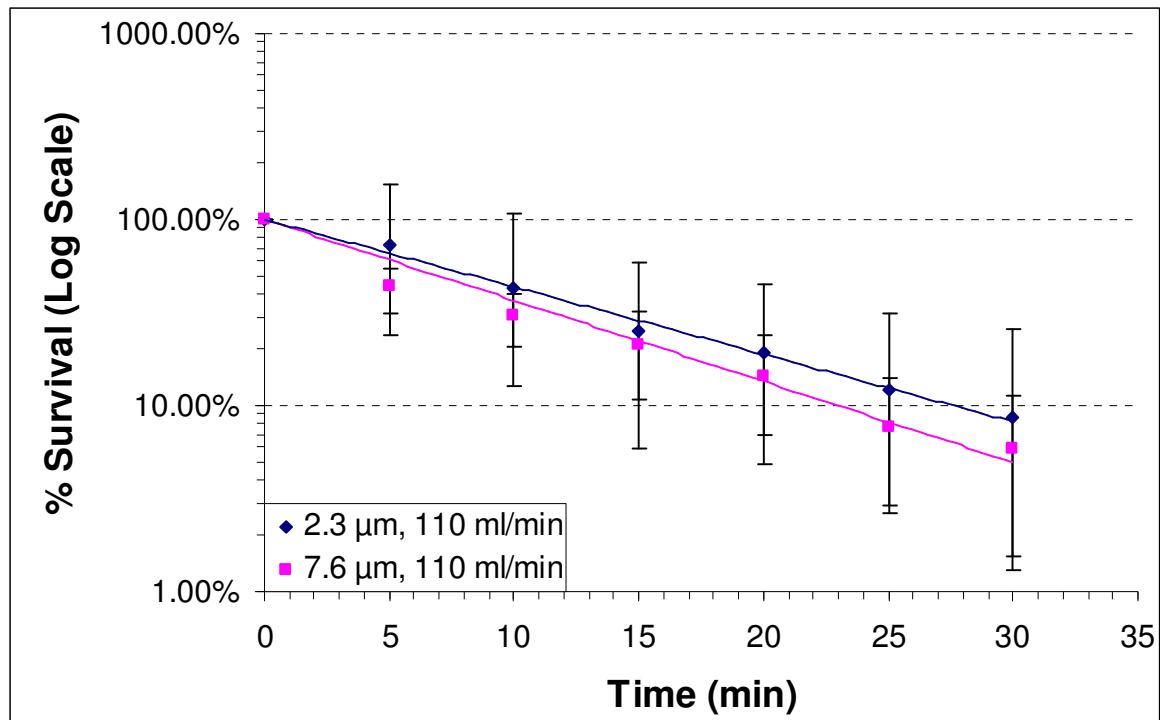


Figure 6-4 – Bacterial inactivation of *E. coli* K12 using the continuous flow set up for vibration input amplitudes of 2.3 and 7.6 μm

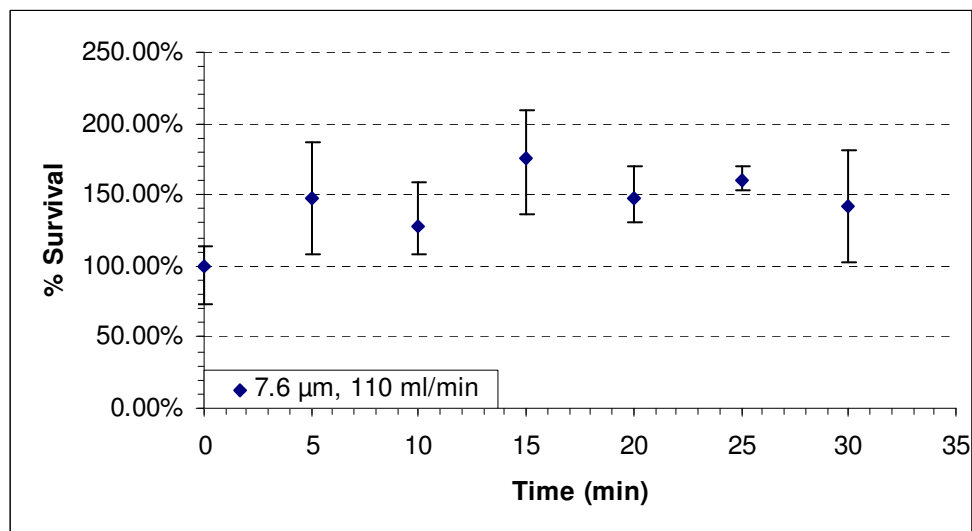


Figure 6-5 – Bacterial inactivation of *S. aureus* 24 using the continuous flow set up

## 6.5 Discussion

The results using *S. aureus* 24 indicate that this organism is extremely resistant to ultrasonic treatment as was discovered in the previous chapter. Analysing the results of the continuous flow set up it can be observed that the average results indicate an increase in

bacteria numbers. This is likely due to the disaggregating effect ultrasonic vibrations have on bacteria clumps. Since one would expect slower inactivation at lower amplitudes, further tests were not continued as it was deemed fruitless in light of these results.

Inactivation rates using *E. coli* K12 in the continuous flow set up are in agreement with what was found in the previous Chapter. Although the D-value calculated from Figure 6-4 for the 7.6  $\mu\text{m}$  case indicates a value of 22 min, it is necessary to adjust this for the actual time the fluid spent in the cavitation field. At 22 min during the continuous flow test, the fluid has been subject to the cavitation field for 78 s. This is comparable with results obtained in the previous chapter that found the D-value to be 1.5 min for the R0 mode radial horn at 7.6  $\mu\text{m}$  indicating the cavitation field is not greatly affected by slow flow rates.

## **6.6 Conclusions**

This chapter has reported preliminary results on the use of a R0 mode radial horn for bacterial inactivation in a continuous flow arrangement. It has been shown that *S. aureus* is again extremely resistant to ultrasonic treatment, even at extremely low flow rates. Results using *E. coli* have shown that similar inactivation rates are obtained when referenced against the actual time the fluid spent in the cavitation field.

---

## Chapter 7 – Conclusions

---

The hypothesis of this thesis was that radially vibrating ultrasonic devices are better at invoking bacterial inactivation within fluid suspensions and have several advantages compared to both traditional chemical and light based methods as well as the current ultrasonic method using a probe type device. The work was investigated in four stages. Firstly the horns were designed and manufactured. Next the cavitation fields caused by these devices were assessed before testing the efficacy of the devices on *Escherichia coli* K12 and *Staphylococcus aureus* 24. These results were then compared to other published research. Finally a radial mode ultrasonic horn was designed and manufactured to incorporate a continuous flow of fluid and the efficacy of this device was then assessed.

A review of the literature indicated that there have been several research groups interested in this area and have published excellent research on this topic. However, all the previous research has focussed on the probe type device with little research on any alternative devices. The mechanism of inactivation has been found to be high intensity bubble collapse called cavitation caused by the vibrations of these devices. Significant research and several books have been written on the physics of cavitation bubbles and their behaviour but the behaviour of cavitation fields is still not well understood and appropriate physical equations have yet to be elucidated. Of the research undertaken in using ultrasound to enact bacterial inactivation, one conclusion is consistently drawn; the use of ultrasound alone is not sufficient to be industrially useful due to the excessive exposure times required to reduce bacteria numbers to acceptable levels. Thus several of these studies have used a combination of technologies and have found improvements in requiring lower temperatures or fewer chemicals for the same inactivation rate when used in combination with ultrasonication. This research focussed on isolating the bacterial inactivation caused by ultrasonication alone as it enabled comparisons to be made between

the different devices and configurations without the need to ensure that thermal inactivation effects were consistent.

The ultrasonic devices were designed using the finite element analysis package ABAQUS and the modal characteristics were confirmed using experimental modal analysis. Several devices were designed and manufactured for the tests. Three radial horns and a booster horn were made. While a commercial probe horn was used for the experiments, it was also analysed using FEA and EMA for completeness. There were two R0 mode radial horns which had different internal and external diameters and an R3 mode radial horn. A booster horn was designed such that it could be used in two configurations; one which provided a gain of 2.0 and the other a gain of 0.5. Comparisons could then be drawn between the bacterial inactivation of different horns at several different ultrasonic amplitudes. These horns were successfully designed and manufactured with their modal characteristics confirmed through EMA. Further finite element analysis was carried out to determine the stresses within the horns when vibrating to ensure the stresses were considerably below the yield strength of the material.

A finite element analysis study of the probe device as well as the R0 and R3 mode radial horns was carried out to estimate the pressures caused by the ultrasonic vibrations on the fluid and determine whether these would be of significant magnitude to cause cavitation. A model of the horn with fluid cavity was constructed and analysed. The relationship between the internal diameter of the horn and the pressure field generated was investigated for the R0 radial horn device as was the relationship between ultrasonic amplitude and the pressure field. This study showed that the pressure field generated by the R0 horn consists of a high pressure zone in the centre of the horn reducing to a lower pressure at the vibrating surface. Thus a concentration effect was predicted. It was also found that an increase in amplitude caused a linear increase in the maximum pressure obtained in the fluid cavity. Also, it was shown that the inner diameter of the horn affected both the maximum pressure obtained for a given ultrasonic amplitude but also how the pressure was distributed. Smaller diameters result in a more uniform pressure field with a much smaller difference between the maximum and minimum pressures in the cavity while the opposite holds for larger diameters. It was also found that the smaller diameter horns had a lower maximum pressure compared to the larger diameter horns for the same ultrasonic

amplitude. This study predicted that the R3 radial horn would display six distinct areas of high pressure located at the anti-node locations.

To verify the results of the FEA, and since it is known that cavitation is the primary cause of cell death, the cavitation fields were investigated using photographs, chemiluminescence and aluminium foil. Photographs of the cavitation field were possible due to the bubbles causing reflection and refraction of light, meaning clear images could be obtained using simple backlighting. This was done for both R0 mode radial horns as well as the R3 radial horn and probe horn. It was found that the R0 mode radial horns created a focused cavitation cloud in the centre of the fluid cavity away from the vibrating surfaces with streamers of cavitation bubbles extending to the extremities of the cavity. The FEA predicted an area of large negative pressure in the centre of the fluid cavity which is where the cavitation cloud occurred in the photographs and chemiluminescence tests giving confidence in the FEA predictions. The R3 mode radial horn exhibited an interesting area of cavitation. Due to the six anti-nodes present in the R3 mode, cavitation occurred close to the vibrating surface but was much stronger at the anti-node locations, causing a hexagonal shape to be observed in the centre of the fluid cavity which was not undergoing cavitation. This is in excellent agreement with the acoustic pressure predictions made using FEA. The probe horn displayed a cone like cavitation field emanating from the probe tip due to bubble radiation forces, with strong cavitation at the horn tip quickly dissipating further from the tip.

Using aluminium foil it was possible to assess the relative strength of these cavitation fields. Bubble collapse near a surface occurs asymmetrically, so that a high speed jet of fluid forms and impinges on the surface causing erosion. The strength and density of bubble collapse can be inferred from the damage caused to a piece of aluminium foil exposed to the cavitation field. Aluminium foil was placed around the inner surface of the radial horns and several configurations were tested. Photographs were used to assess the damage. It was found as expected that in all cases, the longer the aluminium foil was exposed to the cavitation field the more damage was caused. In the case of both of the R0 horns it was found that the foil displayed consistent damage over the entire piece of foil. This is due to the R0 mode causing a uniform vibration of the horn surface. That is to say, there are no nodes on the circumference of the horn. The R3 mode radial horn, however, has six nodes and six anti-nodes. It was found that, in this case, the foil displayed 6 distinct areas of

damage equally spaced around the circumference with the other areas displaying little or no damage. The areas of severe damage were found to coincide with the anti-nodes of the R3 mode while the undamaged areas occurred at the node positions. An assessment was carried out to determine the damage caused to aluminium foil for both R0 horns and the R3 horn at different ultrasonic amplitudes. The amplitude was adjusted using a booster horn to provide two different gains as well as using the amplitude adjustment on the ultrasonic generator. It was observed that higher vibration amplitudes caused increased damage to the aluminium foil for the same exposure time. Thus it was hypothesised that an increase in amplitude will cause an increase in the rate of bacterial inactivation.

Further visualisation experiments were carried out using the chemiluminescence of luminol to determine the areas undergoing cavitation and the strength of that cavitation. This is possible due to the collapse of cavitation bubbles releasing free radicals which react with luminol solution causing a photon of light to be emitted in the blue spectrum. These radicals also have a biocidal effect but this is small compared to that caused by the collapse of cavitation bubbles. Photographs of the chemiluminescence were obtained for all three radial horns and the probe horn. This was done for pH 9.5 and pH 12 as the chemiluminescent effect is highly dependant on the pH of the fluid. It was found that the R0 horn with smaller internal diameter displayed a blue light on the inner surface of the horn at the lower pH but a uniform light was observed at the higher pH. The light observed at the lower pH is due to reactions taking place at the inner surface of the horn. The aspherical collapse of cavitation bubbles at the inner surface of the horn causes the luminol solution to be exposed to the aluminium surface having stripped away the aluminium oxide layer. The exposure of the luminol solution to aluminium is known to cause the reactions necessary to emit the blue light. The uniform emitance of light at the higher pH indicates that cavitation takes place throughout the fluid and not only in the central region where the cavitation cloud is observed in the photographs. Further, carrying out the same tests using the larger diameter R0 mode radial horn, it was observed that in addition to the light at the inner surface there was also a light emitted in the centre of the fluid cavity with visible streamers extending to the outer surface confirming the observations of the photographs taken using backlighting. Using the R3 mode radial horn, light was observed to occur at the anti-node points only. The probe horn displayed a cone like light emitance in agreement with the photographs. Comparing the amount of light emitted by these devices it was observed that the radial horns gave out more light than the probe horn indicating that

the reaction is stronger using these devices. It is thus concluded that the radial horn designs give a stronger cavitation field than that caused by the probe horn and has the potential to be better at bacterial inactivation.

This thesis has investigated the use of radial mode ultrasonic devices to enact bacterial inactivation in fluid suspensions. The bacterial inactivation rates were investigated with both *Escherichia coli* K12 and *Staphylococcus aureus* 24 using two R0 mode radial horns with different internal diameters as well as a R3 mode horn and a probe horn. In addition to the inactivation rates, the power consumption of the devices in the configurations used was determined to find out which device configuration has the greatest inactivation rate per unit power consumed. Microbiological tests using *S. aureus* yielded slow inactivation rates with results using the R3 radial mode horn indicating a single log reduction in bacteria numbers to take in 60 min exposure. *S. aureus* are gram positive bacteria and hence have a much thicker cell wall compared to *E. coli*. Coupled with their spherical shape this provides greater structural strength and makes the cell extremely resistant to physical inactivation through cavitation collapse. The spread of results was also found to be significant. The use of ultrasound alone is not sufficient to inactivate this type of cell at rates that would be commercially viable.

Tests using *E. coli*, a gram negative organism with significantly thinner cell wall, were considerably more successful. Microbiological tests yielded up to 4 log reduction in viable bacteria cells for an exposure of less than 5 min. Although these D-values are not commercially attractive they are encouraging for use in combination with other technologies which has been shown in the literature to be considerably more effective. Using *E. coli* as the sample organism it has been shown that radial mode ultrasonic devices are more efficient at enacting bacterial inactivation when compared to the results using the probe device and to other published work in this area. Further analysis of the results indicates there is a possible relationship between the decimal reduction time and the input power. Further detailed work is required to confirm or refute this hypothesis due to the experimental errors associated with the methodology of measuring the power input to the system. These tests have also shown that the D-value of the system is dependent on the initial bacterial concentration. Using the radial mode ultrasonic horns it has been shown that larger initial concentrations result in increased D-values. This is consistent with other studies investigating the concentration effect on heat, pressure and UV radiation. However,



it was also shown that the probe type horn displayed the opposite effect, indicating this mechanism is not as straightforward as initially thought.

Based on the encouraging results of the non flow tests, a R0 mode ultrasonic horn was designed to enable a continuous flow of fluid to be treated. Microbiological tests were carried out using both *E. coli* K12 and *S. aureus* 24 with a flow rate of 110 ml/min under a number of different configurations. Results again showed that the inactivation of *S. aureus* was minimal with a large spread of results observed. Results using *E. coli* were more successful with a measured D-value of 78 s exposure time at a vibration input of 7.6  $\mu\text{m}$ . This is in agreement with the results obtained by the non-flow system and indicates that the cavitation field is not greatly affected by the slow flow rate used in these experiments. It is concluded that the inclusion of a continuous flow does not significantly change the inactivation rates observed. Further research is required to seek designs to improve the cavitation field characteristics during continuous flow operations such that lower D-values may be obtained. The effect of increasing flow rate should also be examined.

In conclusion, it has been found that radial mode ultrasonic horns are more efficient at enacting bacterial inactivation, in terms of D-value per unit power, with significant benefits being realised over the traditional probe device. The bacterial inactivation rates of these devices are not sufficient to be commercially viable as a replacement for traditional bacterial inactivation techniques such as the use of heat, UV radiation and chemicals. However, it is expected that similar gains can be expected from the radial mode horns as has been achieved using the probe device when used in combination with these other technologies. In addition, the use of ultrasound to inactivate the more hardy bacteria *S. aureus* resulted in excessively long D-values making the use of other technologies in combination with ultrasound inevitable if the system were to be commercialised since it is likely that the product being treated has a number of different bacterial organisms requiring inactivation.

---

## Chapter 8 – Future Work

---

The work presented in this thesis has shown a good basis from which further research should be carried out. Outlined below are some areas where further research would be beneficial.

- Increasing ultrasonic amplitude/ power – Previous literature and this thesis have shown that the rate at which bacteria is inactivated is highly dependent upon the strength of the cavitation field generated. The finite element studies in this thesis have also shown that the maximum pressure generated by these devices is dependant on the ultrasonic amplitude and it is known that the ability to drive larger amplitudes lies with more powerful generators. Using higher power generators should lead to greater bacterial inactivation in both no-flow and flow conditions. It may also allow for larger flowrates to be treated.
- It has been observed in this thesis that the rate of inactivation is much lower when a continuous flow process is introduced. The reason for this has not yet been elucidated and should be determined in order for the system to be a viable option in the arsenal of processes making liquid foods safe. This could be carried out using a coupled fluid structure interaction analysis to evaluate the pressure fields generated by the radial horn in the continuous flow environment and comparing it with results from the no-flow pressure fields.
- It would also be useful to validate the pressure fields predicted by the FEA studies experimentally using a hydrophone or other pressure measurement device.
- Currently the main theory of bacterial inactivation through ultrasound is based on the pressure shock waves created upon cavitational collapse. This is supported by microscopic analysis of the cells after treatment. It would be advantageous to support this theory further using a finite element model of a bacteria cell interacting

with a pressure wave from a collapsing bubble. There is literature which determines the mechanical properties of the bacteria cell wall for several species which would assist the researcher undertaking this task.

- The finite element studies of the pressure fields generated by horns vibrating in the first radial mode, R1, gave the interesting result of large pressure fields being generated, greater than that achieved at the centre of the R0 mode horn. It would be interesting to determine whether this was the case and if so what affect it had on bacterial inactivation.
- This thesis focussed on isolating the ultrasonic bacterial inactivation effect from other factors such as thermal inactivation. The literature has shown that ultrasonic treatment with probe devices is inefficient in isolation but coupled with other methods can provide much better inactivation results. Further research should be carried out into developing the radial horn in combination with other methods such as heat, chemicals, UV and pressure.
- This thesis focussed solely on bacteria suspended in nutrient broth. Further research should be carried out into the effect of using ultrasonic inactivation when bacteria are suspended in other more industrially relevant fluids such as milk or fruit juices. The effect ultrasonic processing has on the taste and texture of these fluids should also be considered.

---

## References

---

1. [http://en.wikipedia.org/wiki/Miasma\\_theory\\_of\\_disease](http://en.wikipedia.org/wiki/Miasma_theory_of_disease), last accessed 07/08/07
2. [http://en.wikipedia.org/wiki/Germ\\_theory\\_of\\_disease](http://en.wikipedia.org/wiki/Germ_theory_of_disease), last accessed 07/08/07
3. [http://en.wikipedia.org/wiki/Louis\\_Pasteur](http://en.wikipedia.org/wiki/Louis_Pasteur), last accessed 07/08/07
4. <http://en.wikipedia.org/wiki/Pasteurization>, last accessed 07/08/07
5. I.R. Grant, H.J. Ball, S.D. Neill, M.T. Rowe, Inactivation of Mycobacterium paratuberculosis in cows' milk at pasteurization temperatures, Applied and environmental microbiology, Feb. 1996, Vol. 62, No. 2, pp. 631-636
6. The national study on the microbiological quality and heat processing of cows' milk, <http://www.food.gov.uk/multimedia/pdfs/map-positives.pdf>, last accessed 08/08/07
7. [http://en.wikipedia.org/wiki/Ignaz\\_Semmelweis](http://en.wikipedia.org/wiki/Ignaz_Semmelweis), last accessed 08/08/07
8. Life Magazine, 1997
9. [http://en.wikipedia.org/wiki/Hypochlorous\\_acid](http://en.wikipedia.org/wiki/Hypochlorous_acid), last accessed 08/08/07
10. [http://en.wikipedia.org/wiki/Water\\_purification](http://en.wikipedia.org/wiki/Water_purification), last accessed 08/08/07
11. J. Mir, J. Morato, F. Ribas, Resistance to chlorine of freshwater bacterial strains, Journal of applied microbiology, Jan. 1997, Vol. 82, No. 1, pp. 7-18
12. <http://en.wikipedia.org/wiki/Cryptosporidium>, last accessed 08/08/07
13. [http://en.wikipedia.org/wiki/Ultraviolet\\_Germicidal\\_Irradiation](http://en.wikipedia.org/wiki/Ultraviolet_Germicidal_Irradiation), last accessed 08/08/07
14. <http://www.uvcomparison.com/uvscience.php>, last accessed 08/08/07
15. Downes A, Blount T.P, Proceedings of the Royal Society of London, 1877, Vol. 26, 1877, PP.488-500, Researches on the Effect of Light upon Bacteria and other Organisms
16. <http://en.wikipedia.org/wiki/UVGI>, last accessed 08/08/07
17. <http://www.lateral-science.co.uk/marum/index.html>, last accessed 08/08/07

18. M.B. Rubin, The history of ozone. The Schönbein period, 1839-1868, Bulletin for the History of Chemistry, 2000, Vol. 26, No. 1, pp. 40-56
19. <http://en.wikipedia.org/wiki/Ozone>, last accessed 08/08/07
20. Virus inactivation by ozone, D. Adachi, 2001, Masters thesis
21. V. Camel, A. Bermond, The use of ozone and associated oxidation processes in drinking water treatment, Water Research, Nov. 1998, Vol. 32, No. 11, pp. 3208-3222
22. B. Thanomsub, V. Anupunpisit, S. Chanphetch, T. Watcharachaipong, R.Poonkhum, C. Srithsukonth, Effects of ozone treatment on cell growth and ultrastructural changes in bacteria, Journal of general and applied microbiology, 2002, Vol. 48, pp. 193-199
23. <http://en.wikipedia.org/wiki/Piezoelectricity>, last accessed 08/08/07
24. <http://www.ob-ultrasound.net/langevin.html>, last accessed 08/08/07
25. M. Versluis, B. Schmitz, A von der Heydt, D. Lohse, How Snapping Shrimp Snap: Through Cavitating Bubbles, 2000, Science, Vol. 289, pp. 2114-2117
26. K.S. Norris, B. Mohl, Can Odontocetes Debilitate Prey with Sound?, The American Naturalist, Jul. 1983, Vol. 122, No. 1, pp. 85-104
27. <http://www.cbsnews.com/stories/2007/08/07/tech/main3142664.shtml>, last accessed 08/08/07
28. Alliger, H., American Laboratory, Oct 1975, PP 75-84, "Ultrasonic Disruption"
29. Mason, T.J., Duckhouse, H., Joyce, E., Lorimer, J.P., WCU 2003, Paris, Sept 7-10, pp.423-426, "Uses of ultrasound in the biological decontamination of water"
30. Mir, J. et al., Journal of Applied Microbiology, Vol.82, Issue 1, Jan 1997, PP.7-18, "Resistance to chlorine of freshwater bacterial strains"
31. Grant, I.R., Applied and Environmental Microbiology, Vol.62, No.2, Feb 1996, PP.631-636, "Inactivation of *Mycobacterium paratuberculosis* in Cows' Milk at Pasteurization Temperatures"
32. Klijn, N. et al., Journal of Applied Microbiology, Vol.91, 2001 PP.697-704, "Heat inactivation data for *Mycobacterium avium* subsp. *Paratuberculosis*: Implications for Interpretation"
33. Nelson, T.R. and Pretorius, D.H., Ultrasound in Medicine and Biology, Vol.24 No.9, PP.1243-1270, 1998, "Three Dimensional Ultrasound Imaging"
34. Bond, L.J. et al., IEE Proceedings, Part A: Physical Science, Measurement and Instrumentation, Management and Education, Vol.131, No.4, pt.A, Jun 1984,

- PP.265-274, "Review of some Recent Advances in Quantitative Ultrasonic NDT."
35. Thoe T.B et al., International Journal of Machine Tools and Manufacture, Vol.38, No.4, 1998, PP.239-255, Review on Ultrasonic Machining
  36. Lucas, M. et al., CIRP Annals – Manufacturing Technology, Vol.50, No.1, 2001, PP.149-152, Design and characterisation of ultrasonic cutting tools
  37. Lambert B, Engineering (London), Vol.219, No.3, Mar 1979, PP.329-331, "Ultrasonic Cleaning Aids to Production"
  38. Tittman, B.R et al., Proceedings of the Twelfth Annual Review of Progress in Quantitative Nondestructive Evaluation, Vol.5B, 1986, PP.1533-1541, "Enhanced Castings By the use of Ultrasonics"
  39. Petukhow, V.I et al., Light Metal Age, Vol.31, No.5-6, Jun 1973, PP.6-8, "Extrusion of Aluminium in an Ultrasonic Field"
  40. Ueoka, T, Tsujino, J, Japanese Journal of Applied Physics, Vol.41, Part 1, No.5B, May 2002, PP.3237-3242, Welding Characteristics of Aluminium and Copper Plate Specimens Welded by a 19 kHz Complex Vibration Ultrasonic Seam Welding System
  41. Neppiras E.A, Physics reports, Vol.61, No.3, 1980, PP.159-251, Acoustic cavitation
  42. Frenkel J., Kinetic theory of liquids, 1955, New York: Dover
  43. Mason T.J. and Lorimer, J.P., Sonochemistry theory, applications and uses of ultrasound in chemistry, 1988, PP. 51-53, Ellis Horwood, ISBN 0-7458-0240-0
  44. Williams, P.R. and Williams, R.L., Molecular Physics, Vol.102, No.19-20, Oct. 2004, PP.2091-2102, "Cavitation and the Tensile Strength of Liquids Under Dynamic Stressing"
  45. Abramov O.V., 1998, High Intensity Ultrasonics, Gordon and Breach Science Publishers
  46. Leighton, T.J., In: The Acoustic Bubble, Academic Press
  47. Mason T.J., Sonochemistry, 1999, Oxford Chemistry Primers, Vol. 70, PP. 11-12, ISBN 0-19-850371-7
  48. Mason T.J. and Lorimer J.P, Applied Sonochemistry , 2002, Wiley VCH
  49. Lord Rayleigh, Philosophy Magazine, Vol.34, 1917, PP.94-98, "On the Pressure Developed in a Liquid During the Collapse of a Spherical Cavity"

50. Plesset, M.S., Journal of Applied Mechanics, Sept. 1949, PP.277-282, "The Dynamics of Cavitation Bubbles"
51. Noltingk, B.E. and Neppiras, E.A., Proceedings of the Physics Society B, Vol.63, 1950, PP.674-, "Cavitation Produced by Ultrasonics"
52. Neppiras, E.A. and Noltingk, B.E., Proceedings of the Physics Society B, Vol.64, 1951, PP.1032-, "Cavitation Produced by Ultrasonics: Theoretical Conditions for the Onset of Cavitation"
53. Poritsky, H., Proceedings of the 1<sup>st</sup> US national congress on applied mechanics, 1952, PP.813-821, "The Collapse or Growth of a Spherical Bubble or Cavity in a Viscous Fluid"
54. Neppiras, E.A., Physics Reports, Vol.61, No.3, 1980, PP.159-251, "Acoustic Cavitation"
55. Apfel, R.E., Journal of the Acoustical Society of America, Vol.69, Issue.6, June 1981, "Acoustic Cavitation Prediction"
56. Flynn, H.G., Journal of the Acoustical Society of America, Vol.57, 1975, PP.1379-1396, "Cavitation Dynamics: I, A Mathematical Formulation"
57. Flynn, H.G., Journal of the Acoustical Society of America, Vol.58, No.6, Dec 1975, PP.1160-1170, "Cavitation Dynamics. II. Free Pulsations and Models for Cavitation Bubbles"
58. Blake F.J., The onset of cavitation in liquids: I. Acoustics Research Laboratory, Harvard University, 1949, Tech. memo. No. 12
59. Holland, C.K. and Apfel, R.E., IEEE Transactions on Ultrasonics, Ferroelectrics, and frequency control, Vol.36, No.2, March 1989, PP.204-208, "An Improved Theory for the Prediction of Microcavitation Thresholds"
60. Apfel, R.E. and Holland, C.K., Ultrasound in Medicine and Biology, Vol.17, No.2, 1991, PP.179-185, "Gauging the Likelihood of Cavitation from Short-Pulse, Low-Duty Cycle, Diagnostic Ultrasound"
61. Alliger, H., American Laboratory, Oct 1975, PP 75-84, "Ultrasonic Disruption"
62. Harvey E.N, Barnes D.K, McElroy W.D, Whitely A.H, Pease D.C and Cooper K.W, 1944, Journal of Cellular Comparative Physiology, Vol.24, Iss.1, PP.1-22, Bubble formation in animals. I. Physical factors
63. <http://www.brl.uiuc.edu/Downloads/sakai/SakaiChapter1.pdf>
64. Leighton, T.J., In: The Acoustic Bubble, PP. 341-367, Academic Press

65. Wood R.W, Loomis A.L, *Philosophy Magazine*, 4, 417, 1927, The physical and biological effects of high frequency sound waves of high intensity
66. Richards W.T., The Chemical Effects Of High Frequency Sound Waves II. A Study Of Emulsifying Action, *Journal American Chemical Society*, 1929, Vol.51, PP. 1724–1729
67. Higgins D.M. and Skauen D.M., Influence of power on quality emulsions prepared by ultrasound, *Journal of Pharmaceutical Sciences*, Vol.61, No.10, PP.1567-1570
68. Abismail J.P., Canselier J.P., Wilhelm A.M., Delmas H., Gourdon C., Emulsification by ultrasound: drop size distribution and stability, *Ultrasonics Sonochemistry*, Vol.6, 1999, PP.75-83
69. Freitas S., Heilscher G., Merkle H.P., Gander B., Continuous contact- and contamination-free ultrasonic emulsification – a useful tool for pharmaceutical development and production, *Ultrasonics Sonochemistry*, Vol.13, 2006, PP.76-85
70. Richards W.T, Loomis A.L, *Journal of the American Chemical Society*, Vol.49, Iss.12, 1927, PP.3086-3100, The chemical effects of high frequency sound waves I. A preliminary survey
71. Fang X, Mark G and von Sonntag C, *Ultrasonics Sonochemistry*, Vol.3, Iss.1, 1996, PP.57-63, OH radical formation in aqueous solutions part I: the chemistry underlying the terephthalate dosimeter
72. Mark G, Tauber A, Laupert R, Schuchmann H.P, Schulz D, Mues A, von Sonntag C, *Ultrasonics Sonochemistry*, Vol.5, 1998, PP.41-52, OH radical formation by ultrasound in aqueous solution part II: Terephthalate and Fricke dosimetry and the influence of various conditions on the sonolytic yield
73. Sochard S, Wilhelm A.M, Delmas H., *Ultrasonics Sonochemistry*, Vol.4, 1997, PP.77-84, Modelling of free radical production in a collapsing gas-vapour bubble
74. Hart E.J, Henglein A, *Journal of physical chemistry*, Vol.89, 1985, PP.4342-4347, Free radical and free atom reactions in the sonolysis of aqueous iodine and formate solutions
75. Colussi A.J., Weavers L.K, Hoffmann M.R, *Journal of physical chemistry A*, Vol.102, 1998, PP.6927-6934, Chemical bubble dynamics and quantitative sonochemistry



76. Makino K, Mossoba M, Riesz P, Journal of physical chemistry, Vol.87, 1983, PP.1369-1377, Chemical effects of ultrasound on aqueous solutions. Formation of hydroxyl radicals and hydrogen atoms
77. Suslick K.S, Hammerton D.A, Cline R.E, The Journal of the Acoustical Society of America, 1986, Vol.108, PP.5641-5642, The Sonochemical Hotspot
78. Doktycz S.J and Suslick K.S, Science, Vol.247, Iss.4946, PP.1067-1069, Interparticle collisions driven by ultrasound
79. Thompson L.H and Doraiswamy L.K, Industrial Engineering Chemical Research, 1999, Vol.38, PP.1215-1249, Sonochemistry: Science and Engineering
80. Suslick K.S and Price G.J, Annual Review Materials Science, 1999, Vol.29, PP.295-326, Applications of ultrasound to materials chemistry
81. Peters D., Journal of materials chemistry, 1996, Vol.6, Iss.10, PP.1605-1618, Ultrasound in materials chemistry
82. Suslick K.S, Homogeneous sonochemistry, In: Ultrasound. It's chemical, physical and biological effects, VCH Publishers, New York, 1988
83. Taleyarkhan R.P, West C.D, Cho J.S, Lahey Jr. R.T, Nigmatulin R.I, Block R.C, Science, 2002, Vol. 295, No.5561, PP.1868-1873, Evidence for Nuclear Emissions During Acoustic Cavitation
84. Taleyarkhan R.P, Cho J.S, West C.D, Lahey Jr. R.T, Nigmatulin R.I, Block R.C, Physical Review E, Vol.69, 2004, PP, Additional evidence of nuclear emissions during acoustic cavitation
85. Xu Y. and Butt A., Nuclear Engineering and Design, 2005, Vol. 235, Iss.1317, PP.1317-1324, Confirmatory Experiments for Nuclear Emissions During Acoustic Cavitation
86. Fry F.J, Sanghvi T., Foster R.S, Bihrl R., Hennige C., Ultrasound in medicine and biology, Vol.21, No.9, 1995, PP.1227-1237, Ultrasound and microbubbles: their generation, detection and potential utilization in tissue and organ therapy – experimental
87. Kennedy J.E, Haar G.R, Cranston D., The British journal of radiology, Vol.76, 2003, PP.590-599, High intensity focused ultrasound: surgery of the future?
88. Sun X.Z, Zhang Z.W, Asian journal of surgery, Vol.29, No.1, 2006, PP.36-39, Shock wave lithotripsy for uric acid stones

89. Harvey E.N, Loomis A.L, Journal of bacteriology, Vol.17, 1929, PP.373-379, The destruction of luminous bacteria by high frequency sound waves
90. Scherba, G, Weigel R.M, O'Brien W.D, American Society for Microbiology, Vol.57, No.7, 1991, PP.2079-2084, "Quantitive Assessment of the Germicidal Efficacy of Ultrasonic Energy"
91. Sala, F.J. et al., In: New Methods of Food Preservation, Chapter 9, PP.176-204, "Effect of heat and ultrasound on micro organisms and enzymes"
92. Rahman, M.S., Light and Sound in Food Preservation, In: Handbook of food preservation, PP.669-685
93. Earnshaw, R.G, Appleyard, J, Hurst R.M, International Journal of Food Microbiology, Vol.28, 1995, PP.197-219, Understanding Physical Inactivation Processes: Combined Preservation Opportunities Using Heat, Ultrasound and Pressure
94. Wu J, Ultrasound in Medicine and Biology, Vol.28, No.1, 2002, PP.125-129 Theoretical Study on Shear Stress Generated By Microstreaming Surrounding Contrast Agents Attached to Living Cells
95. Wu J, Progress in biophysics and molecular biology, Vol.93, 2007, PP.363-373, Shear stress in cells generated by ultrasound
96. Ohta S, Suzuki K, Tachibana K, Yamada G, Genesis, Vol.37, 2003, PP.91-101, Microbubble-enhanced sonoporation: efficient gene transduction technique for chick embryos
97. Deng C.X, Sieling F, Pan H, Cui J, Ultrasound in medicine and biology, Vol.30, No.4, PP.519-526, Ultrasound-induced cell membrane porosity
98. Okada K, Kudo N, Niwa K, Yamamoto K, Journal of medical ultrasonics, Vol.32, 2005, PP.3-11, A basic study on sonoporation with microbubbles exposed to pulsed ultrasound
99. Liu Y, Yang H, Sakanishi A, Biotechnology advances, Vol.24, 2006, PP.1-16, Ultrasound: Mechanical gene transfer into plant cells by sonoporation
100. Wamel A, Kooiman K, Harteveld M, Emmer M, Cate F.J, Versluis M, Jong N, Journal of controlled release, Vol.112, 2006, PP.149-155, Vibrating microbubbles poking individual cells: drug transfer into cells via sonoporation
101. Kinoshita M, Hynynen K, Biochemical and biophysical research communication, In press, 2007, Key factors that affect sonoporation efficiency in vitro settings: the importance of standing wave in sonoporation

102. Bekeredjian R, Kuecherer H.F, Kroll R.D, Katus A, Hardt E, Urology, Vol.69, No.2, 2007, PP.386-389, Ultrasound-targeted microbubble destruction augments protein delivery into testes
103. Madigan M.T, Martinko J.M, Parker J, Brock Biology of Microorganisms, 10<sup>th</sup> edition, Prentice Hall, ISBN 0130491470
104. <http://en.wikipedia.org/wiki/Peptidoglycan>, last accessed 21/09/07
105. Hedges, M. et al., International Journal of Radiation Biology, Vol.37, No.1, 1980, PP.103-108, The Effect of Ultrasound at 1.5MHz on *Escherichia Coli*
106. Allison, D.G. et al., Journal of Basic Microbiology, Vol.36, No.1, 1996, PP.3-11, The Effect of ultrasound on *Escherichia coli* viability
107. Miles, C.A. et al., Journal of Applied Bacteriology, Vol.78, 1995, PP.47-54, Principals of Separating Micro-organisms from Suspensions Using Ultrasound
108. Phull S.S, Newman A.P, Lorimer J.P, Pollet B, Mason T.J, Ultrasonics Sonochemistry, Vol.4, 1997, PP.157-164, "The development and evaluation of ultrasound in the biocidal treatment of water
109. Duckhouse H, Mason T.J, Phull S.S, Lorimer J.P, Ultrasonics Sonochemistry, Vol.11, 2004, PP.173-176, The effect of sonocation on microbial disinfection using hypochlorite
110. Burleson, G.R., Applied Microbiology, Vol.29, No.3, 1975, PP.340-344, Inactivation of Viruses and Bacteria by Ozone With and Without Sonication
111. Garcia, M.L. et al., Journal of Applied Bacteriology, Vol.67, 1989, PP.619-628, Effect of Heat and Ultrasonic Waves on the Survival of Two Strains of *Bacillus Subtilis*
112. Lee et al. Food Microbiology, Vol.6, 1989, PP.143-152, Thermal ultrasonic and ultraviolet inactivation of *Salmonella* in thin films of aqueous media and chocolate
113. Raso, J. et al., Journal of Applied Microbiology, Vol.85, 1998, PP.849-854, Inactivation of *Bacillus Subtilis* spores by Combining Ultrasonic Waves Under Pressure and Mild Heat Treatment
114. Joyce E, Phull S.S, Lorimer J.P, Mason T.J, Ultrasonics Sonochemistry Vol.10, 2003, PP.315-318, The development and evaluation of ultrasound for the treatment of bacterial suspensions. A study of frequency, power and sonication time on cultured *Bacillus* species

115. Pagan R, Manas P, Alvarez I, Condon S, Food Microbiology, Vol.16, 1999, PP.139-148, Resistance of *Listeria Monocytogenes* to Ultrasonic Waves Under Pressure at Sub-Lethal (Manosonication) and Lethal (Manothermosonication) Temperatures
116. Manas P, Pagan R, Raso J, Sala F.J, Condon S, Journal of food protection, Vol.63, No.4, 2000, PP.451-456, Inactivation of *Salmonella* Enteritidis, *Salmonella* Typhimurium, and *Salmonella* Senftenberg by ultrasonic waves under pressure
117. Save S.S, Pandit A.B, Joshi J.B, Transactions of the institute of chemical engineers, Vol.75, Part C, 1997, Use of hydrodynamic cavitation for large scale microbial cell disruption
118. Lopez-Malo A, Guerrero S, Alzamora S.M, Journal of food protection, Vol.62, No.10, 1999, PP.1215-1217, *Saccharomyces cerevisiae* thermal inactivation kinetics combined with ultrasound
119. Tsukamoto I, Yim B, Stavarache C.E, Furuta M, Hashiba K, Maeda Y, Ultrasonics Sonochemistry, Vol.11, 2004, PP.61-65, Inactivation of *Saccharomyces cerevisiae* by ultrasonic irradiation
120. Ciccolini L, Taillandier P, Wilhem A.M, Delmas H, Strehaiano P, Chemical engineering journal, Vol.65, 1997, PP.145-149, Low frequency thermo-ultrasonication of *Saccharomyces cerevisiae* suspensions: effect of temperature and of ultrasonic power
121. Guerrero S, Lopez-Malo A, Alzamora S.M, Innovative food science and emerging technologies, Vol.2, 2001, PP.31-39, Effect of ultrasound on the survival of *Saccharomyces cerevisiae*: influence of temperature, pH and amplitude
122. Lanchun S, Bochu W, Liancai Z, Jie L, Yanhong Y, Chuanren D, Colloids and surfaces B: Biointerfaces, Vol.30, 2003, PP.61-66, The influence of low-intensity ultrasonic on some physiological characteristics of *Saccharomyces cerevisiae*
123. Tsukamoto I, Constantinoiu E, Furuta M, Nishimura R, Maeda Y, Ultrasonics sonochemistry, Vol.11, 2004 PP.167-172, Inactivation effect of sonication and chlorination on *Saccharomyces cerevisiae*. Calorimetric analysis

124. Guerrero S, Tognon M, Alzamora A.M, Food control, Vol.16, 2005, PP.131-139, Response of *Saccharomyces cerevisiae* to the combined action of ultrasound and low weight chitosan
125. Hulsen U, European dairy magazine, Vol.3, 1999, PP.20-24, Alternative heat treatment processes
126. Ahmed F.I, Russell C, Journal of applied bacteriology, Vol.39, Iss.1, 1975, PP.31-40, Synergism between ultrasonic waves and hydrogen peroxide in the killing of micro-organisms
127. Jacobs, S.E., Journal of Applied Bacteriology, Vol.67, 1989, PP.619-628, Effect of Heat and Ultrasonic Waves on the Survival of Two Strains of *Bacillus Subtilis*
128. Jacobs S.E, Thornley M.J, Journal of applied bacteriology, Vol.17, 1954, PP.38-55, The lethal action of ultrasonic waves on bacteria suspended in milk and other liquids
129. Mason T.J, Paniwnyk L, Lorimer J.P, Ultrasonics sonochemistry Vol.3, 1996, PP. S253-S260, The uses of ultrasound in food technology
130. Piyasena P, Mohareb E, McKellar R.C, International journal of food microbiology, Vol.87, 2003, PP.207-216, Inactivation of microbes using ultrasound: a review
131. Blume, T. and Neis, U, Ultrasonics Sonochemistry, Vol.11, 2004, PP.333-336, Improved wastewater disinfection by ultrasonic pre-treatment
132. Gennaro L, Cavella S, Romano R, Masi P, Journal of food engineering, Vol.39, 1999, PP.401-407, The use of ultrasound in food technology I: inactivation of peroxidase by thermosonication
133. Joyce E, Mason T.J, Phull S.S, Lorimer J.P, Ultrasonics Sonochemistry Vol.10, 2003 PP.231-234, The development and evaluation of electrolysis in conjunction with power ultrasound for the disinfection of bacterial suspensions
134. Pagan R, Manas P, Raso J, Condon S, Applied and environmental microbiology, Vol.65, Iss.1, 1999, Pp.297-300, Bacterial resistance to ultrasonic waves under pressure at nonlethal (manosonication) and lethal (manothermosonication) temperatures
135. Jyoti K.K, Pandit A.B, Ultrasonics Sonochemistry, Vol.10, 2003, PP.255-264, Hybrid cavitation methods for water disinfection: simultaneous use of chemicals with cavitation

136. Gonze E, Fourel L, Gonthier Y, Boldo P, Bernis A, Chemical engineering journal, Vol.73, 1999, PP.93-100, Wastewater pretreatment with ultrasonic irradiation to reduce toxicity
137. Cleofé, Campos-Pozuelo et al., 2005, Ultrasonics Sonochemistry, Vol.12 PP.79-84, "Experimental and theoretical investigation of the mean acoustic pressure in the cavitation field"
138. Villamiel M, Jong P, Journal of food engineering, Vol.45, 2000, PP.171-179, Inactivation of *Pseudomonas fluorescens* and *Streptococcus thermophilus* in trypticase soy broth and total bacteria in milk by continuous flow ultrasonic treatment and conventional heating
139. Borthwick, K.A.J, Coakley W.T, McDonnell M.B, Nowotny H, Benes E, Groschl M, Journal of Microbiological Methods, Vol.60, 2005, PP.207-216, Development of a Novel Compact Sonicator for Cell Disruption
140. ABAQUS theory manual, section 2.5
141. [http://en.wikipedia.org/wiki/Helium-neon\\_laser](http://en.wikipedia.org/wiki/Helium-neon_laser), last accessed 26/01/08
142. Lucas, M., Ultrasonics Vol.34, Iss.1, 1996, pp35-41, Vibration sensitivity in the design of ultrasonic forming dies
143. Peshkovsky S. L. and Peshkovsky, A.S., Ultrasonics Sonochemistry, Vol. 14, 2007, PP.314-322, Matching a transducer to water at cavitation: Acoustic horn design principles
144. Renaudin V., Gondrexon N., Boldo P., Petrier C., Bernis A., Gonthier Y., Ultrasonics Sonochemistry, Vol.1, Iss.2, 1994, PP.S81-S85, Method for determining the chemically active zones in a high frequency ultrasonic reactor
145. Schneider Y., Zahn S., Hofmann J., Wecks M., Rohm H., Ultrasonics Sonochemistry, Vol.13, 2006, PP.117-120, Acoustic cavitation induced by ultrasonic cutting devices: A preliminary study
146. McMurray H.N., Wilson B.P., Journal of physical chemistry A, Vol.103, 1999, PP.3955-3962, Mechanistic and special study of ultrasonically induced luminol chemiluminescence
147. Reisz P., Free radical generation by ultrasound in aqueous solutions of volatile and non-volatile solutes, In: Advances in Sonochemistry, Mason T.J., Vol.2, 1991, JAI Press, PP.23-64, ISBN 1-55938-267-8

148. Makino K., Mossobna M., Riesz P., Journal of physical chemistry, Vol.87, 1983, PP.1369-1377, Chemical effects of ultrasound on aqueous solutions. Formation of Hydroxyl radicals and Hydrogen atoms
149. Moussatov A., Granger C., Dubus B., Ultrasonics Sonochemistry, Vol.10, 2003, PP.191-195, Cone-like bubble formation in ultrasonic cavitation field
150. Campos-Pozuelo C., Granger C., Vanhille C., Moussatov A., Dubus B., Ultrasonics Sonochemistry, Vol.12, 2005, PP.79-84, Experimental and theoretical investigation of the mean acoustic pressure in the cavitation field
151. Kulmala S., Matachescu C., Kulmala A., Papkovsky D., Hakansson M., Ketamo H., Canty P., Analytica Chimica Acta, Vol.453, 2002, PP.253-267, Chemiluminescence of luminol induced by dissolution of oxide-covered aluminium in alkaline aqueous solution
152. <http://textbookofbacteriology.net/growth.html>, last accessed 14/02/08
153. Davies R., Biochimica et Biophysica Acta, Vol. 33, 1959, PP.491-493, Observations on the use of ultrasound waves for the disruption of microorganisms
154. Hua, I., Thompson, J.E., Water Research, Vol.34, No.15, 2000, PP.3888-3893, Inactivation of *Escherichia Coli* by sonication at discrete ultrasonic frequencies
155. Watts, R.J. et al., Water Research, Vol.29, No.1, 1995, PP.95-100, Photocatalytic inactivation of coliform bacteria and viruses in secondary effluent
156. Sung, N., Collins, M.T., Applied and Environmental Microbiology, Vol.63, Iss.3, Mar. 1998, PP.999-1005, Thermal tolerance of *Mycobacterium paratuberculosis*
157. Furukawa, S., et al., International journal of Food Science and Technology, 2002, Vol.37, PP.573-577, Effect of initial concentration of bacterial suspensions on their inactivation by high hydrostatic pressure
158. Brennen C.E., Cavitation and bubble dynamics, Chapter 3, Oxford University Press, 1995
159. [http://commons.wikimedia.org/wiki/Image:Prokaryote\\_cell\\_diagram.svg](http://commons.wikimedia.org/wiki/Image:Prokaryote_cell_diagram.svg), last accessed 28/04/08
160. [http://en.wikipedia.org/wiki/Image:Animal\\_cell\\_structure.svg](http://en.wikipedia.org/wiki/Image:Animal_cell_structure.svg), last accessed 28/04/08
161. <http://researchnews.osu.edu/archive/proreg.htm>, last accessed 28/04/08

162. [http://www.biology4kids.com/extras/dtop\\_micro/7821.html](http://www.biology4kids.com/extras/dtop_micro/7821.html), last accessed 28/04/08
163. <http://web.mpiib-berlin.mpg.de/cgi-bin/pdbs/2d-page/extern/index.cgi>, last accessed 28/04/08
164. <http://www.americanaquariumproducts.com/images/graphics/bacteria.jpg>, last accessed 28/04/08
165. ABAQUS analysis user's manual, sections 14.1.4
166. [http://www.polytec.com/eur/158\\_425.asp](http://www.polytec.com/eur/158_425.asp), last accessed 28/04/08
167. O'Shea, K., ASME Design Engineering Division DE, Vibration Analysis - Analytical and Computational, Vol.DE-37, 1991, pp259-265, Enhanced vibration control of ultrasonic tooling using finite element analysis
168. [http://www.maxim-ic.com/appnotes.cfm/an\\_pk/729](http://www.maxim-ic.com/appnotes.cfm/an_pk/729), last accessed 04/05/08
169. Cifuentes A. O., Kalbag A., Finite Elements in Analysis and Design, 1992, Vol.12 Iss.3-4, PP.313-318, A performance study of tetrahedral and hexahedral elements in 3-D finite element structural analysis



---

## Bibliography

---

1. Brock Biology of Microorganisms, 10<sup>th</sup> edition, Madigan, M. T., Martinko, J.M., Parker, J., Prentice Hall, ISBN 0-13-049147-0
2. Modal Testing theory, practice and application, 2<sup>nd</sup> edition, Ewins, D. J., Research studies press ltd., ISBN 0-86380-218-4
3. The Acoustic Bubble, Leighton, T. G., Academic Press, ISBN 0124419216
4. Modal Space, In our own little world, Avitable, P.,  
<http://macl.caeds.eng.uml.edu/umlspace/mspace.html>
5. <http://en.wikipedia.org/>
6. Ultrasound in Food Processing, Mason, T.J., Povey M.J.W., Springer, ISBN 0751404292

---

## **Publications**

---

1. G. Hunter, M. Lucas, I. Watson, R. Parton, A radial mode ultrasonic horn for the inactivation of *Escherichia coli* K12, *Ultrasonics Sonochemistry*, Volume 15, Issue 2, February 2008, Pages 101-109
2. G. Hunter, Prof. M. Lucas, Dr. I. Watson, Dr. R. Parton, Finite element modelling of the pressure fields created by ultrasonic bacterial inactivation devices, Paper #1111 Presented at the International Congress on Ultrasonics, Vienna, April 9 - 13, 2007, Session R06: Bioeffects of Ultrasound